空调换热器低阻高效技术现状及趋势
(Focus on Airside Improvement)

Chi-Chuan Wang (王啟川), PhD, FASME, FASHRAE

Professor, Department of Mechanical Engineering,
National Chiao Tung University, Hsinchu, Taiwan
E-mail: ccwang@mail.nctu.edu.tw

Dec. 1, 2017 @ 珠海格力电器

Outline

- 基本背景
- 鰭片熱傳性能之改善與演進
  - More Surfaces..
  - Boundary Layer Restarting
    - Intrusion design
    - Grooved design
  - Swirled Flow
  - Oval/Flat tube
  - Combined Design
  - Grooved surface
  - Effective temperature Management
  - Others
- Conclusions

典型氣冷式熱交換器的熱流現象

- 熱傳分析
  - 管側冷媒熱傳
    - 平滑管
    - 微鰭管
    - 增強管
      - 兩相冷凝熱傳
      - 兩相蒸發熱傳
      - 單相熱傳
      - 兩相流譜
      - 壓降
      - 新冷媒熱傳

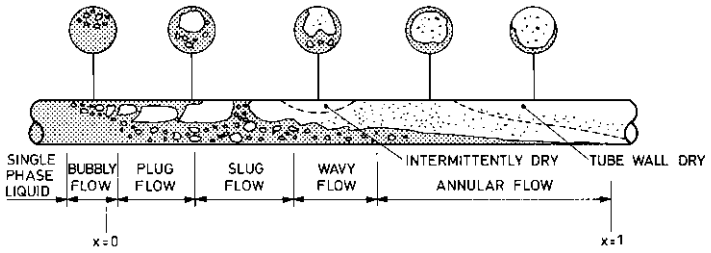

管內兩相流譜之變化

  - 鰭片側空氣熱傳
    - 乾盤管 (室外機)
    - 濕盤管 (室內機)
      - 平板鰭片
      - 百葉窗鰭片
      - 波浪鰭片
      - Convex-Louver鰭片
      - Lanced 鰭片
      - 親水性鰭片

熱傳管尺寸之演變

- 近年來,小管徑熱傳管的使用越來越普遍
  (Ex. 以小型空調機為例;管徑的變化如下
- **Why?**

空調機用熱傳管演進圖

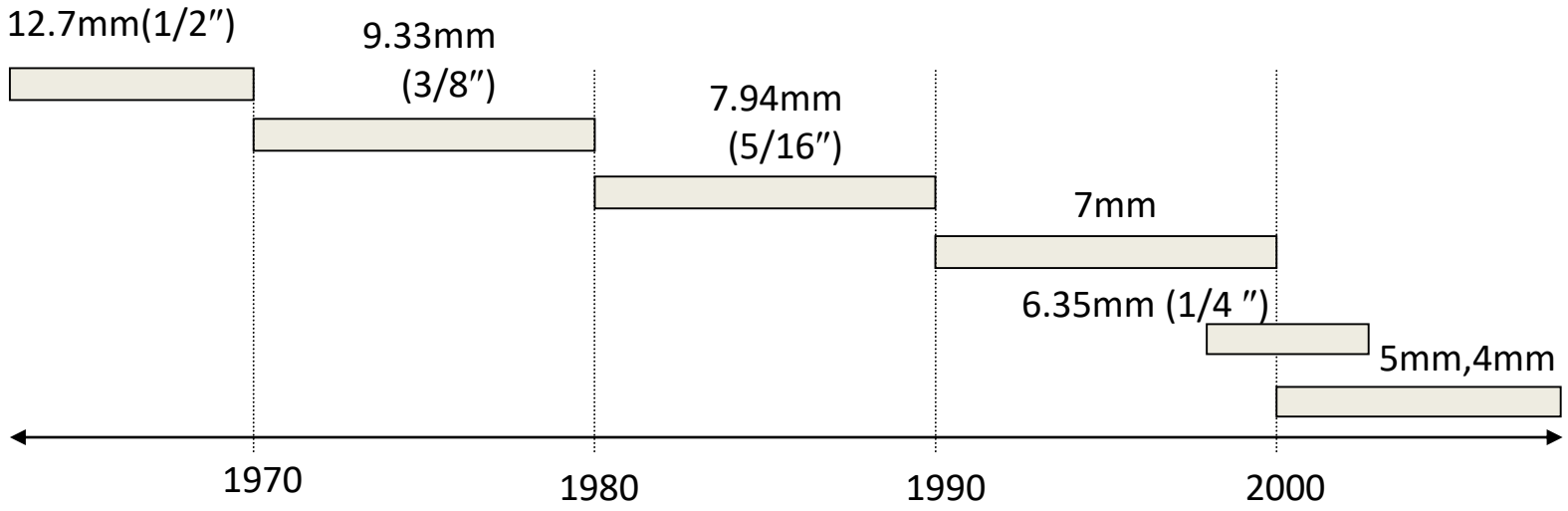

Note: 汽車現在用的扁平管為1 ~ 2 mm

Fundamentals of Heat Transfer

$$Q = UA\Delta T, \quad \frac{1}{UA} = \frac{1}{\eta_o h_o A_o} + \frac{\delta_w}{k_w A_w} + \frac{1}{h_i A_i}$$

$$or \quad Q = \eta_o h_o A_o \Delta T \text{ for electronic cooling}$$

- U: overall heat transfer coefficient
  - h_i, h_o: inside & outside heat transfer coefficient
  - η_o: surface efficiency ($=1-A_f/A_o(1-\eta_f)$)
  - η_f: fin efficiency
- A: surface area
- ΔT: effective Temperature Difference

For Heat Transfer Augmentation. One needs to..

(a) Increase A? (Most effective but limited by ΔP)

(b) Increase U? (Effective but also prone to increasing ΔP)

(c) What else can one do? (Manuplating ΔT?)

各式鰭片

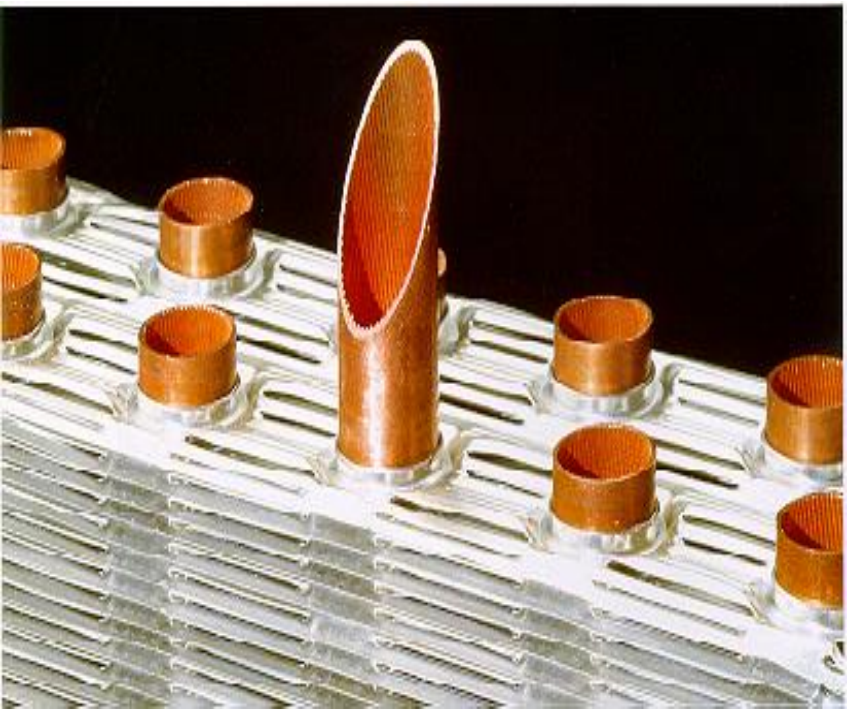

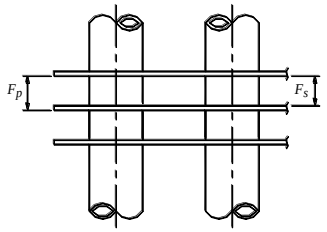

(a) 平板型

Plain fin

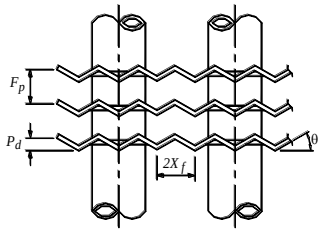

(b) 波浪型

Herringbone wavy fin

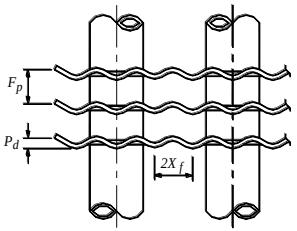

(c) 平滑波浪型

Smooth wavy fin, type (I)

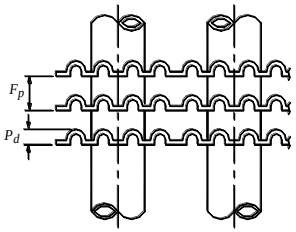

(d) 平滑波浪+平板型

Smooth wavy fin, type (II)

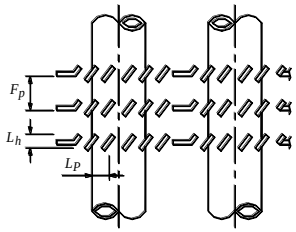

(e) 單向百葉窗型

Louver fin, one-sided

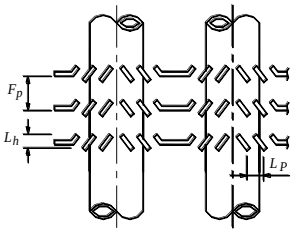

(f) 雙向百葉窗型

Louver fin, with re-direction louver

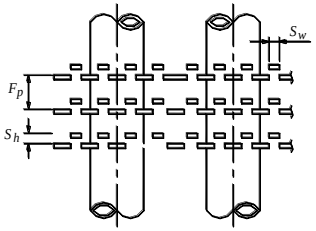

(g) 單向裂口型

Slit fin, one-sided

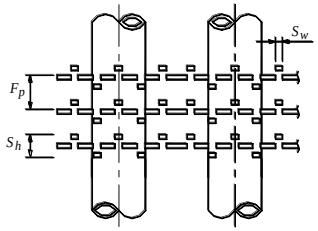

(h) 雙向裂口型

Slit fin, double-sided

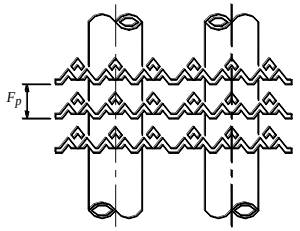

(i) 複和百葉窗型

Convex-louver fin

Fin Type

First generation – Continuous Surface

(wavy)

(plain)

Second generation – Interrupted Surface

(louver)

(louver)

convex louver

(slit)

Concept of Interrupted surfaces

Boundary layer restart & Mixing

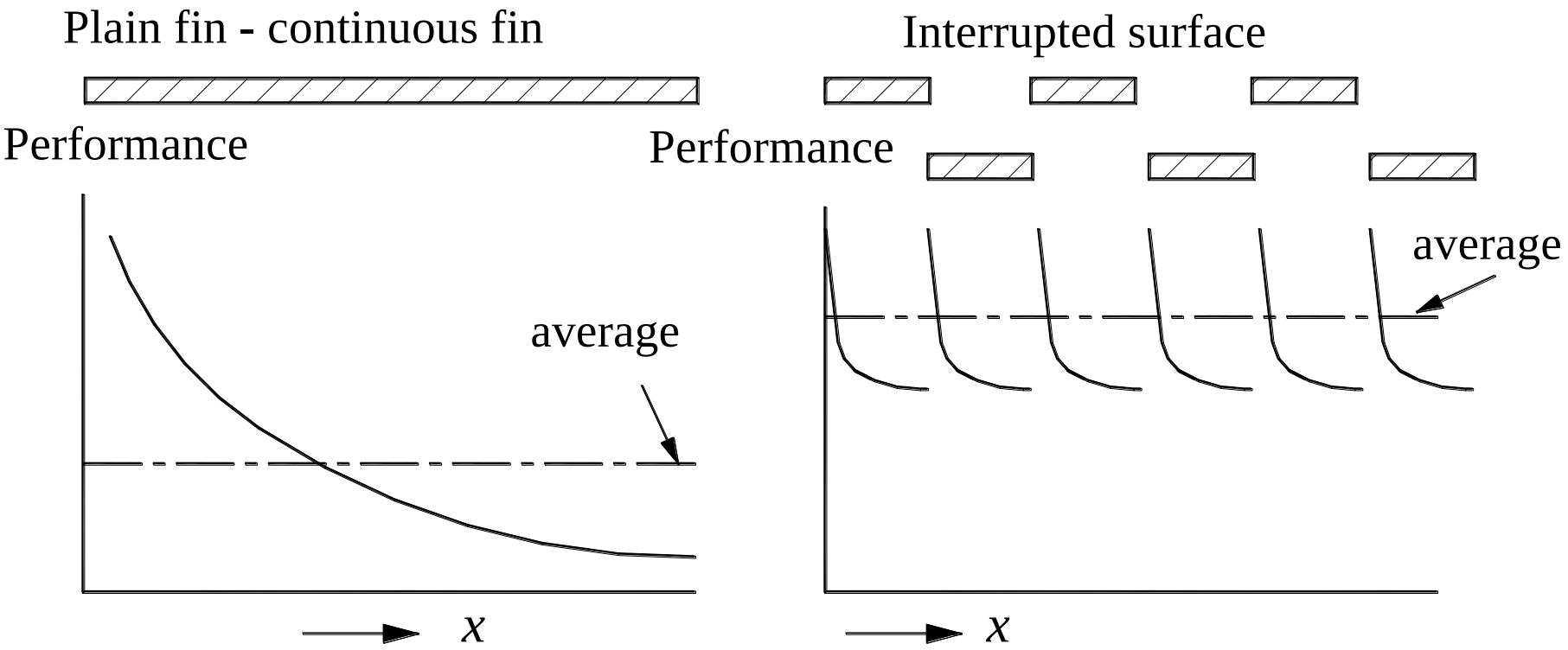

Characteristics: Sufficient Heat Transfer Improvement accompanied with significant pressure drop.

Unable to fulfill heat transfer performance at low velocity operation

Various kinds of improvements - **Implementations**

- Smooth fin: Plain fin featuring heat transfer improvement by increasing heat dissipating surface. Generally, smaller fin spacing is used to accommodate more fin surface.

  Fin spacing can be lower than 1 mm.

- Interrupted fin geometry which improves convective heat transfer coefficient via periodical renewal of boundary layer such as slit or louver fin.

louver fin

slit fin

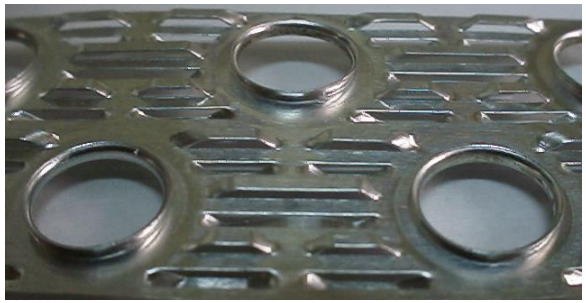

Interrupted surfaces..

- Provide effective heat transfer augmentations at medium and high velocity with significant pressure drop penalty.
- Nearly ineffective at low velocity but still suffer from considerable pressure drop.
  - Duct flow effect.

Low performance at low velocity (normally less than 1.0 m/s of V_{fr})

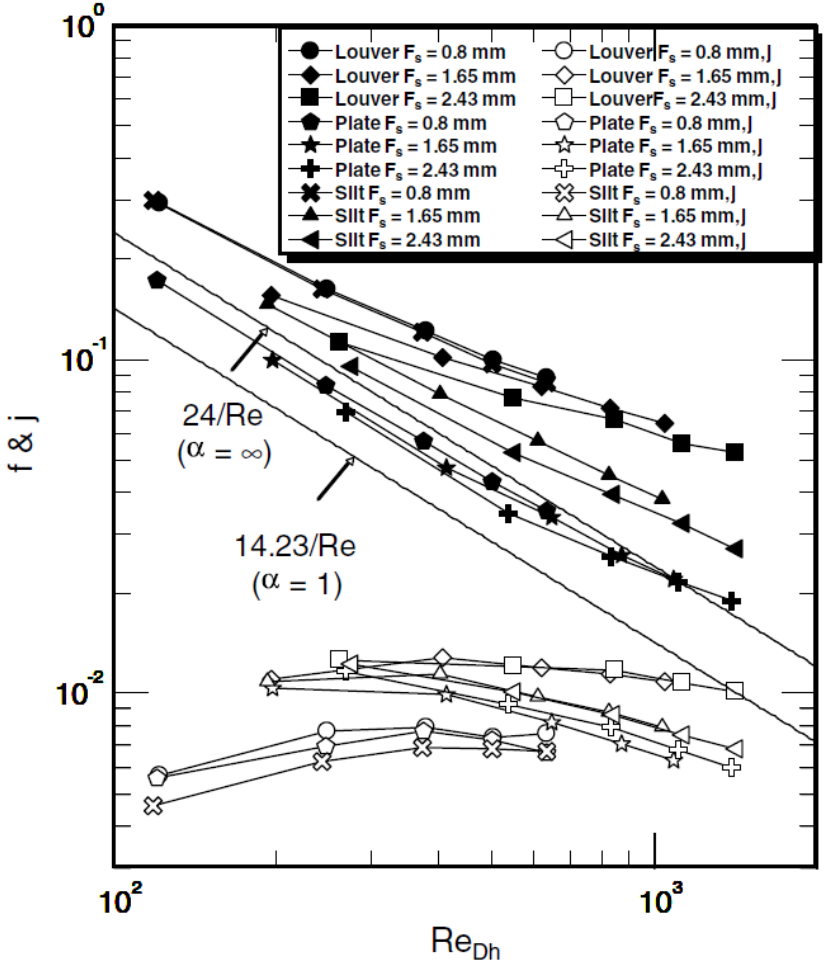

Fig. 6. j & f vs. Re_{D_h} for louver, slit and plate fin.

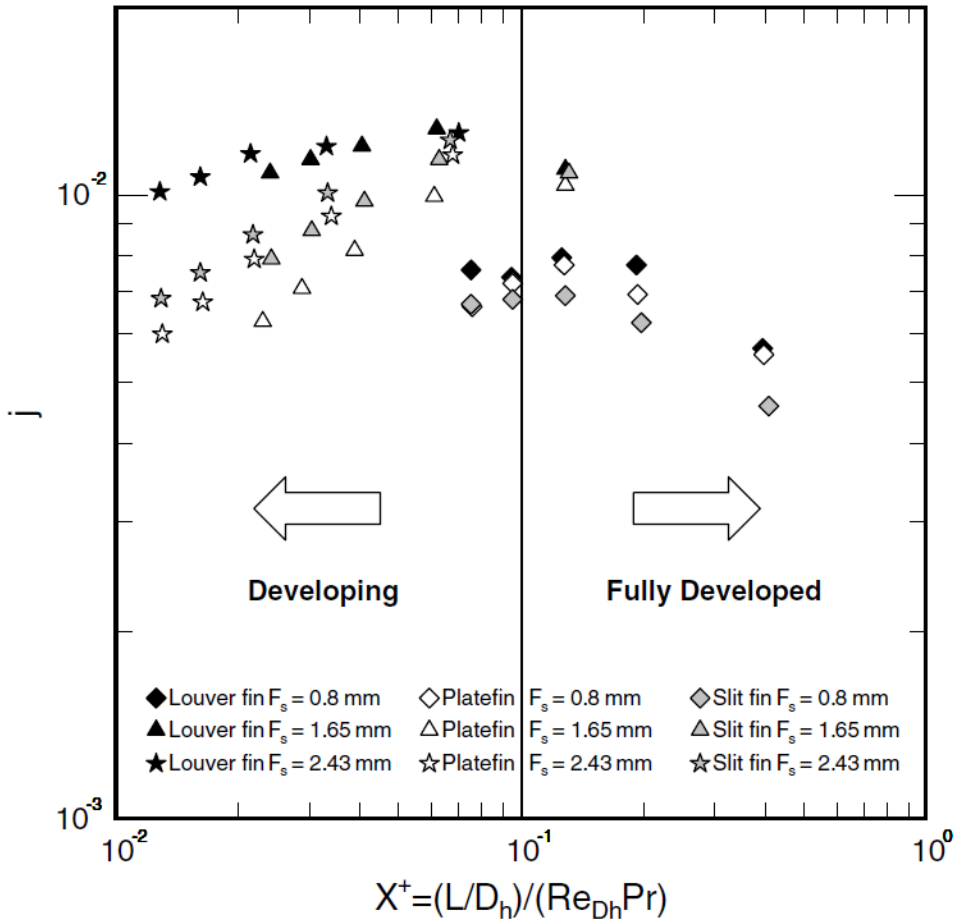

Fig. 7. Inverse Graetz number x^+ vs. j for louver, slit, and plate fin.

Effects of Periodic Entrance/Exit

Air flow

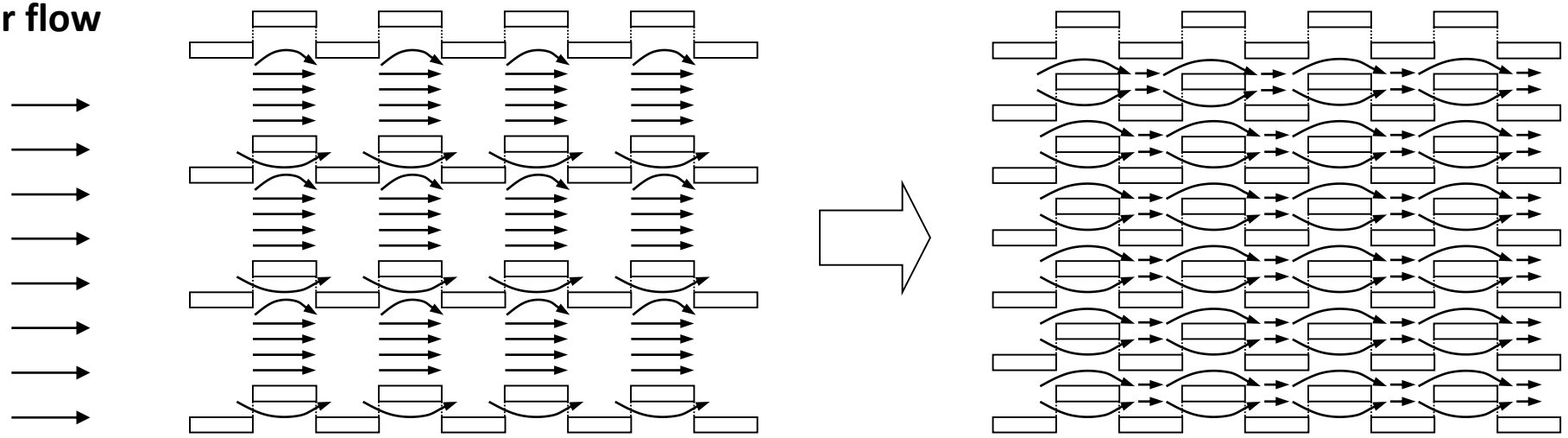

Louver directed vs. fin directed

Air flow

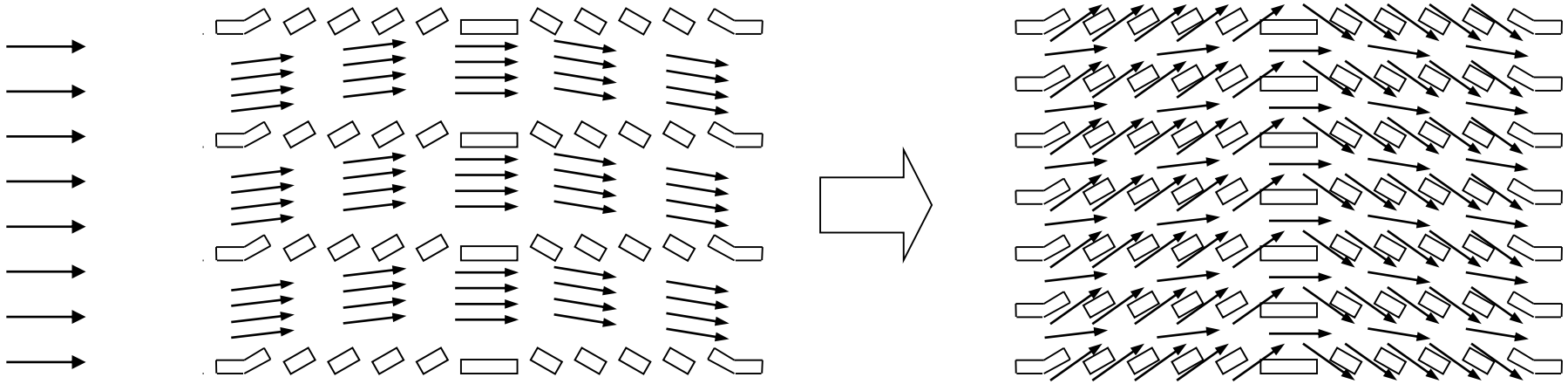

SCHEMATIC OF DUCT FLOW VS. FIN-DIRECTED FLOW FOR LOUVER FIN GEOMETRY AT SMALLER AND LARGER FLOW VELOCITIES. (Yang et al. IJHMT, 2007)

Heat transfer analysis of fin-and-tube heat exchangers with flat and louvered fin geometries, Int. J. Refrig., 45, 160-167

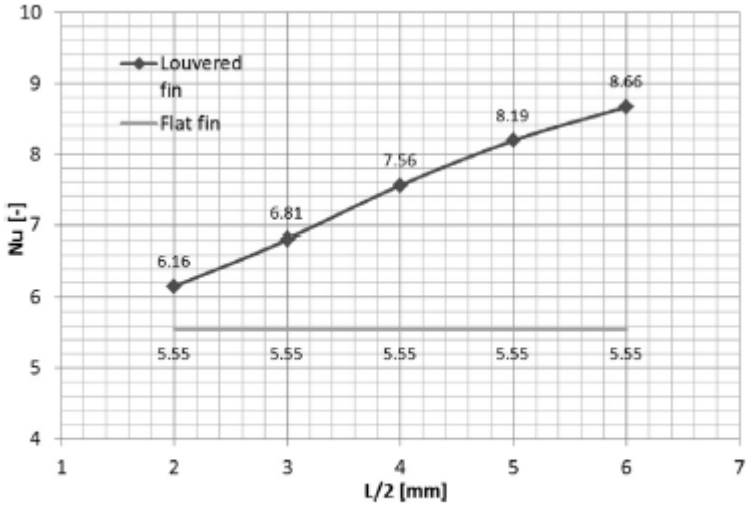

Fig. 7 – Louver length influence on heat transfer performance; $Re_H = 282$.

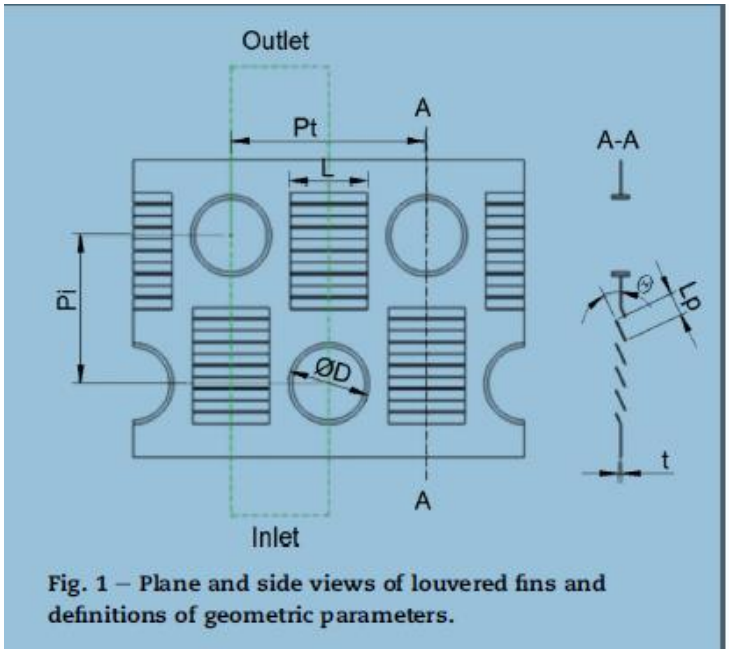

Fig. 1 – Plane and side views of louvered fins and definitions of geometric parameters.

Louver angle is suggested to be less than 20, number of louvers is around 5

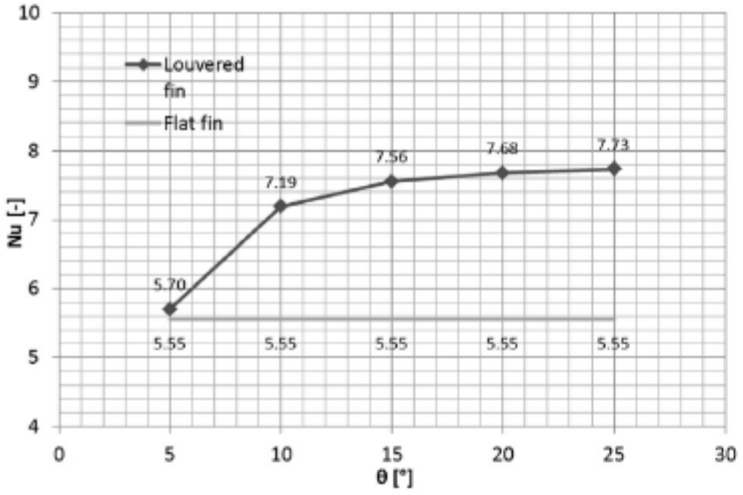

Fig. 8 – Louver angle influence on heat transfer performance; $Re_H = 282$.

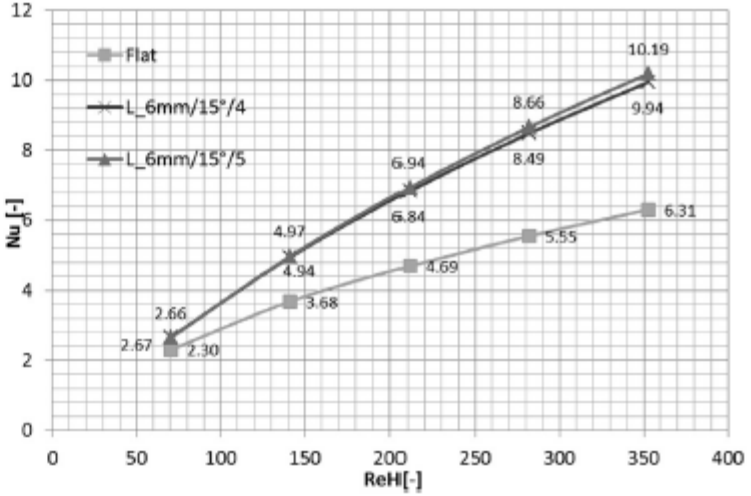

Fig. 10 – The influence of number of louvers on heat exchange.

(10) Pub. No.: US 2016/0245594 A1
(43) Pub. Date: Aug. 25, 2016

- Combination design

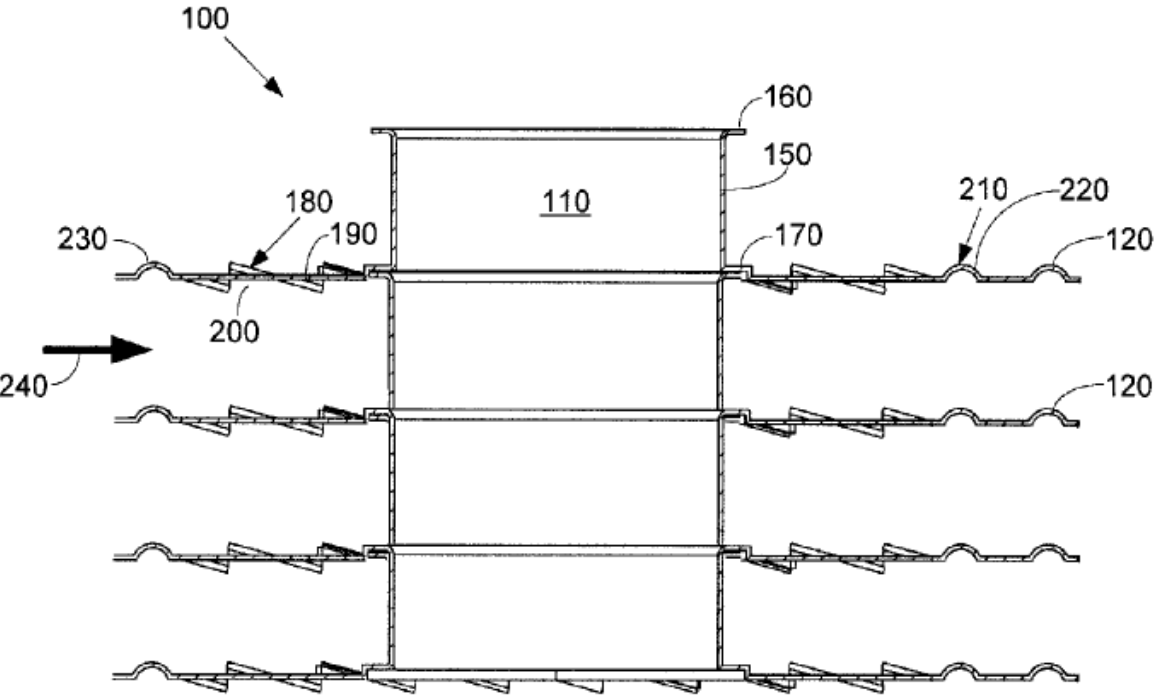

Fig. 1

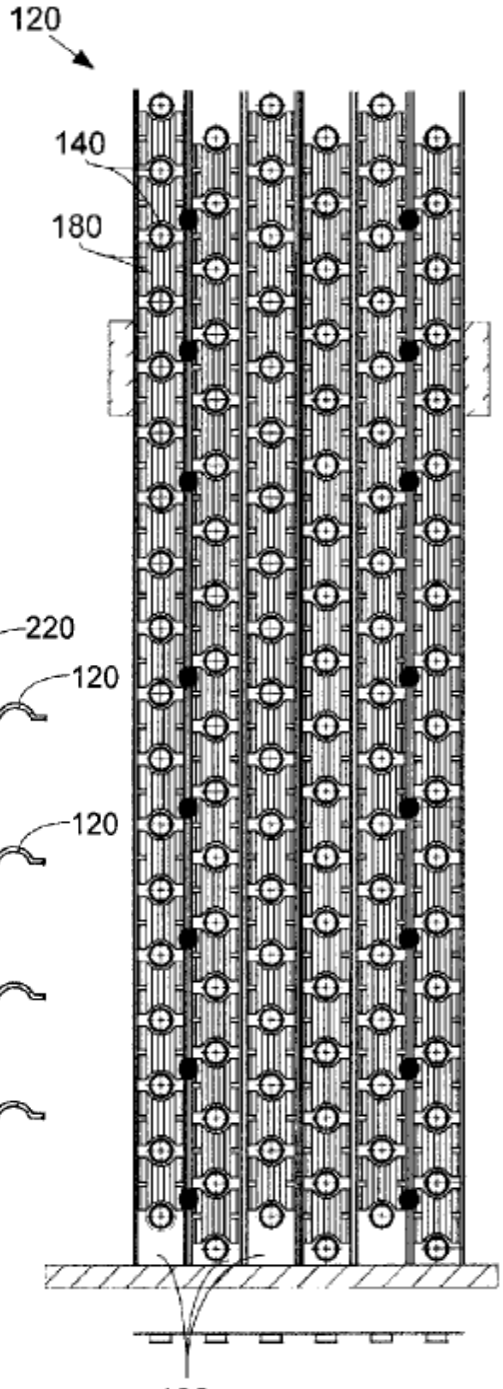

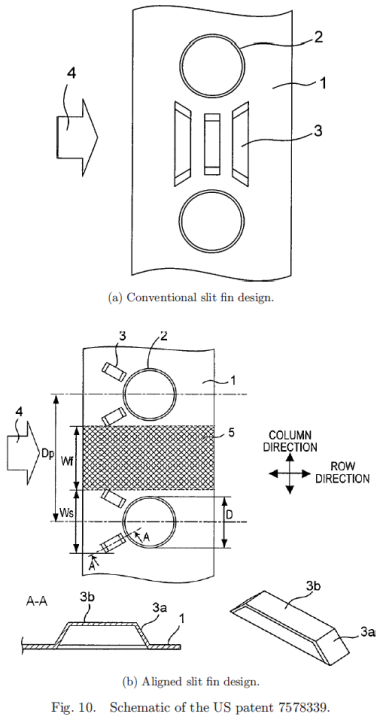

Fig. 10. Schematic of the US patent 7578339.

Role of channel shape on performance of plate-fin heat exchangers: Experimental assessment, International Journal of Thermal Sciences 79 (2014) 183-193

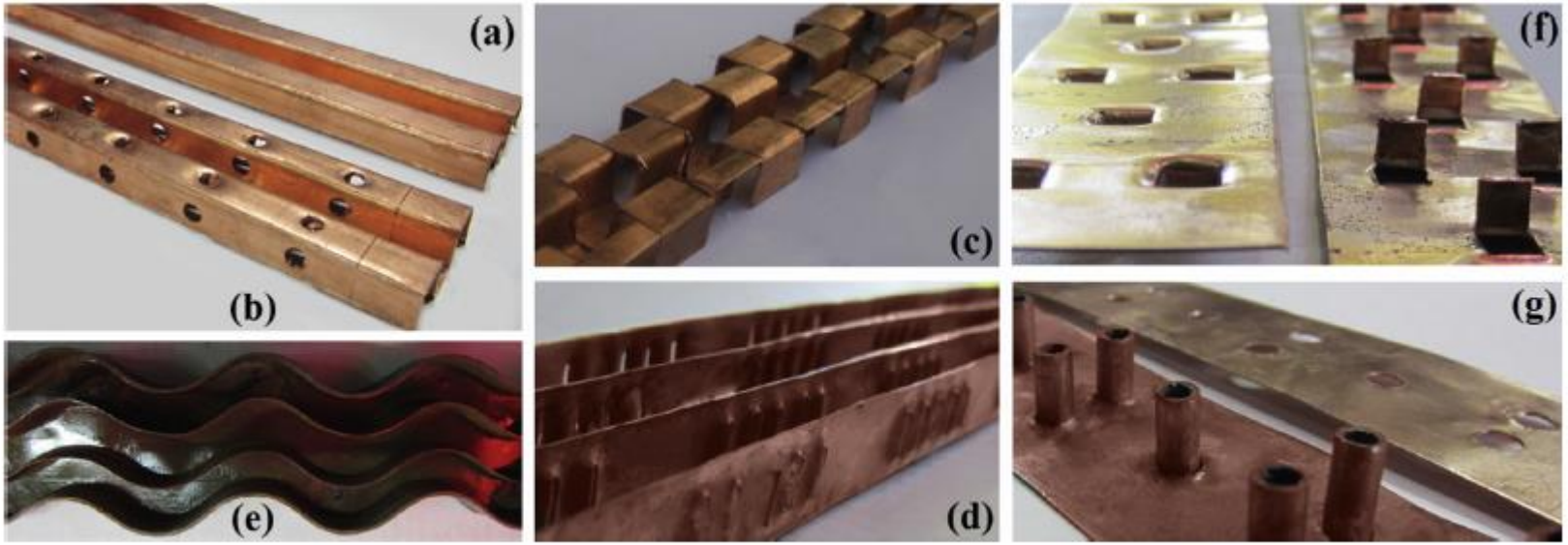

Fig. 3. Plate-fin channels: (a) plain (b) perforated (c) offset strip (d) louvered (e) wavy (f) vortex-generator (g) pin.

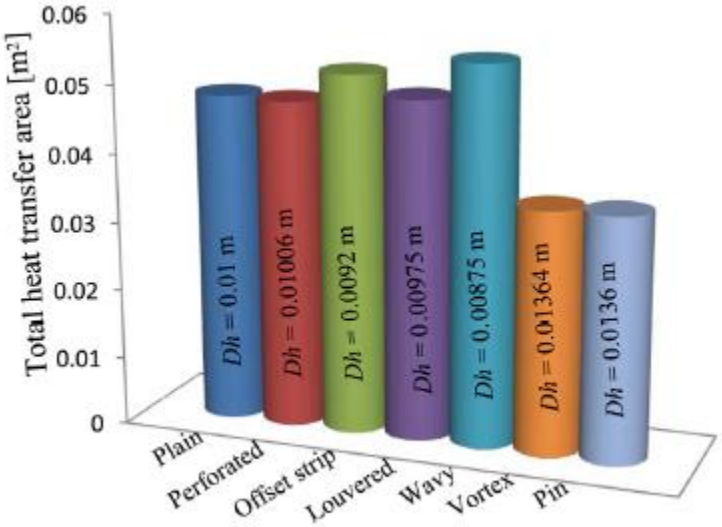

Fig. 6. Total heat transfer area and hydraulic diameter of different plate-fin channels.

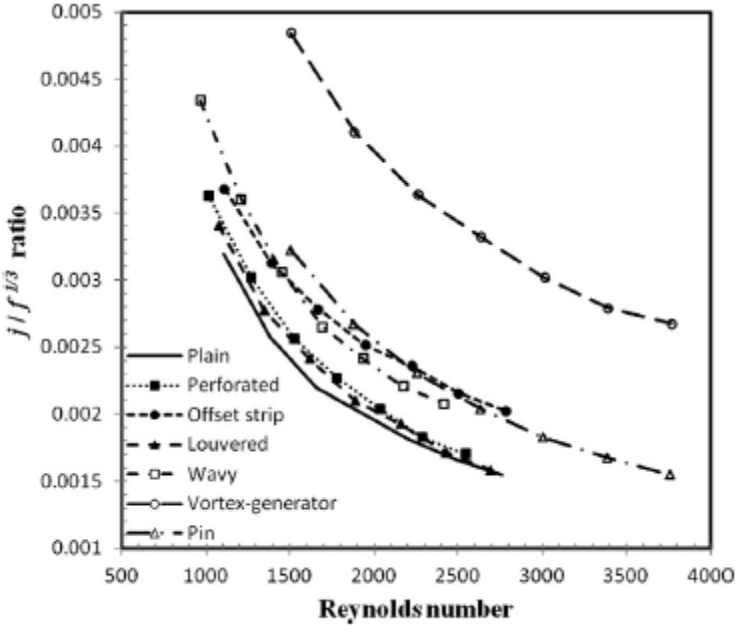

Fig. 9. $jf^{1/3}$ ratio values – Reynolds number for different plate-fin channels.

Enhanced Convex louver Design

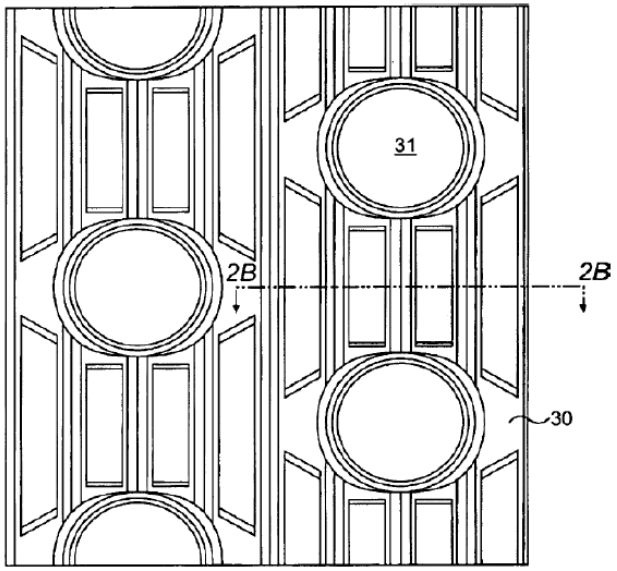

(a) Enlarged view.

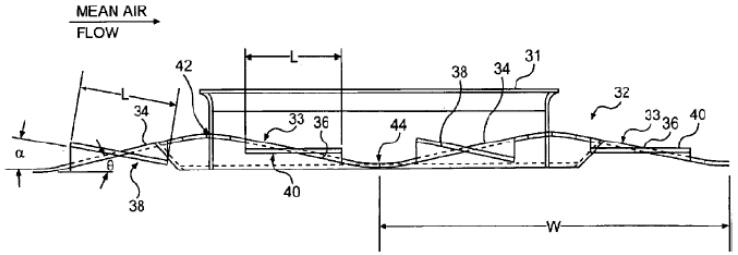

(b) Cross-sectional view.

Fig. 1. Schematic of the US patent 6786724.

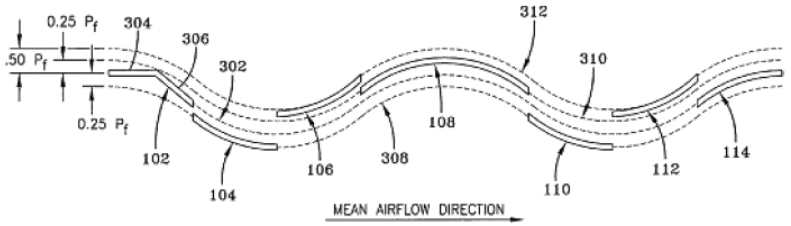

(a) Cross-sectional view.

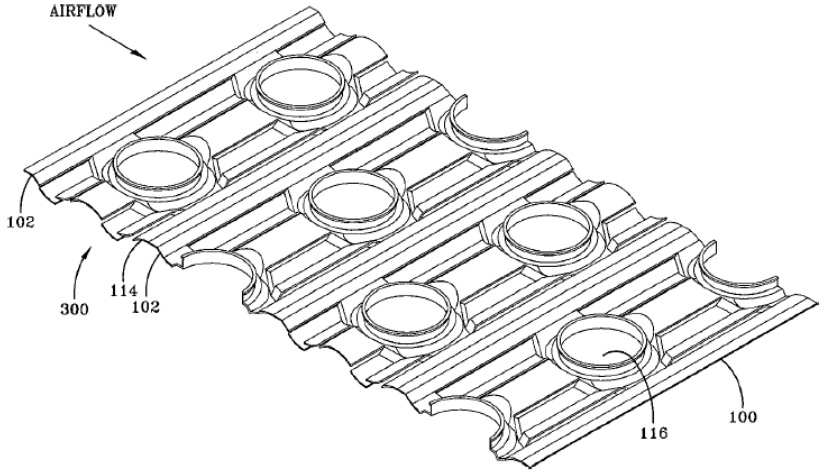

(b) Isometric view.

Fig. 2. Schematic of the US patents of 7124813 and 6976529.

Enhanced Wavy Fin reduced pressure drop design

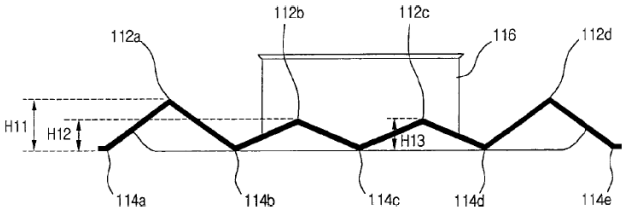

(a) Variable peak/valley design.

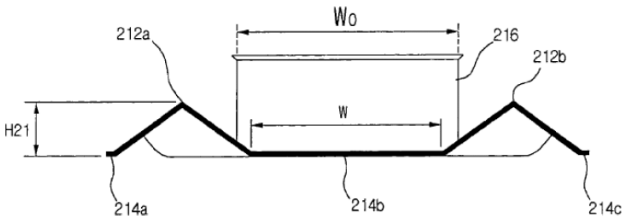

(b) Plain portion amid peaks.

Fig. 3. Schematic of the US patent 7261147.

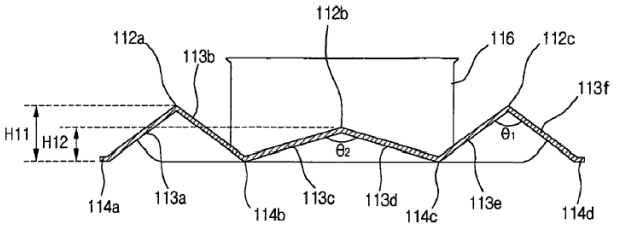

(a) Design with $\theta_1 < \theta_2$.

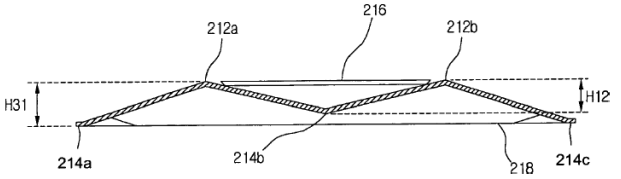

(b) Design with shallow valley.

Fig. 4. Schematic of US patent 7219716.

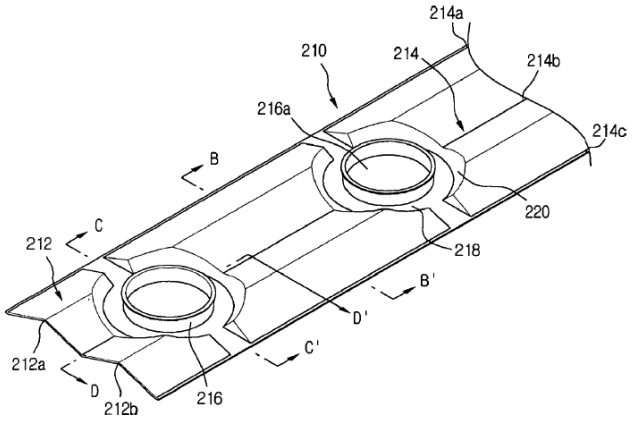

(a) Design with wake removal.

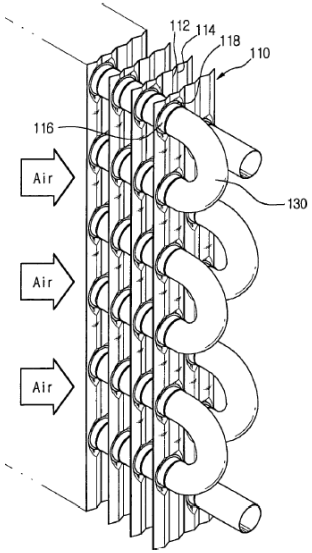

(b) Conventional design.

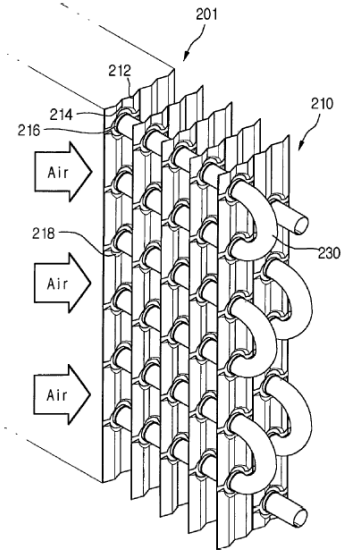

(c) Proposed design.

Fig. 5. Schematic of the US patent 7182127.

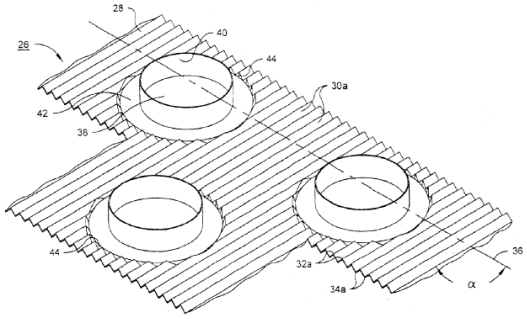

(a) Basic design.

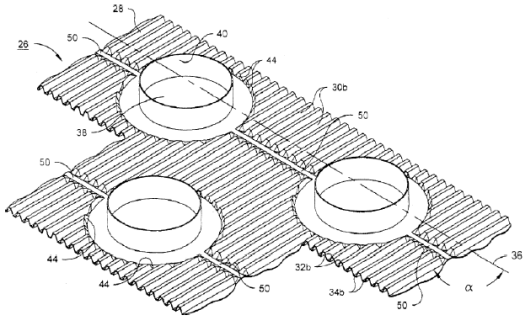

(b) A drainage path design.

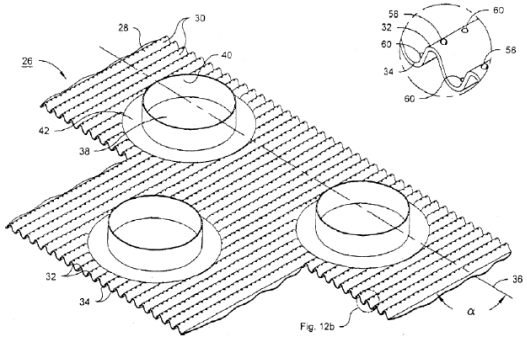

(c) Design with tiny holes to promote mixing between adjacent fins.

Fig. 6. Schematic of the US patent 6889759.

OVAL Tube & Flat Tube

- Lowering wake pressure drop
- Air flow normal to the fin surface, a better fin efficiency
- Reduce the ineffective heat transfer area behind tube

Optimally staggered finned circular and elliptic tubes in forced convection, Int. J. of Heat and Mass Transfer 47 (2004) 1347–1359

- Numerical simulation indicates that the best ellipses eccentricity (e), b/a is around 0.5
- b: smaller ellipse semi-axis
- a: larger ellipse semi-axis
- Confirmed with experiments

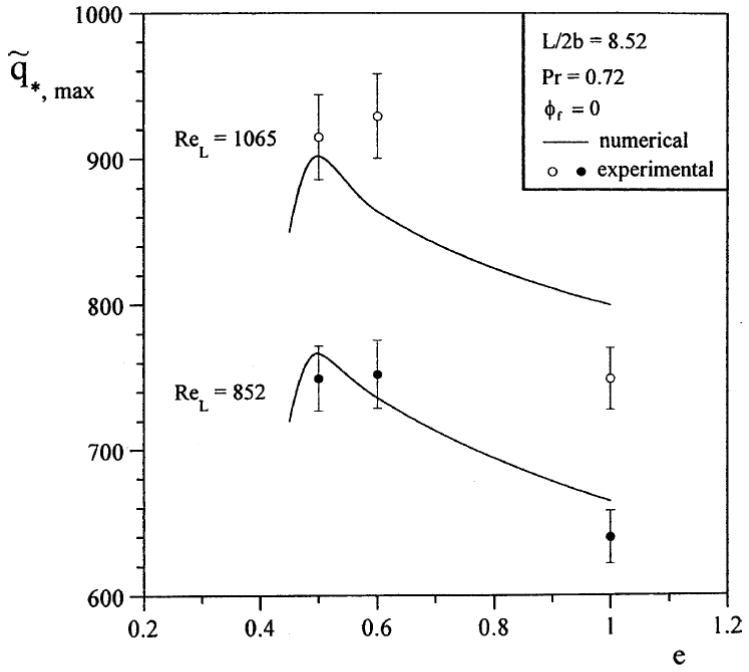

Fig. 4. Numerical and experimental optimization results for non-finned arrangements.

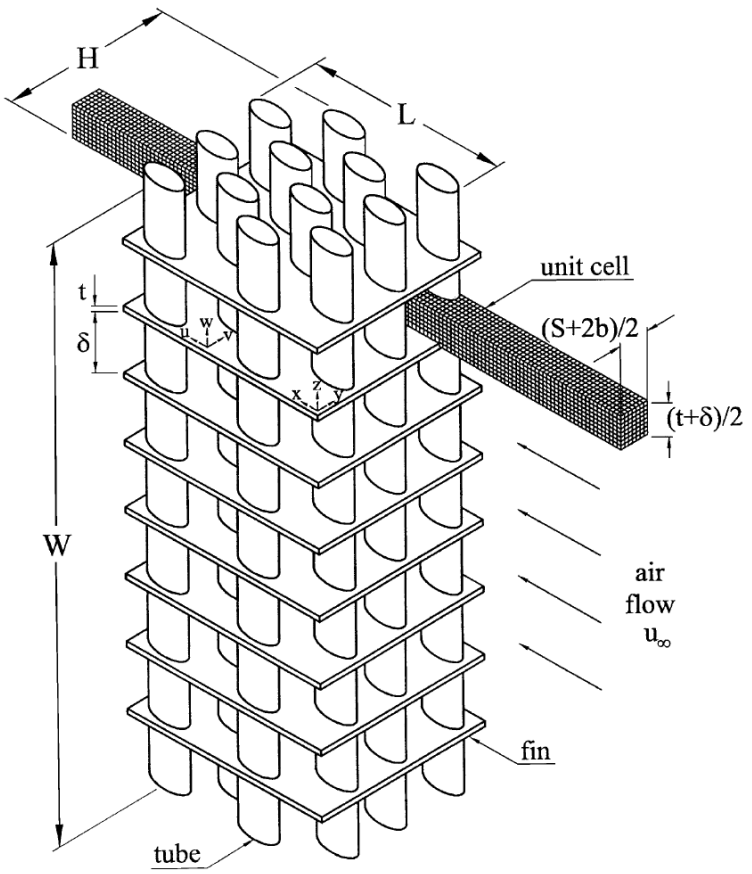

Fig. 1. Arrangement of finned elliptic tubes, and the three-dimensional computational domain.

A numerical study on compact enhanced fin-and-tube heat exchangers with oval and circular tube configurations, Int. J. Heat mass transfer, 65 (2013) 686–695

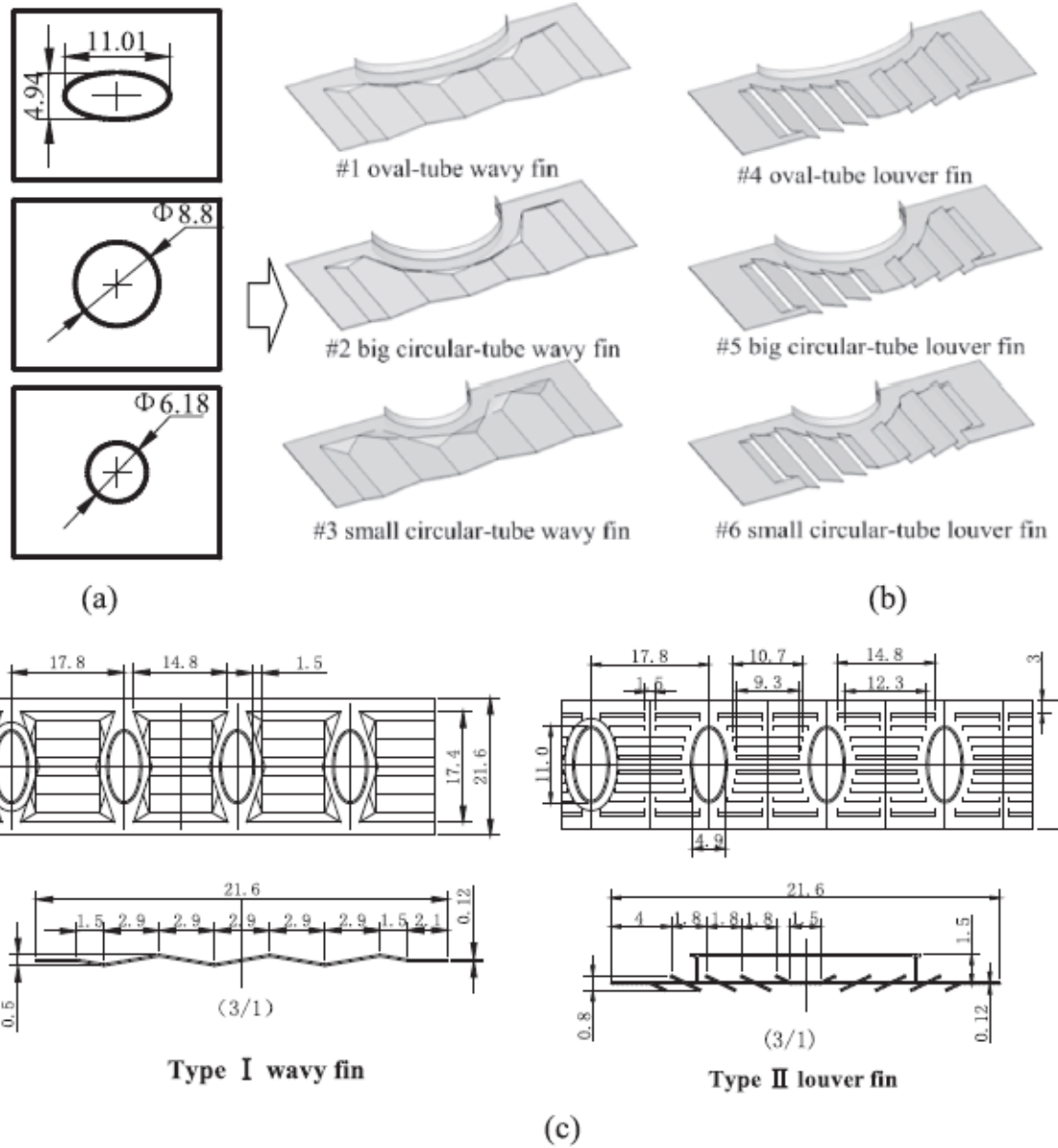

Fig. 1. Schematic diagram of fin-and-tube heat exchangers with oval-tube and circle-tube configurations: (a) geometrical dimensions of heat exchange tubes, (b) fin geometry models, (c) fin dimensions.

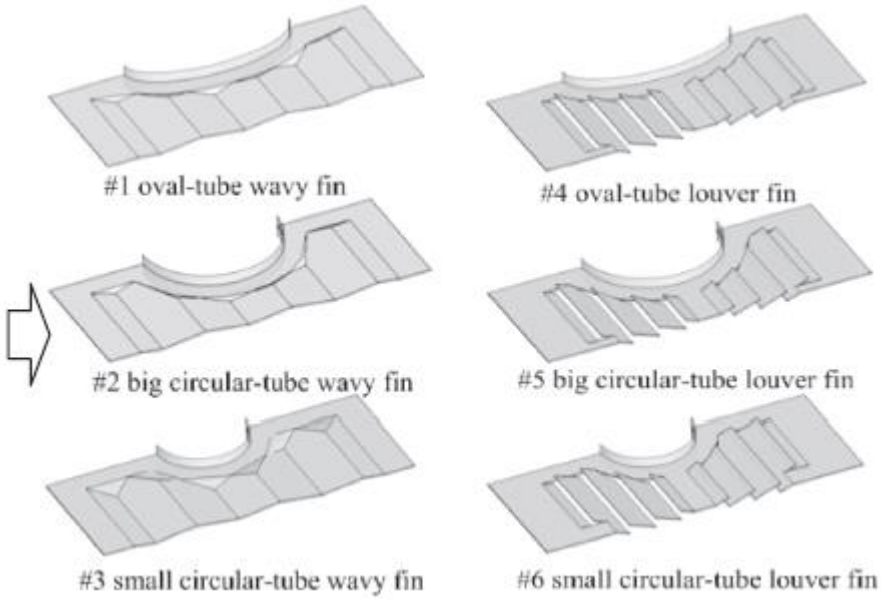

Oval tubes can significantly improve the fin surface temperature distribution along the flow direction, making the temperature distribution more uniform, thereby improving the fin efficiency. Compared to the wavy fins, the fin efficiencies of louvered fins are lower, but a better improvement can be obtained for the fin with oval-tube configuration.

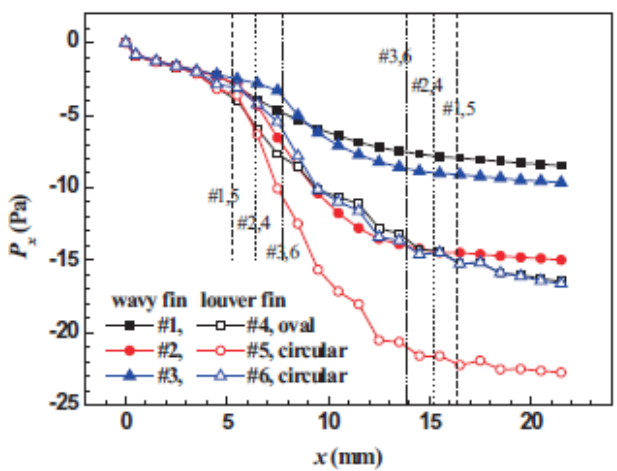

Fig. 5. Distribution of local average pressure drop along the streamwise direction at v_{in} = 1.5 m/s.

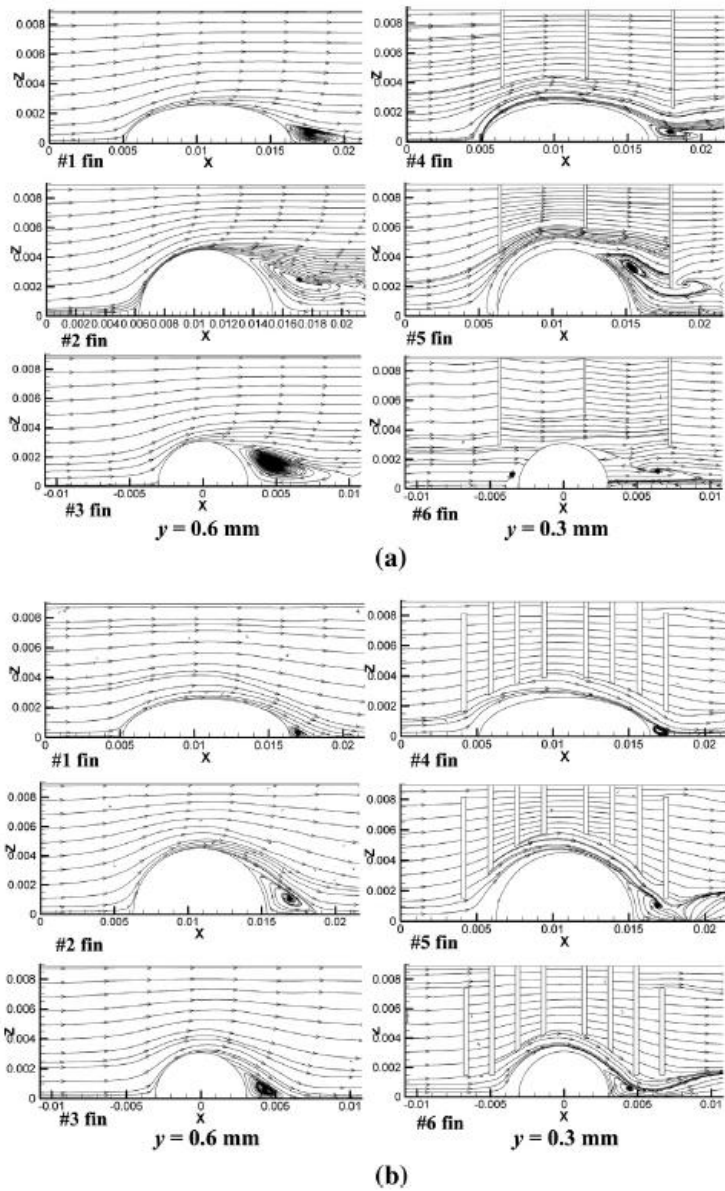

Fig. 4. Streamline plot on the cross-section y = 0.6 mm and y = 0.3 mm for three tubes: (a) wavy fin and (b)

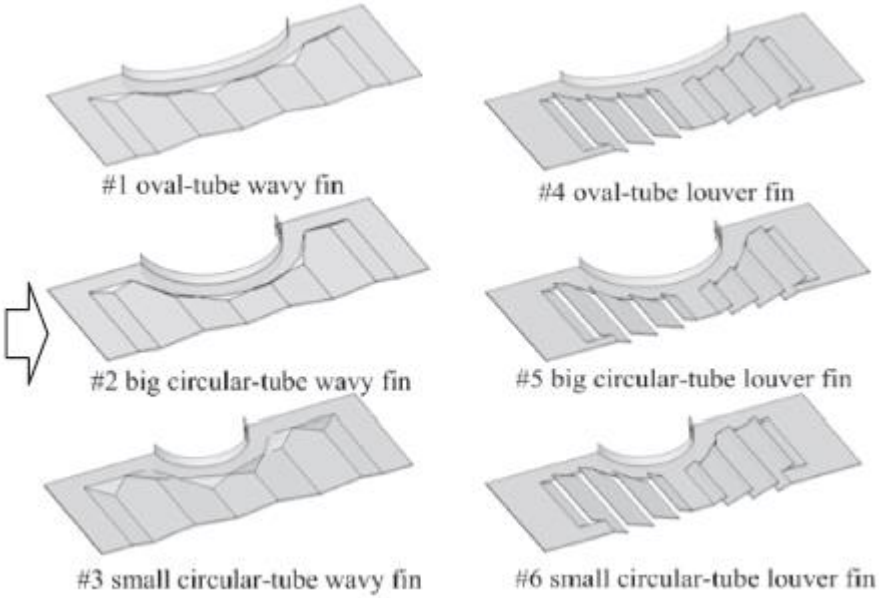

The oval-tube fin shows the better heat transfer performance and lower pressure loss due to the improvement of the flow characteristics in the wake region. Compare to the big and small circular tubes fins, when the wavy fin was employed, the heat transfer coefficient of the oval-tube fin is increased by 0.3–8% and 9.3–10.1%, the pressure drop loss is decreased by 28.5–42.3% and 1.9–24.0%; when the louvered fin was used, the heat transfer coefficient of the oval-tube fin is increased by 3.2–6.6% and 26.0–28.4%, the pressure drop loss is decreased by 22.0% to 31.8% and 1.8% to 3.5%.

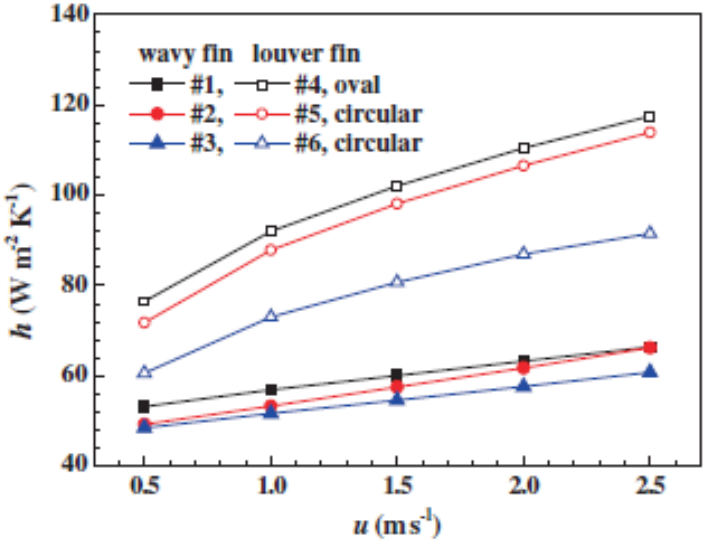

Fig. 10. Heat transfer coefficient versus frontal velocity.

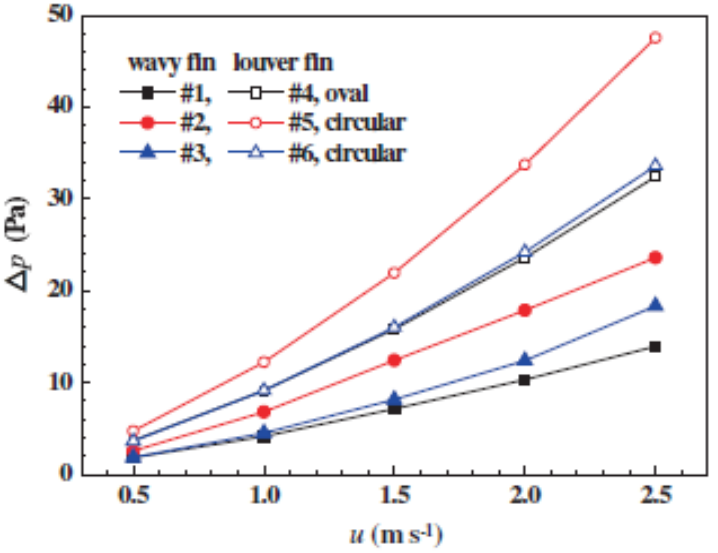

Fig. 6. Pressure drop versus frontal velocity.

Third generation – Fins With Vortex Generator

- More Surface Area
- Thermal Boundary Layer Restart
- Instability
- Thermal Wake Management
- Swirl flow

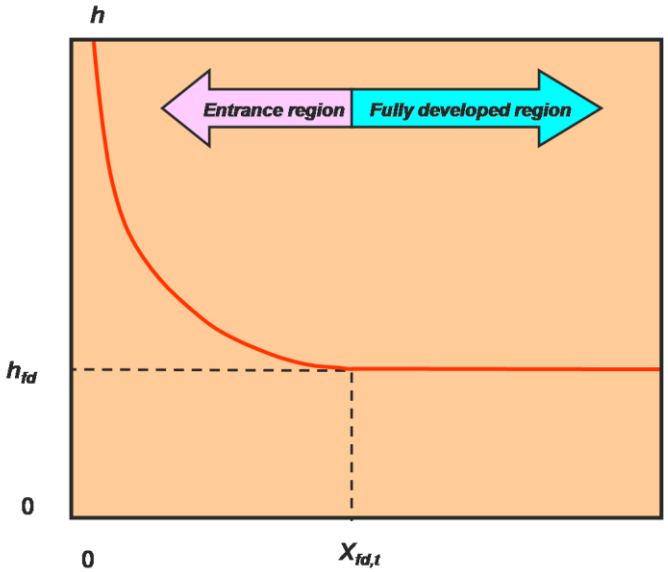

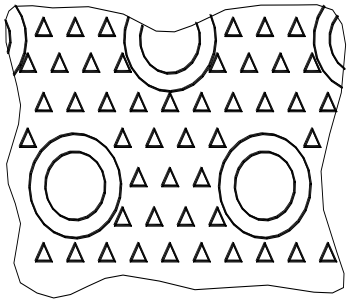

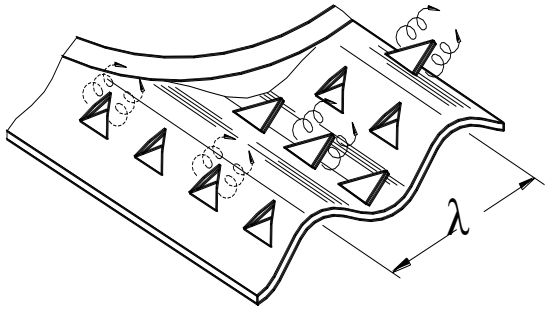

US patent 4817709

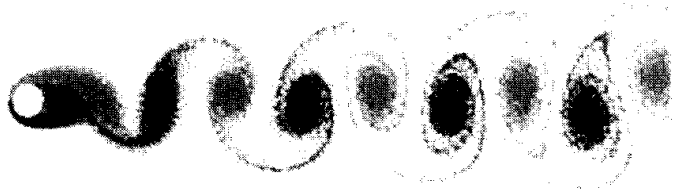

Type of vortex generators

Longitudinal vortex outperforms the transverse vortex

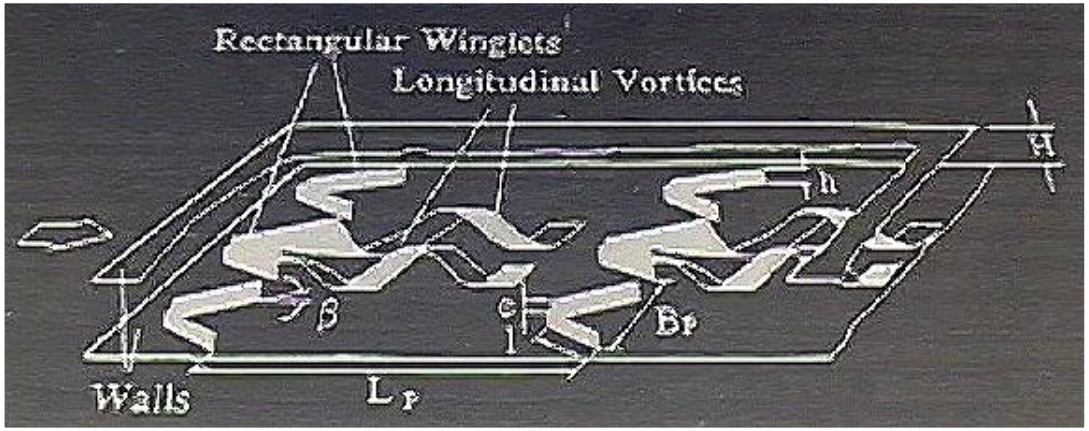

Longitudinal vortex

Transverse vortex

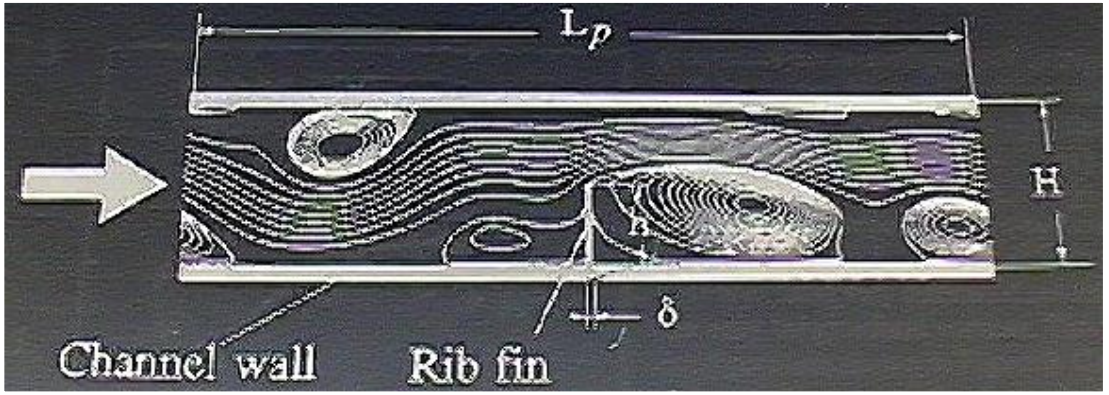

Benefits of vortex generator

- Prevent Boundary Layer separation
- Improve heat transfer performance with acceptable pressure drop

Typical LVGs

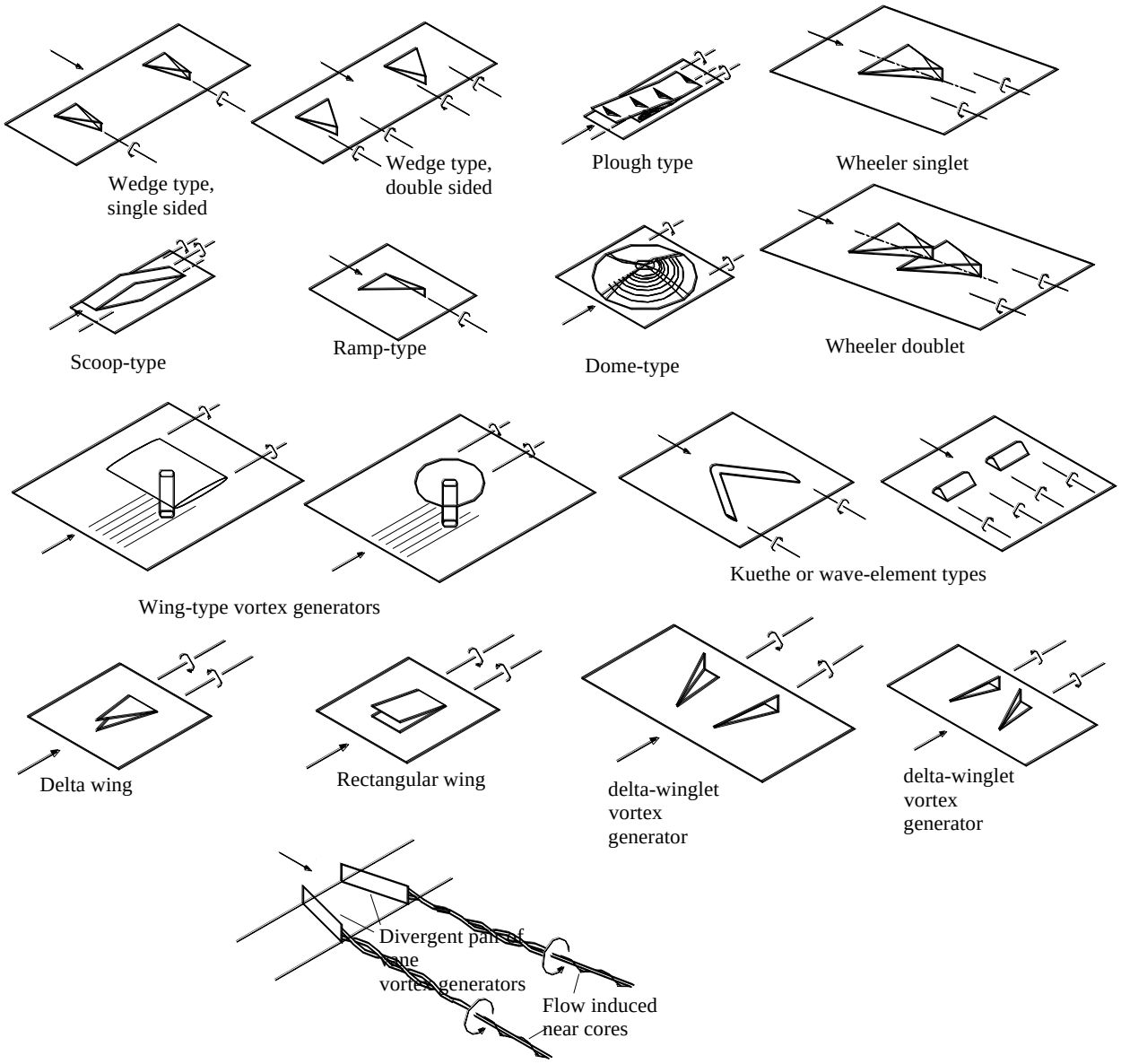

Vortex Generators.. (Applied Thermal Engineering 31, 2011, 1640-1647)

- Effect of cannelure fin configuration on compact aircooling heat sink

Heat sink with dense vortex generator. The enhancements introduce swirl flow, Coanda deflection flow or destabilized flow field from vortex generators or dimple/protrusion structure. The general arrangement is using inline or staggered layout such as semi-circular, delta and dimple vortex generator.

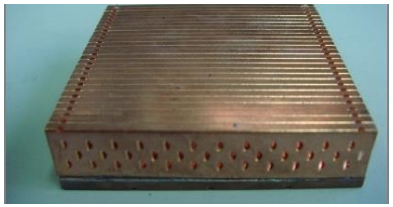

Heat sink with loose vortex generator: The enhancements of this category are still vortex generators or dimple/protrusion structure but with sparse arrangement of vortex generator.

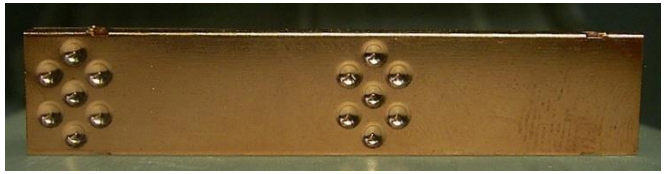

General Guideline for LVG

- No need for numerous LVGS
- More effective @ fully developing region
- More effective @ higher speed region – placing at contraction region down stream may be more effective.
- Attack angle is usually around 30-40 degrees.
- Common flow up is better than common flow down

Int. J. of Heat and Mass Transfer, Vol. 45, pp. 1933-1944.
Int. J. of Heat and Mass Transfer, Vol. 45, pp. 3803-3815.

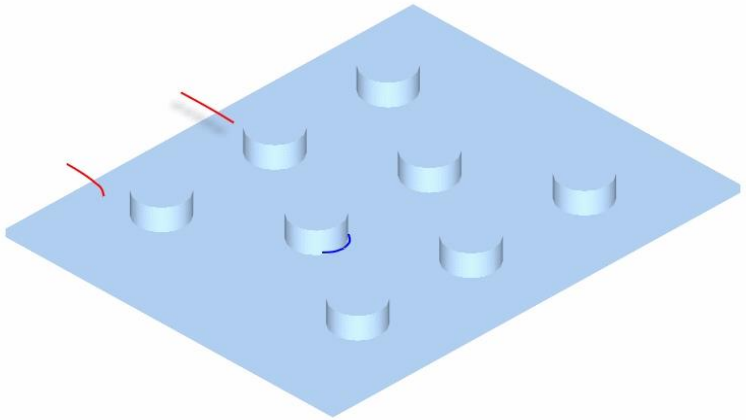

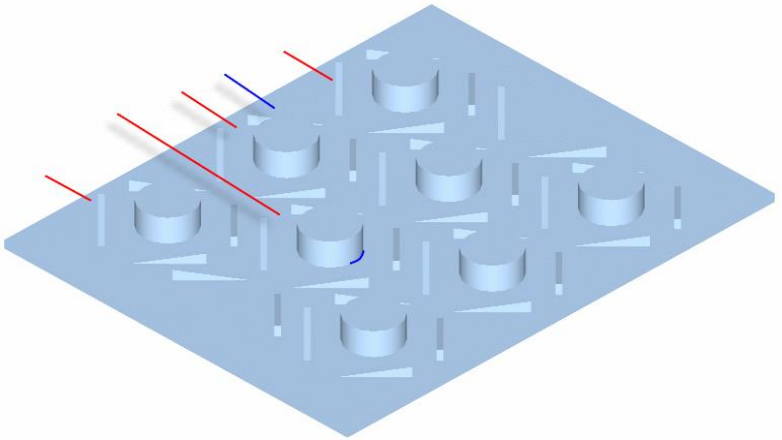

Re=1000,STVG5

Re=1500,STPL

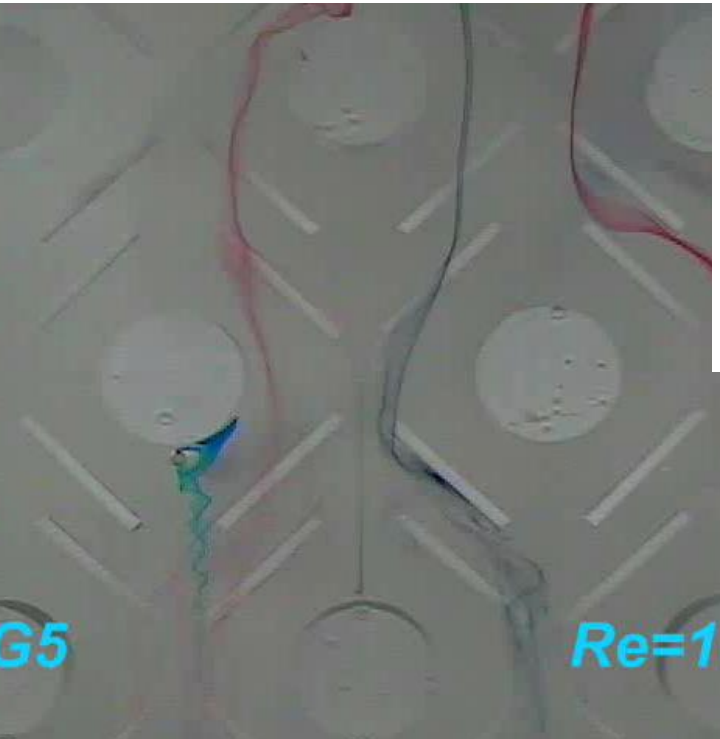

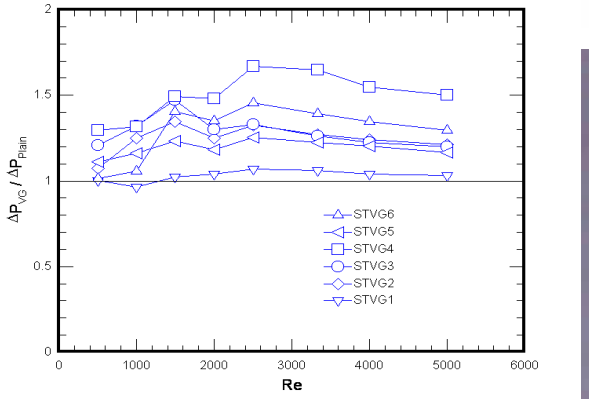

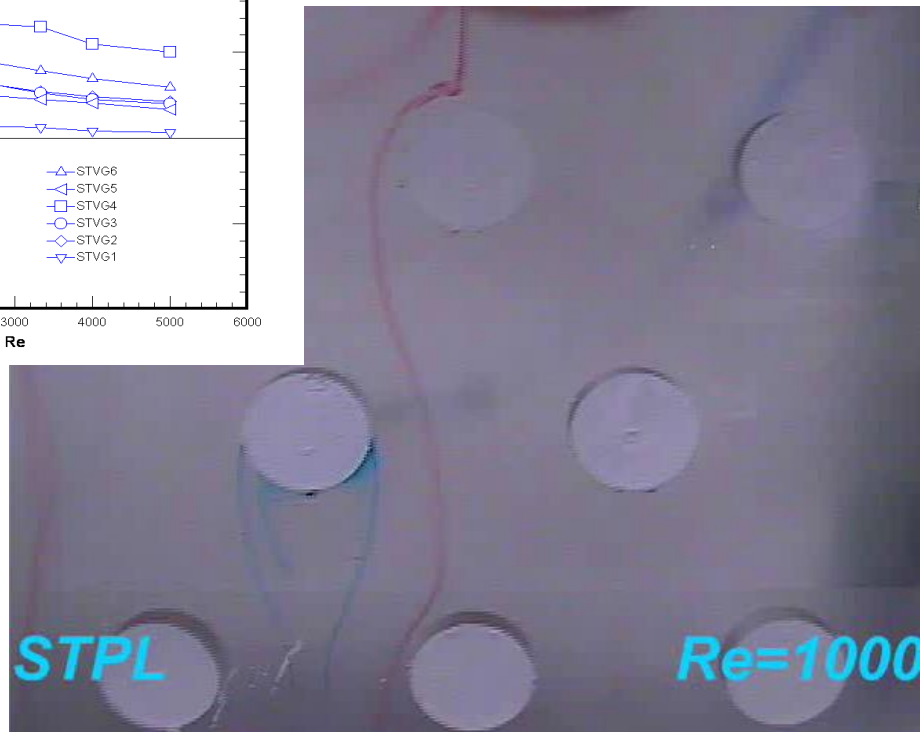

An experimental study of the air-side performance of fin-and-tube heat exchangers having plain, louver, and semi-dimple vortex generator configuration, International Journal of Heat and Mass Transfer 80 (2015) 281–287

(a) Detailed geometry and photo of the Semi-dimple VG (Unit: mm)

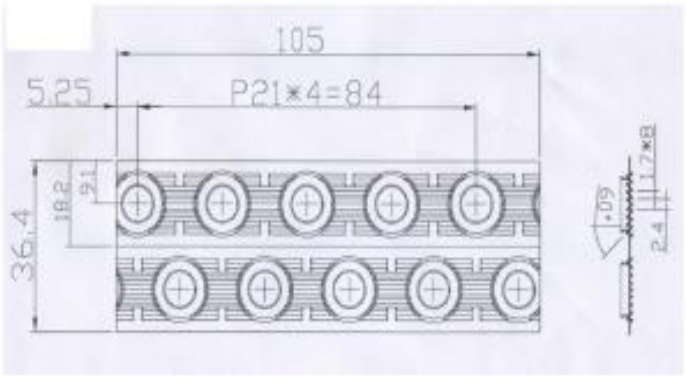

(b) Detailed geometry of the louver fin geometry (Unit: mm)

Fig. 1. Schematic of the semi-dimple VG and louver fin geometry.

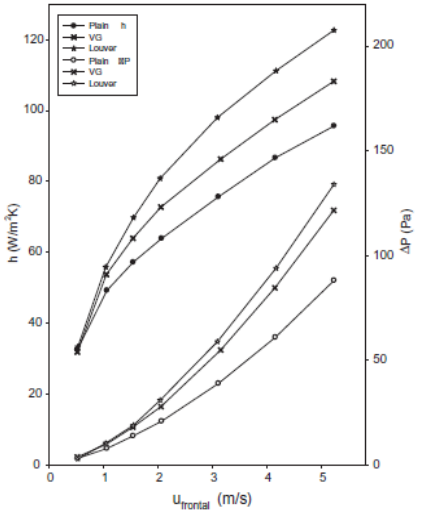

(a) $F_p = 1.6$ mm

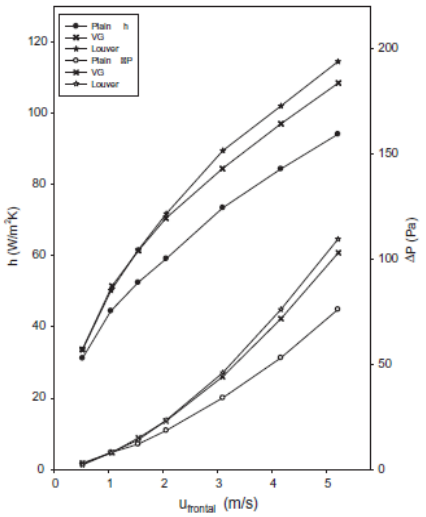

(b) $F_p = 2.0$ mm

Fig. 4. Test results for $N = 2$.

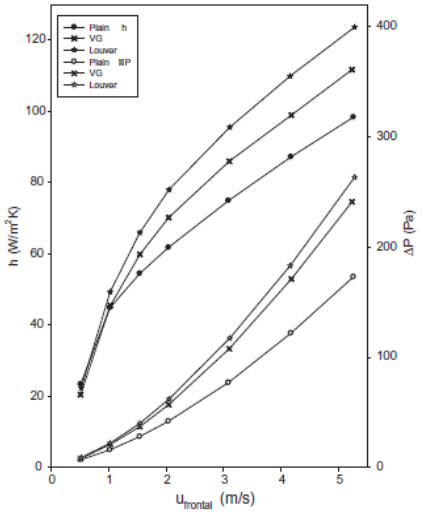

(a) $F_p = 1.6$ mm

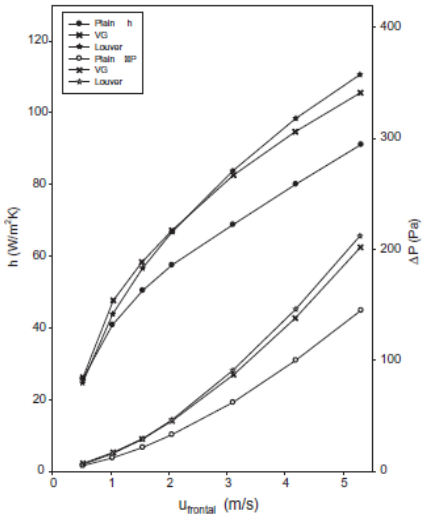

(b) $F_p = 2.0$ mm

Fig. 5. Test results for $N = 4$.

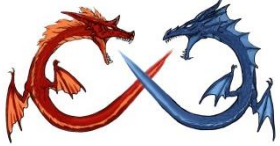

- For N = 1 with a smaller fin pitch of 1.6 mm, the heat transfer coefficient for the louver fin geometry is higher than that of semi-dimple VG and plain fin geometry.
- For a larger fin pitch of 2.0 mm, the semi-dimple VG is marginally higher than that of louver fin geometry when the frontal velocity is lower than 2 m/s due to the increasing effect of swirled motion.
- However, the trend is reversed where the louver fin outperforms that of semi-dimple VG when the velocity is increased further. The heat transfer coefficient for louver fin outperforms that of semi-dimple VG due to appreciable contribution of mixing.
- For N = 2 or N = 4, the heat transfer coefficients for louver fin geometry is about 2–15% higher than those of the semi-dimple VG geometry. The difference is increased with the rising velocity and the results prevail for both fin pitches. However, the difference is smaller at a larger fin pitch due to comparatively effectively swirled motion.
- The effect of the number of tube row on the heat transfer coefficients is negligible for louver fin geometry and is also small for the semi-dimple VG configuration. For the plain fin geometry, the effect of tube row is also small when N > 1. The heat transfer performance for N = 1 is different from N = 2 or N = 4 due to its inline configuration.

Heat Mass Transfer (2015) 51:1523–1536
DOI 10.1007/s00231-015-1521-7

Study on the effect of punched holes on flow structure and heat transfer of the plain fin with multi-row delta winglets

Fig. 1 Schematic view of the plain fin with multi-row delta winglets. **a** Mounted delta winglet. **b** Leeward punched delta winglet. **c** Windward punched delta winglet

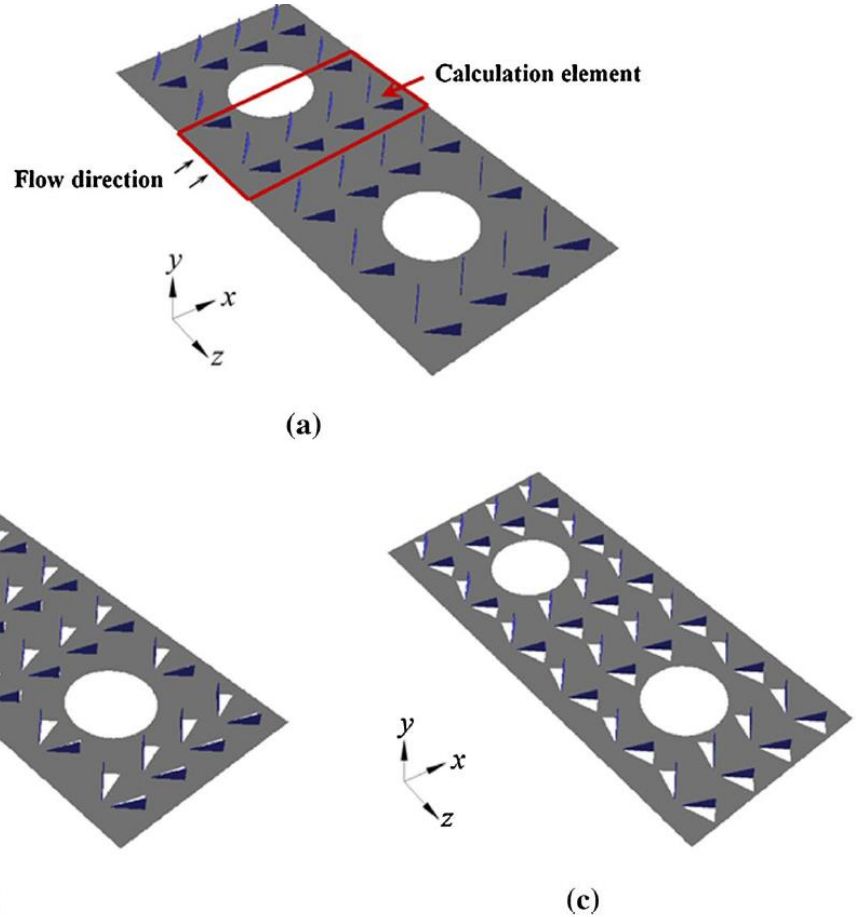

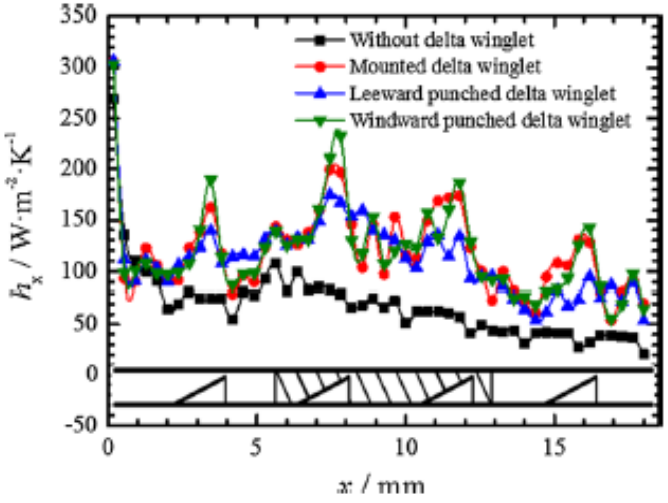

Fig. 10 Distribution of spanwise averaged local heat transfer coeffi cient along the main flow direction

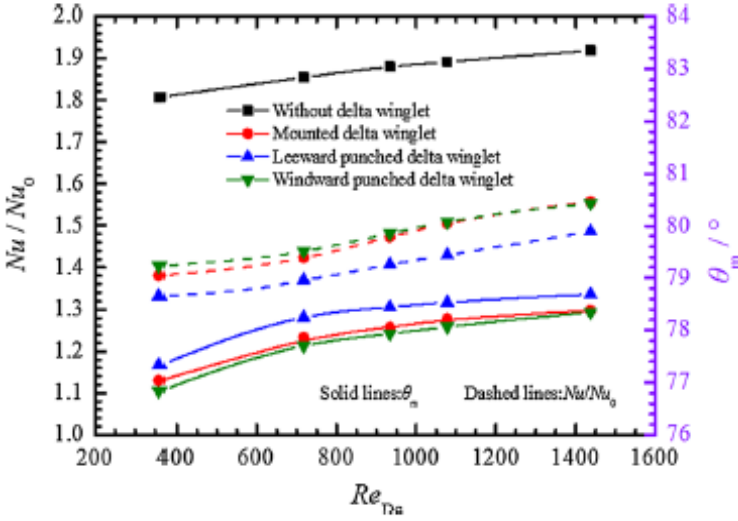

Fig. 12 Variation of average intersection angle and Nu/Nu_0 wit Reynolds number

Experimental study on heat transfer and pressure drop characteristics of fin-and-tube surface with four convex-strips around each tube, International Journal of Heat and Mass Transfer 116 (2018) 1085–1095

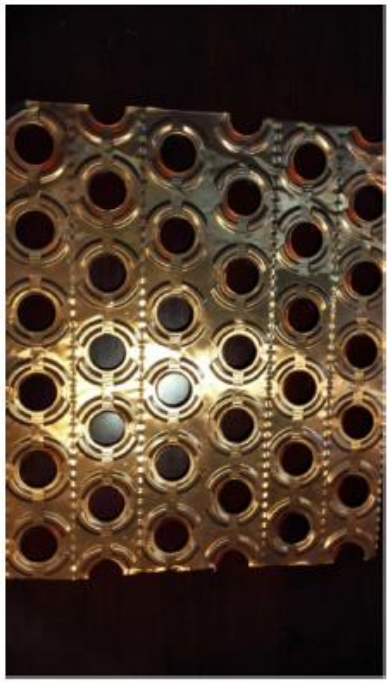

(a) Top view of the fin tested

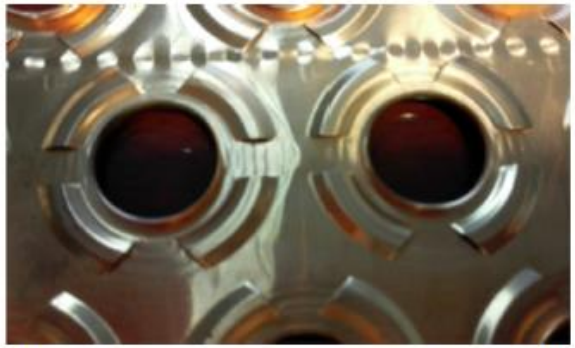

(b) Magnified picture of the four convex-strips around tube

Fig. 1. Tested fin structure.

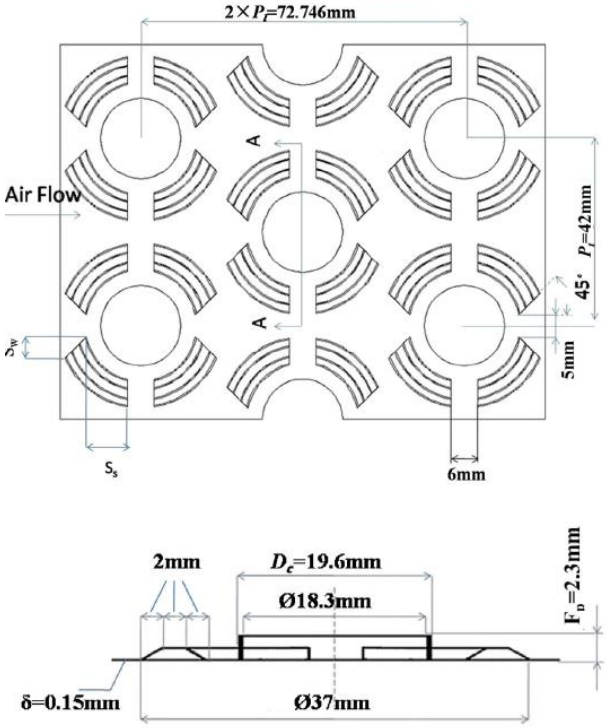

Fig. 3. Geometry of enhanced fin surface.

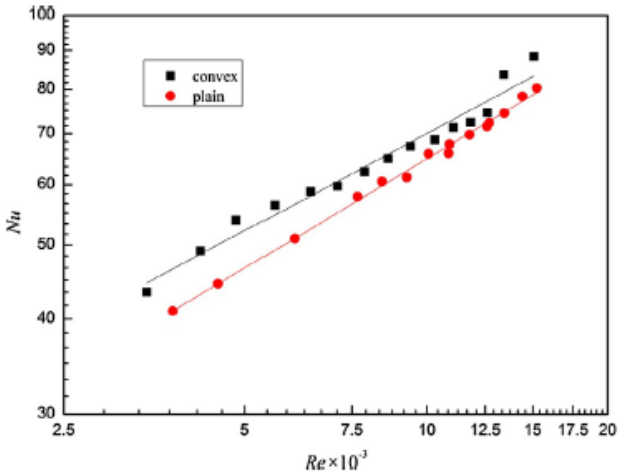

Fig. 7. Nusselt number vs. Reynolds number of convex and plain fin.

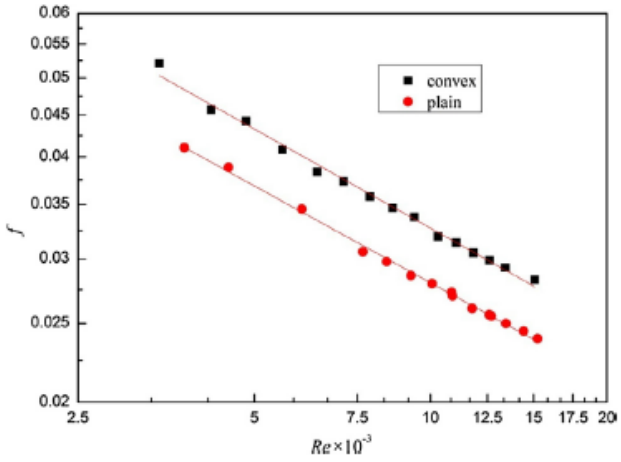

Fig. 8. Friction factor vs. Reynolds number of convex and plain fin.

Table 1
Major parameters of the tested fin surface.

D_c (mm)	F_p (mm)	P_l (mm)	P_t (mm)	δ (mm)	S_w (mm)	S_s (mm)	Row No.
19.6	2.3	36.4	42	0.15	4.24	9.45	11

Heat transfer and pressure drop characteristics of the tube bank fin heat exchanger with fin punched with flow redistributors and curved triangular vortex generators, Heat Mass Transfer (2017) 53:3013–3026

Fig. 3 Schematic view of the studied heat exchanger, **a** fin with flow redistributors, **b** fin with flow redistributors and CTVGs, **c** flow around CTVGs and redistributors

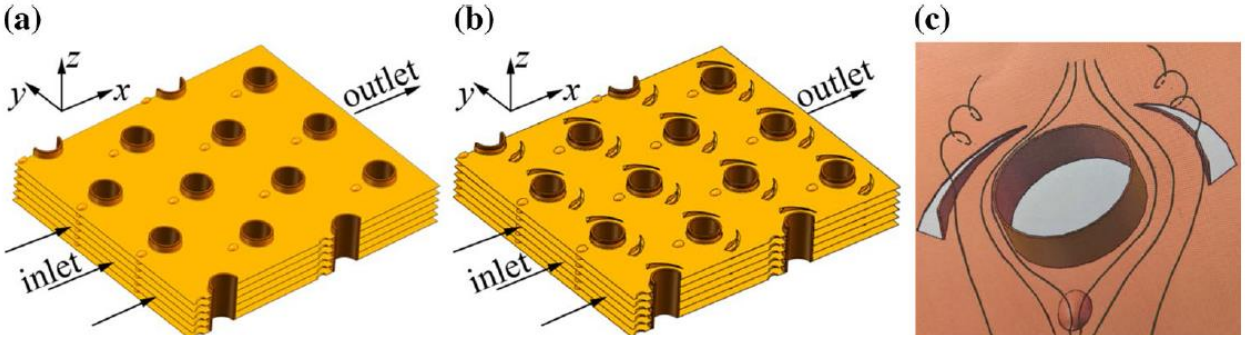

Fig. 4 Fin configuration: **a** plain fin with flow redistributors; **b** fin with CTVG; **c** CTVG-I; **d** CTVG-II

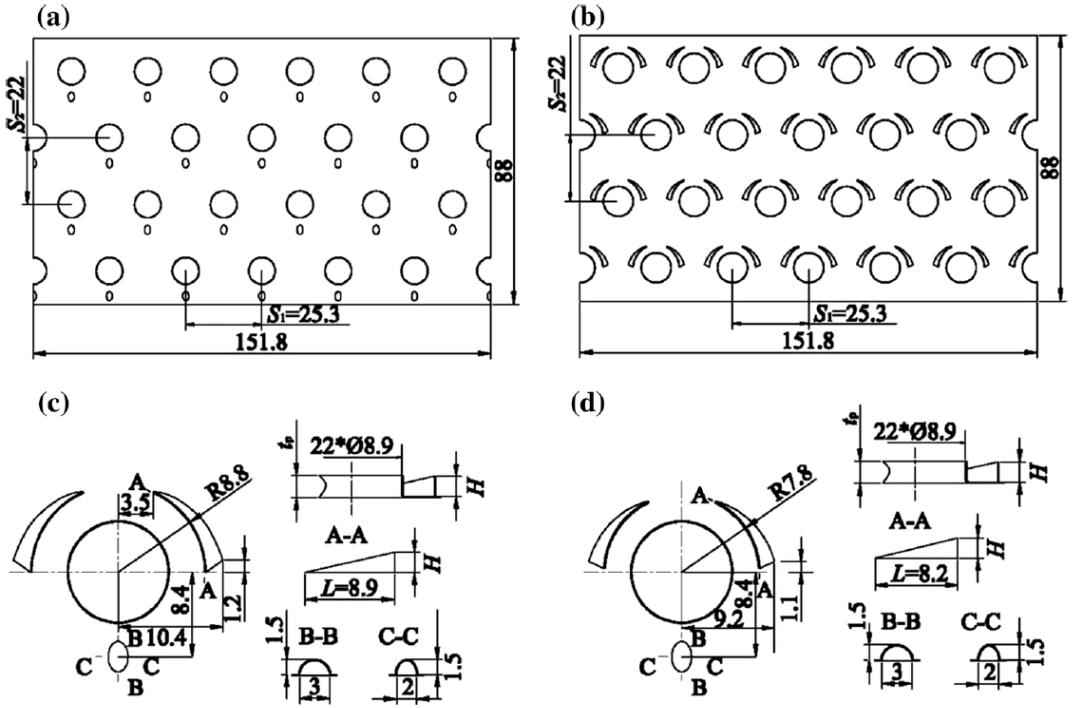

Table 1 Parameters of fin and CTVG

No.	Fin type	T_p (mm)	L (mm)
1	Plain fin	1.7	–
2	Plain fin	2.0	–
3	Plain fin	2.3	–
4	Plain fin with flow redistributors	1.7	–
5	Plain fin with flow redistributors	2.0	–
6	Plain fin with flow redistributors	2.3	–
7	CTVG-I	1.7	8.9
8	CTVG-I	2.0	8.9
9	CTVG-I	2.3	8.9
10	CTVG-II	1.7	8.2
11	CTVG-II	2.0	8.2
12	CTVG-II	2.3	8.2
13	CTVG-I and flow redistributors	1.7	8.9
14	CTVG-I and flow redistributors	2.0	8.9
15	CTVG-I and flow redistributors	2.3	8.9
16	CTVG-II and flow redistributors	1.7	8.2
17	CTVG-II and flow redistributors	2.0	8.2
18	CTVG-II and flow redistributors	2.3	8.2

curved triangular vortex generator (CTVG-I) is L = 8.9 mm and the other one (CTVG-II) is L = 8.2 mm

curved triangular vortex generator (CTVG-I) is L = 8.9 mm and the other one (CTVG-II) is L = 8.2 mm

The existence of flow redistributors can decrease f at the cost of decreasing Nu for the plain fin.

$Nu/f^{1/3}$ for the fin with CTVG-I and flow redistributors is obviously larger than that of the fin with CTVGII and flow redistributors. The maximum value of $Nu/f^{1/3}$ increases by 5.2, 5.5 and 2.6% for Tp = 1.7, 2.0 and 2.3 mm, respectively.

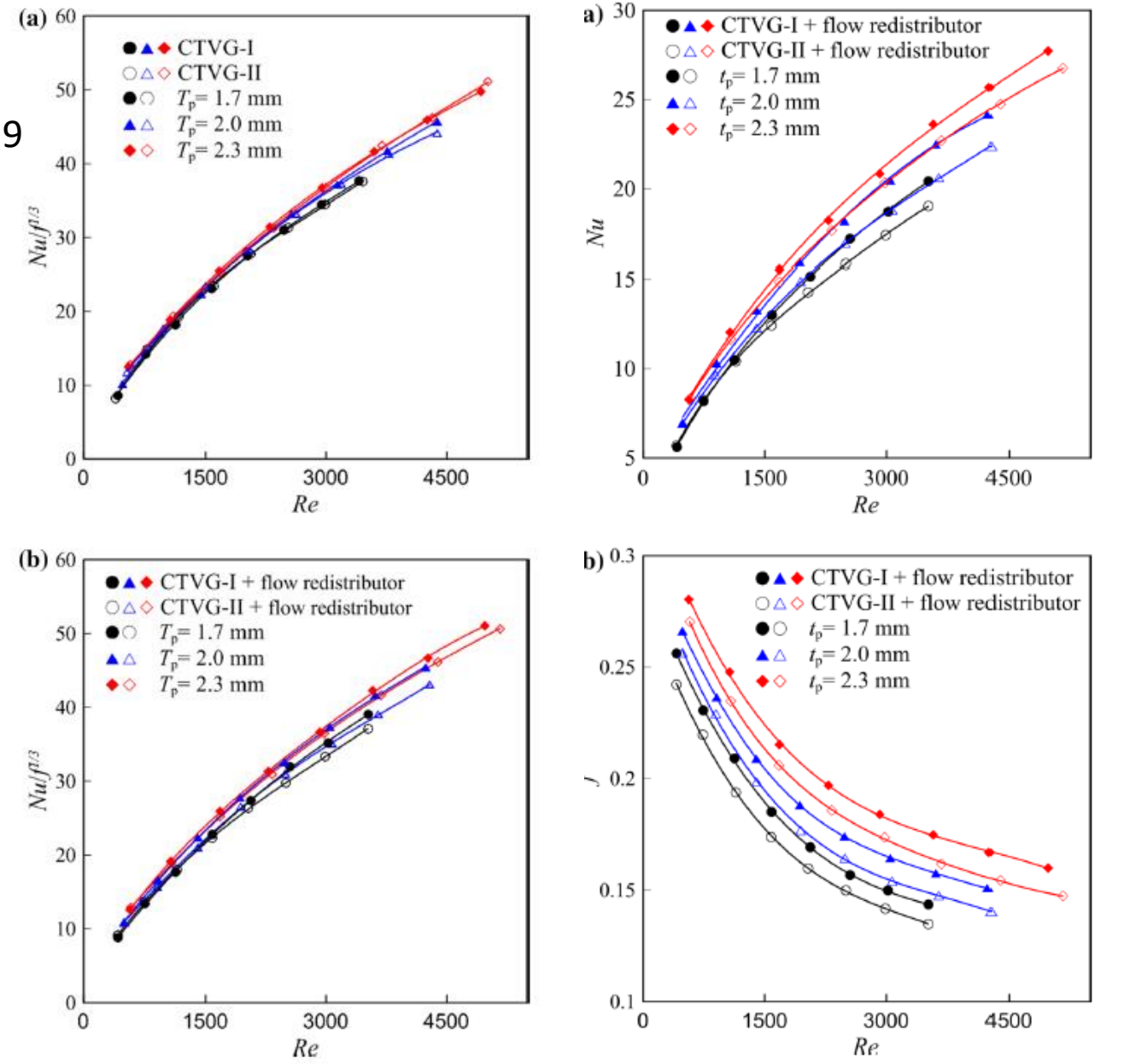

Fig. 13 Comparison of $Nu/f^{1/3}$ between the fins with CTVG-I and CTVG-II: **a** fins with CTVG; **b** fins with CTVG and redistributors

Comparison of Nu and f between fins with VGs and flo butors: **a** Nu; **b** f

VG Design

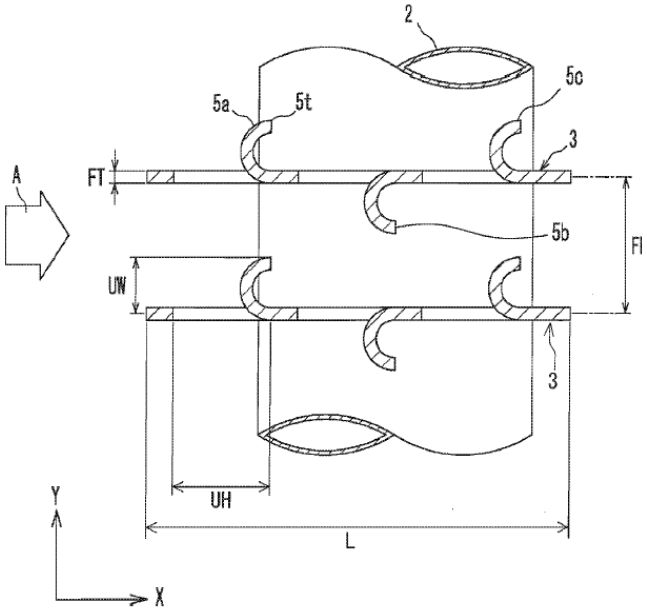

(a) An enlarge view of the fin design.

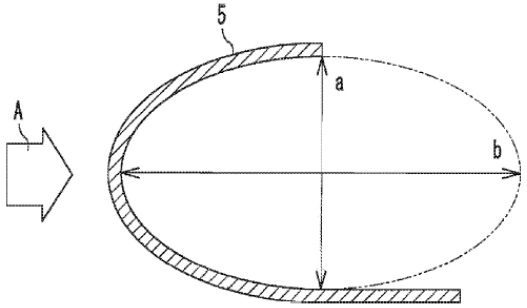

(b) Definition of ellipticity a/b.

Fig. 7. Schematic of the US patent Pub. No. 2009/0050303 A1.

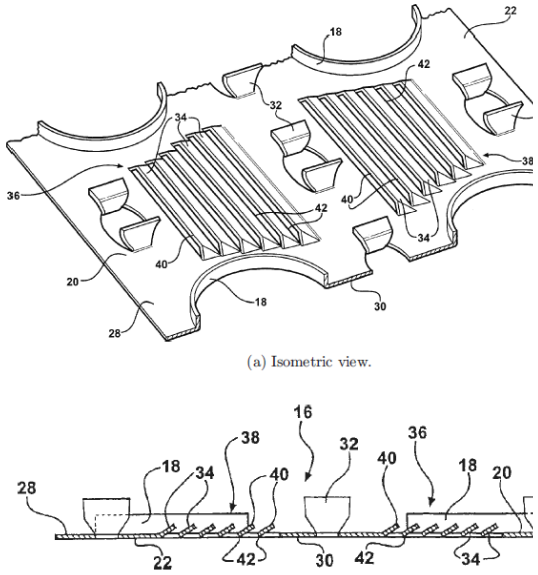

(a) Isometric view.

(b) Cross-sectional view.

Fig. 8. Schematic of the US patent 7021370.

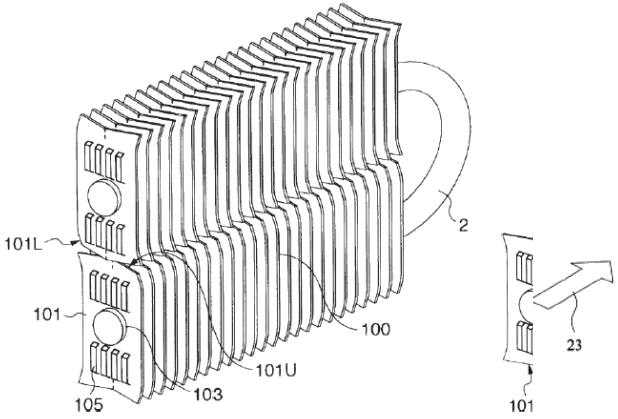

(a) Fin assembly. (b) In

Fig. 9. Schematic of the US patent 6050328.

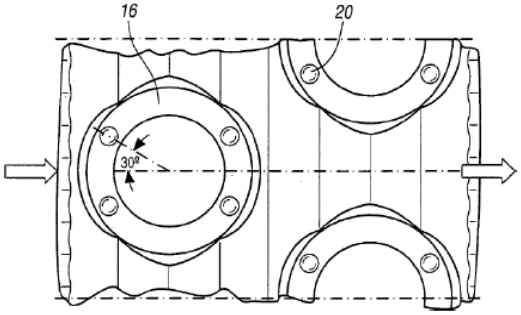

(a) US patent 7004242.

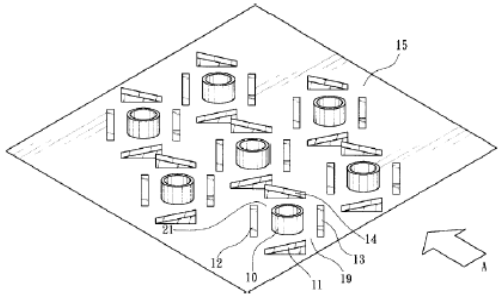

(b) US patent 6578627.

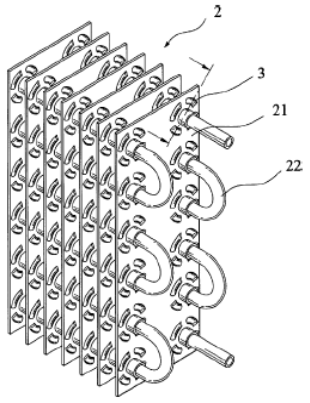

(c) US patent 6349761.

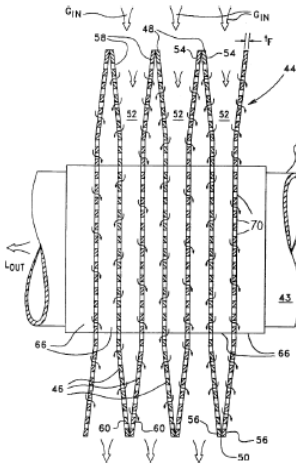

(d) US patent 6378605.

Combined Design

Normally interrupted surface provide higher heat transfer enhancement but with significant pressure drop

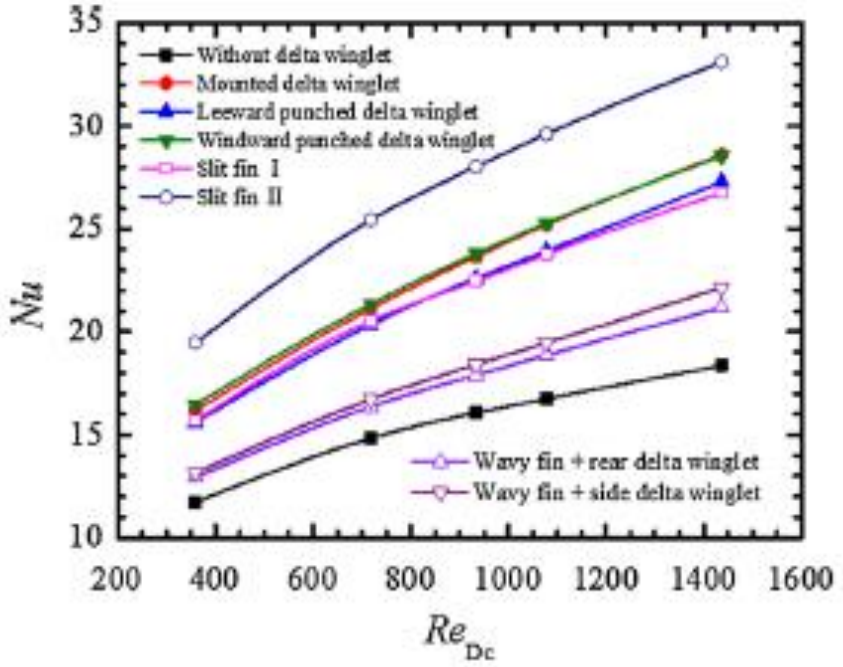

(a)

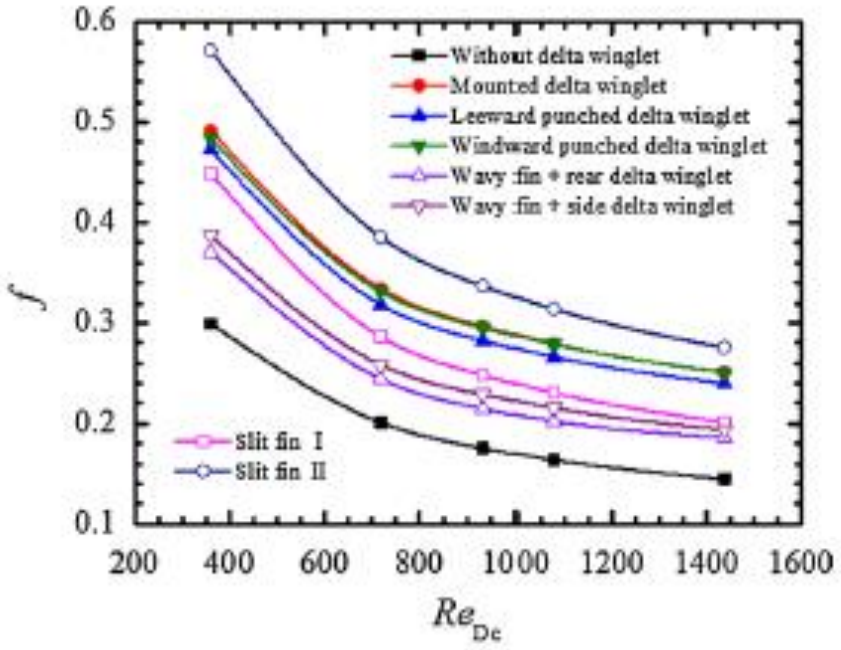

(b)

Slit fin I

Slit fin II

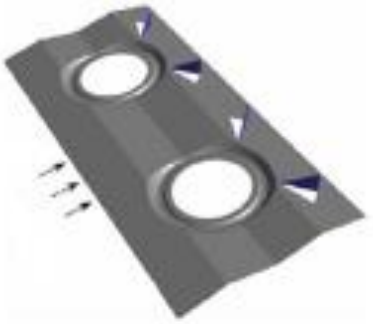

Wavy fin + rear delta winglet

Wavy fin + side delta winglet

Numerical Simulation of Performance Augmentation in a Plate Fin Heat Exchanger Using Winglet Type Vortex Generators, Int. J. of Mechanical Engineering and Mechatronics,1(1):109-120, 2012

Common flow up is better than common flow down

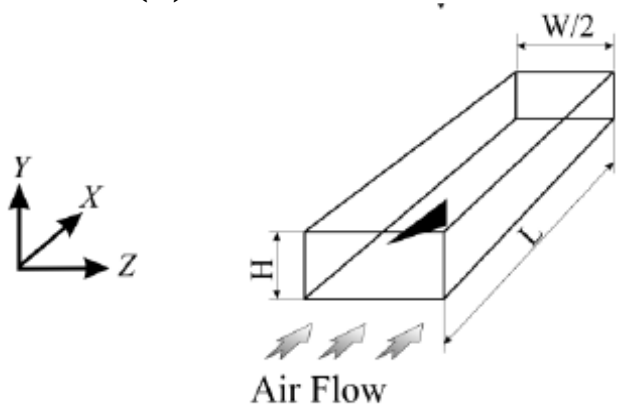

Common Flow Up Configuration

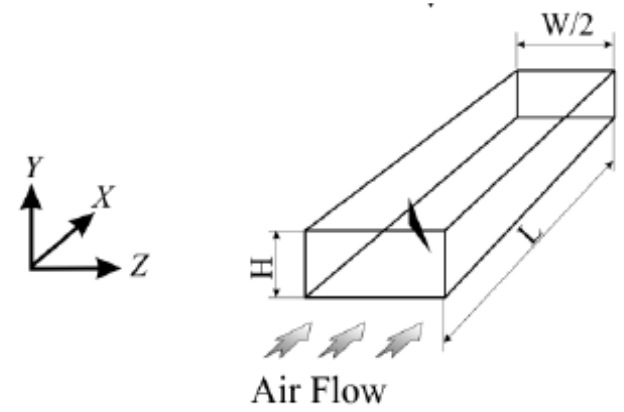

Common Flow Down Configuration

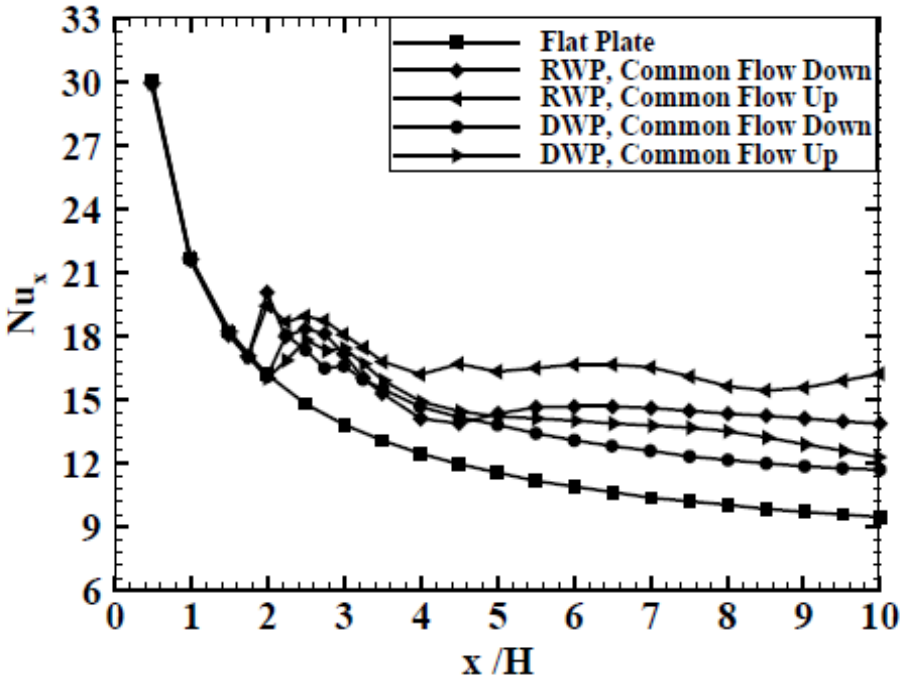

Fig. 11. Variation of Nusselt number in main flow direction (Re=750).

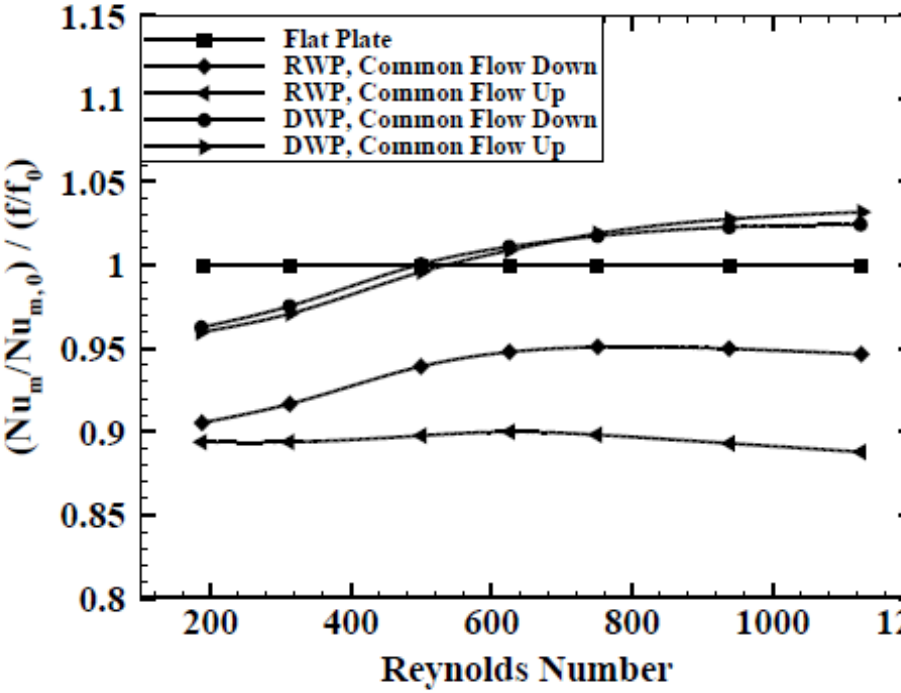

Fig. 14. Overall performance versus Reynolds number for five cases

Three-dimensional numerical study on fin-and-oval-tube heat exchanger with longitudinal vortex generators, Applied Thermal Engineering 29 (2009) 859–876

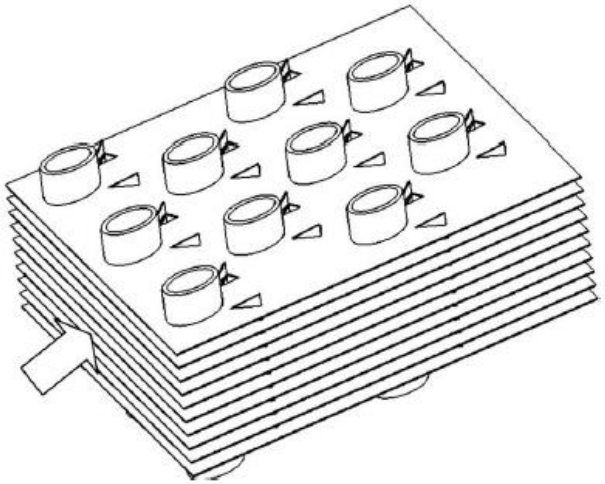

Fig. 1. Schematic diagram of core region of a fin-and-oval-tube heat exchanger with LVGs.

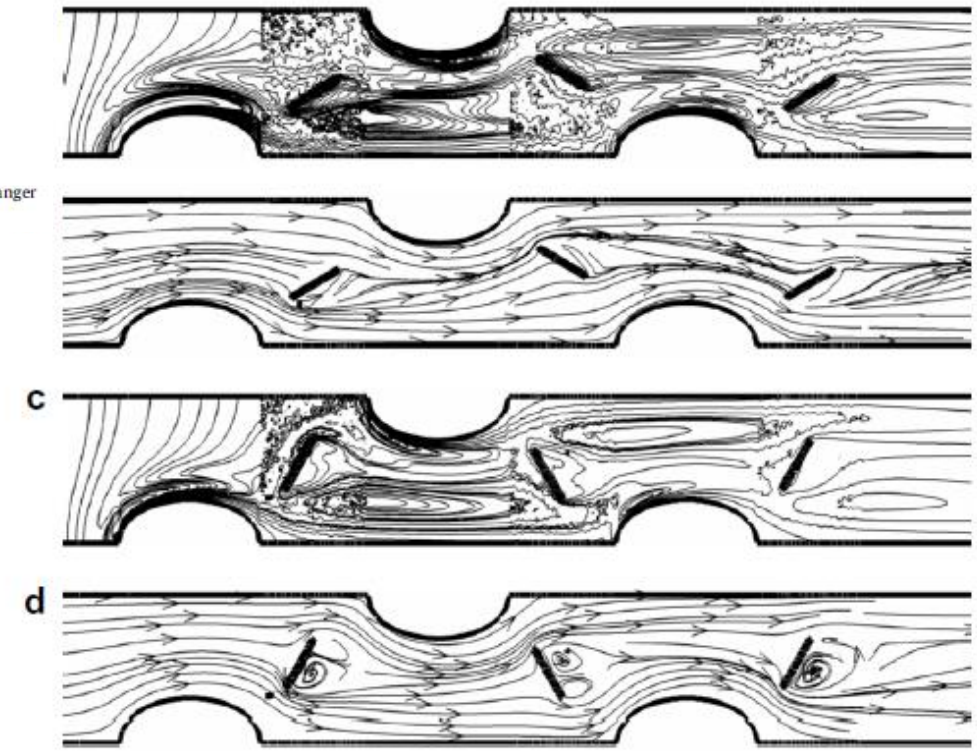

Fig. 24. Distributions of isothermals and streamlines for $\alpha = 30°$ and $\alpha = 60°$ at $Re = 1500$: (a) Isothermal for $\alpha = 30°$; (b) streamline for $\alpha = 30°$; (c) isothermal for $\alpha = 60°$; (d) streamline for $\alpha = 60°$.

- Increase of the angle of attack α ($\alpha < 30$), the strength of the longitudinal vortex is intensified and the average Nu number are increased.
- For $\alpha > 30$, the vortex may break down when the angle of attack α is too large and the average Nu number decreases with the increasing α.
- An optimum angle of attack $\alpha = 30$ at which the average Nu number can reach the maximum.
- The friction factor f always increases with the increasing angle of attack a due to that the larger angle of attack leads to larger form drag

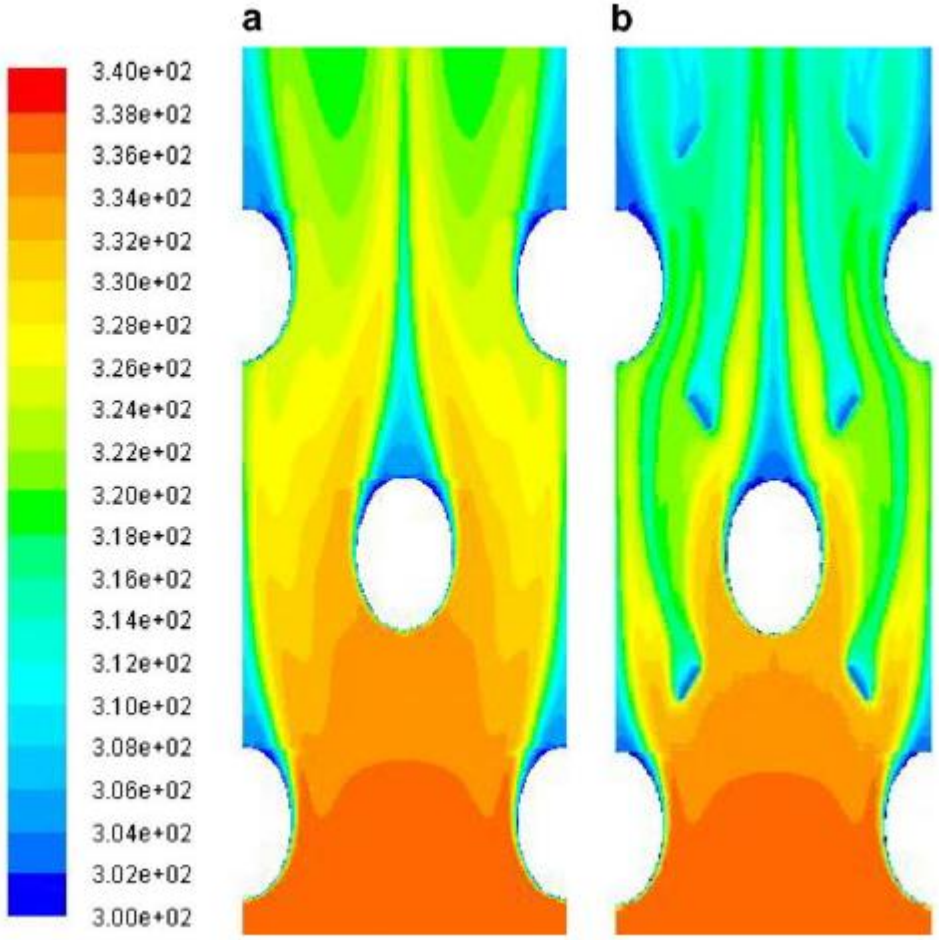

Fig. 14. Local temperature profiles on the middle cross-section for baseline case and modified case with *Re* = 1500: (a) baseline case (b) modified case.

A numerical study on compact enhanced fin-and-tube heat exchangers with oval and circular tube configurations, International Journal of Heat and Mass Transfer 65 (2013) 686–695

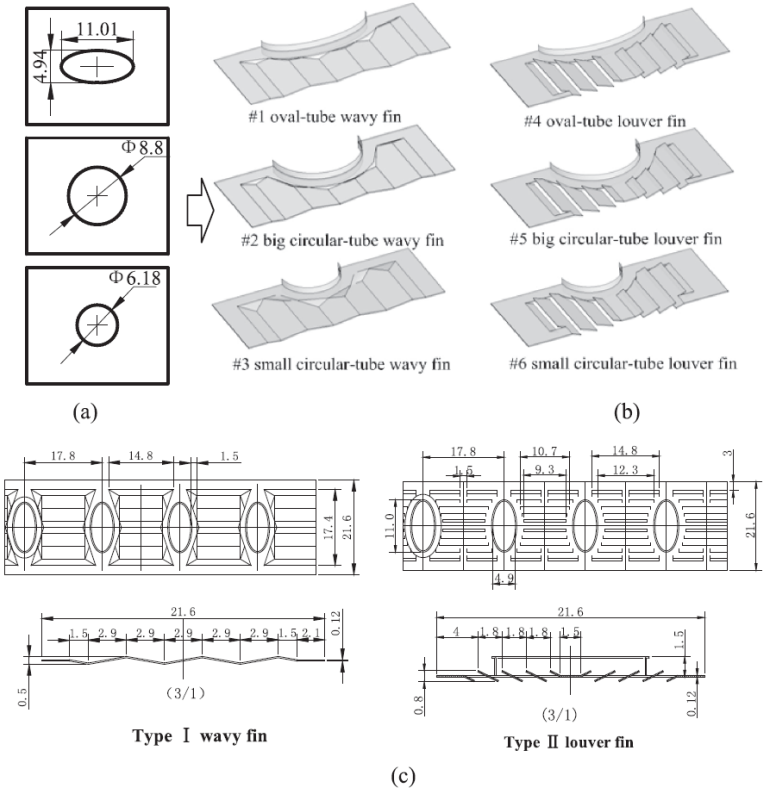

Fig. 1. Schematic diagram of fin-and-tube heat exchangers with oval-tube and circle-tube configurations: (a) geometrical dimensions of heat exchan geometry models, (c) fin dimensions.

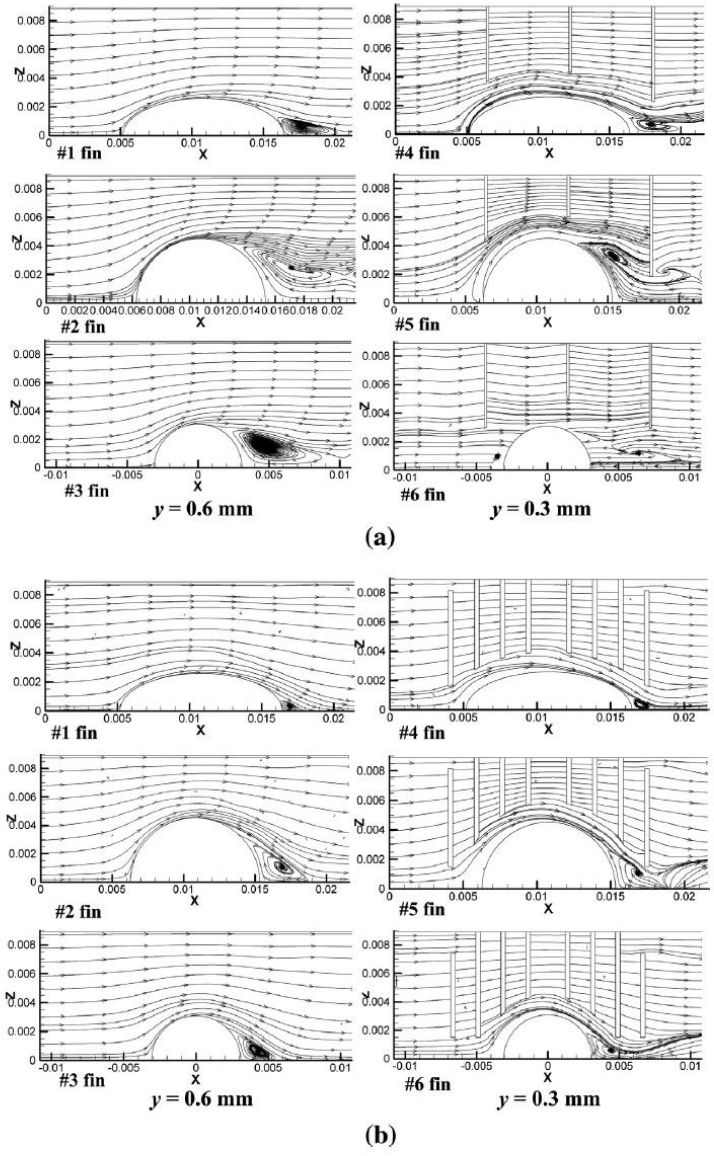

Fig. 4. Streamline plot on the cross-section $y = 0.6$ mm and $y = 0.3$ mm for three tubes: (a) wavy fin and (b) louver fin.

Combination of Elliptic/Circular Design

Air side performance of finned-tube heat exchanger with combination of circular and elliptical tubes, Applied Thermal Engineering 119 (2017) 360–372

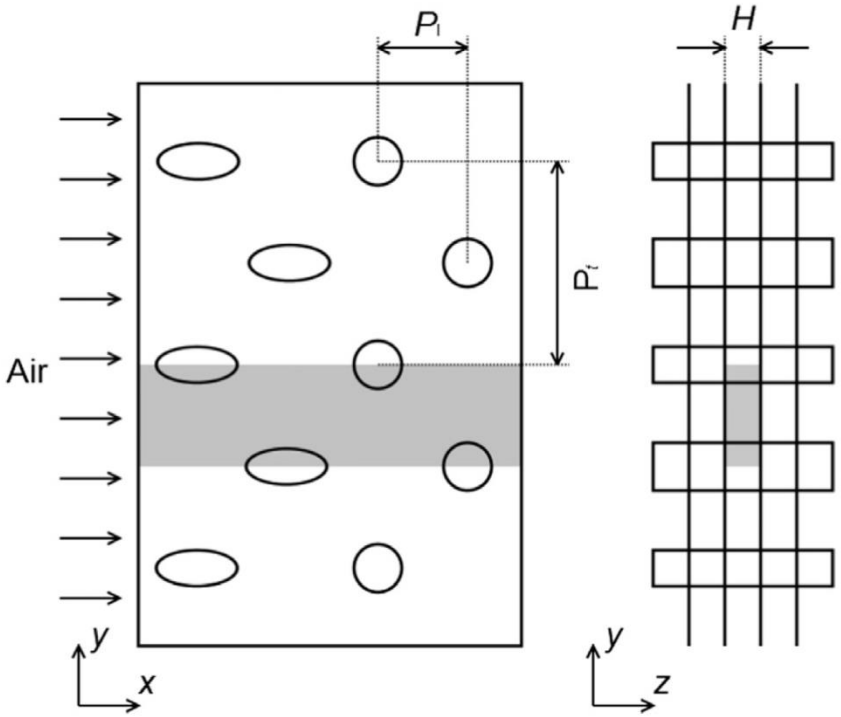

Fig. 1. Schematic representation of heat exchanger with fin and elliptical-circular tubes in staggered arrangement.

Table 1
Geometric details.

Transverse pitch (P_t)	25.4×10^{-3} m
Longitudinal pitch (P_l)	19.05×10^{-3} m
Circular tube diameter (D)	10×10^{-3} m
Perimeter of circular and elliptical tubes	31.42×10^{-3} m
Fin height (H)	2.115×10^{-3} m
Number of rows (N)	2, 4 and 6

Table 2
Combinations of tubes in various arrangements.

Designation	Schematic representation	Category
N2B1		Baseline-1
N2B2		Baseline-2
N2M1		Modified-1
N2M2		Modified-2
N4B1		Baseline-1
N4B2		Baseline-2
N4M1		Modified-1 (Alternate)
N4M2		Modified-2 (Grouped)
N4M3		Modified-3 (Alternate)
N4M4		Modified-4 (Grouped)
N6B1		Baseline-1
N6B2		Baseline-2
N6M1		Modified-1 (Alternate)
N6M2		Modified-2 (Grouped)
N6M3		Modified-3 (Alternate)
N6M4		Modified-4 (Grouped)

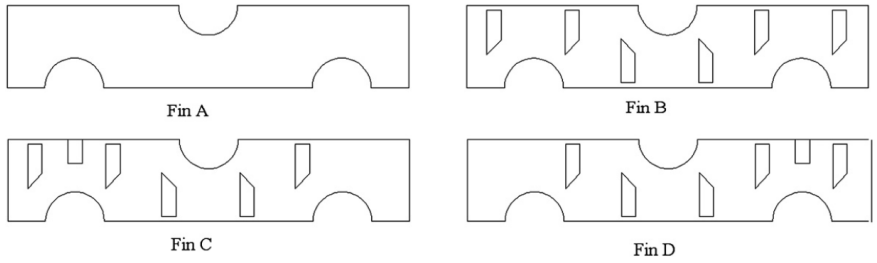

Fig. 9a. Four types of slit fin with the strips at different locations.

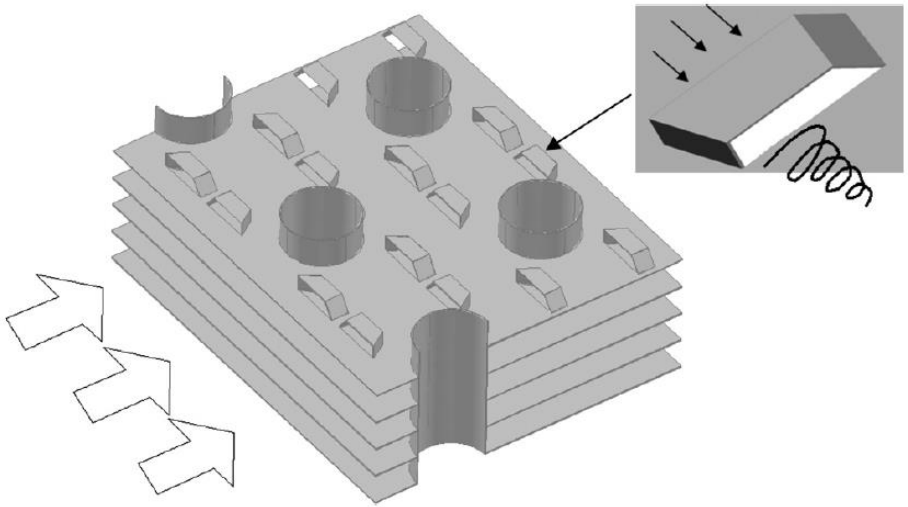

Fig. 1. Schematic diagram of core region of a slit fin-and-tube heat exchanger with longitudinal vortex generators.

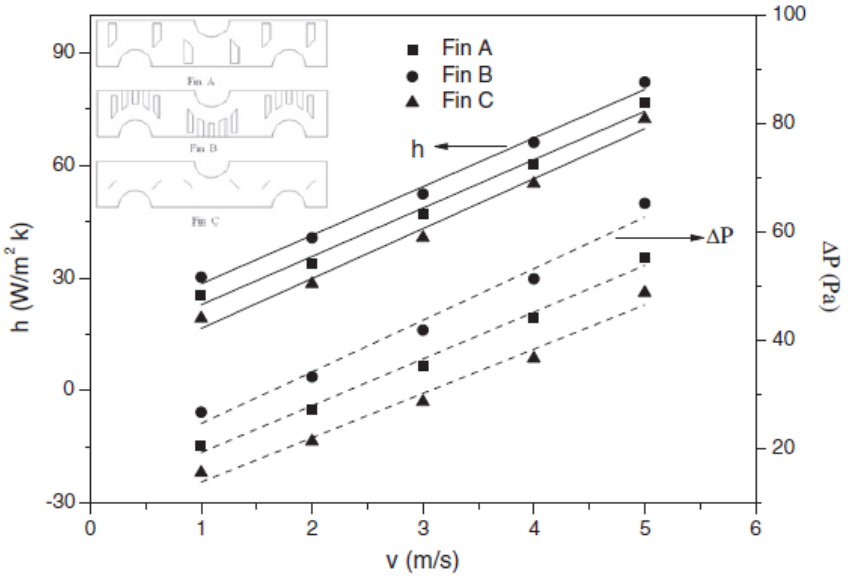

Fig. 10a. Comparison of the heat transfer coefficient and pressure drop versus frontal air velocity of three heat exchangers with different fins.

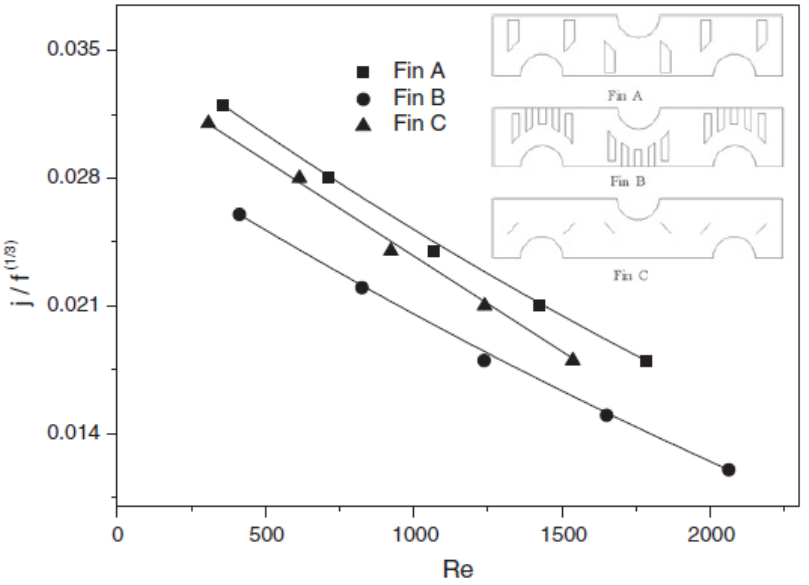

Fig. 10b. Comparison of $j/f^{(1/3)}$ of three heat exchangers with different fins.

Numerical study on a slit fin-and-tube heat exchanger with longitudinal vortex generators
Int J Heat Mass Transfer, 54 (2011) 1743–1751

Heat sink

Nomenclature	Side view	Dimension		Photos of test sample
(a) Plate	-		-	-	
(b) Delta VG	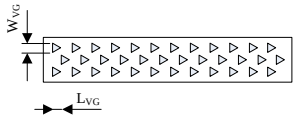	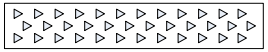	-	-	
(c) Delta VG+Plate		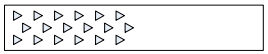	-	-	
(d) Semi-circular VG	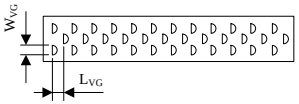	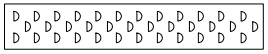	-	-	
(e) Triangular VG	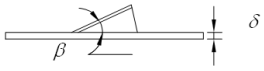	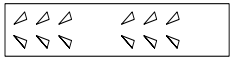	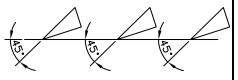	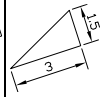	
(f) Triangular Attack VG	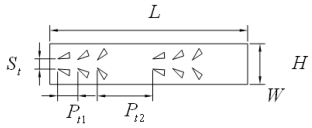	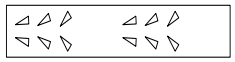	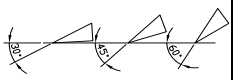	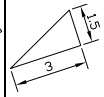	
(g) Dimple VG	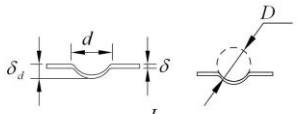	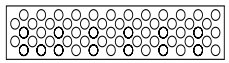	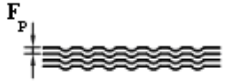	-	
(h) Two Groups Dimple VG		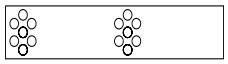		-	

Performance comparison
Fin spacing = 0.8 mm

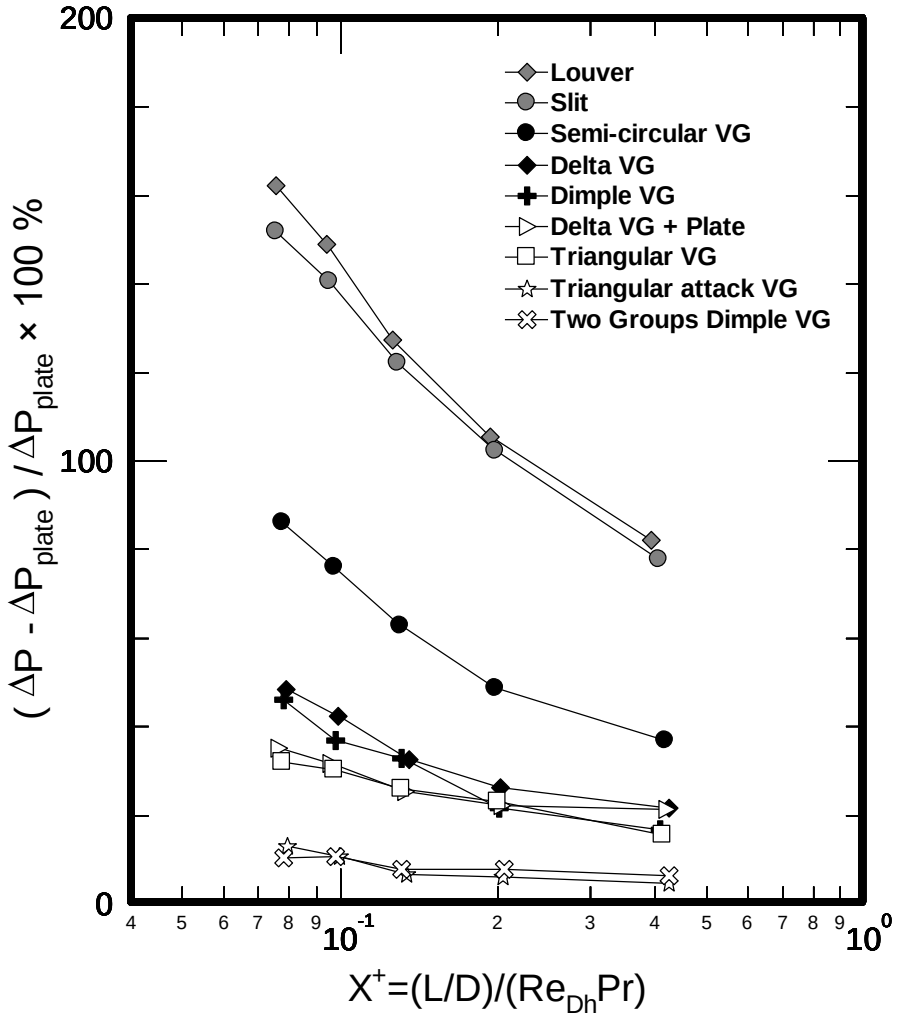

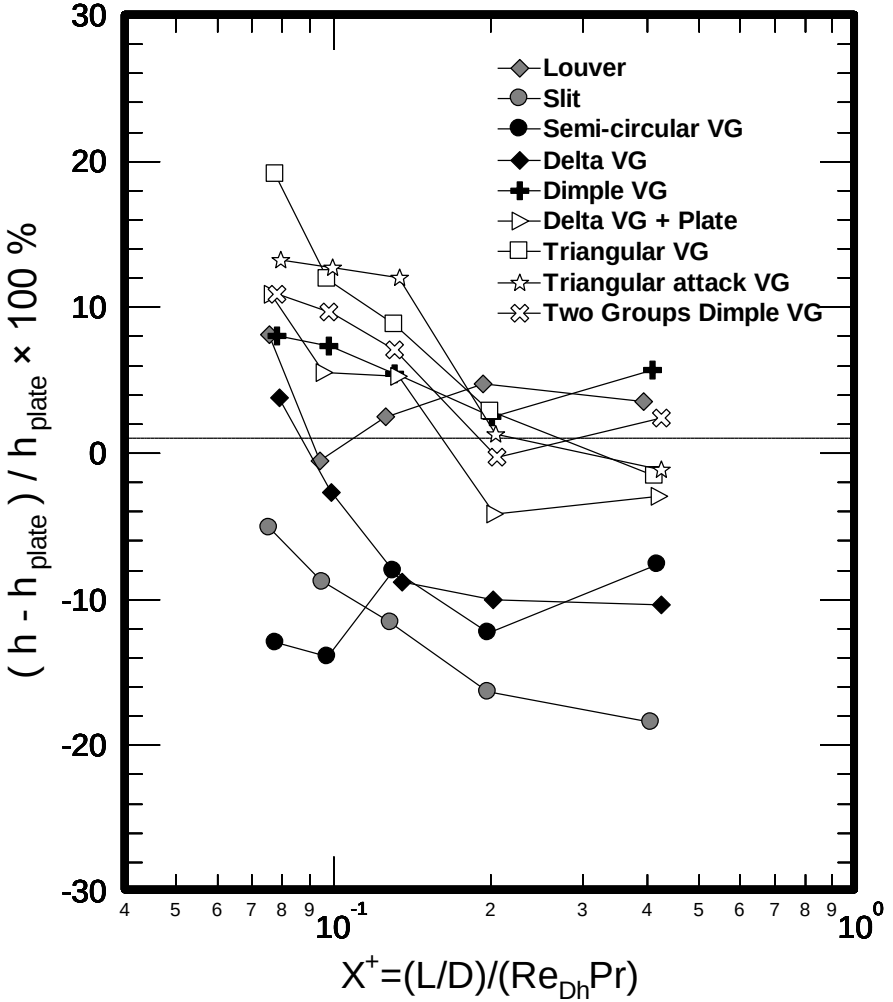

Vortex Generators

Test results & Some conclusions

- Also not so effective when the fin spacing is small.
- The concept is more effective with less number of VGs are employed.
- Less number VG provides much lower pressure drop than other arrangements.

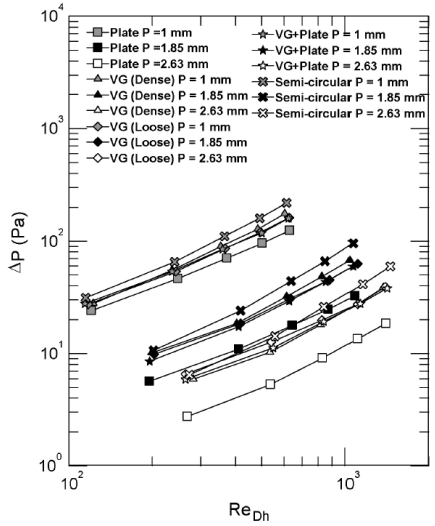

Fig. 3. Pressure drops versus Reynolds number for the test heat sinks.

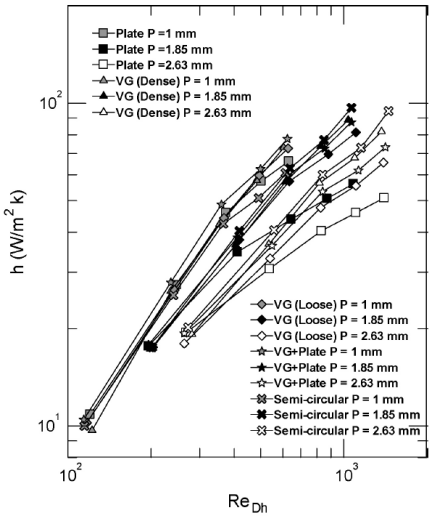

Fig. 4. Heat transfer coefficients versus Reynolds number for the test heat sinks

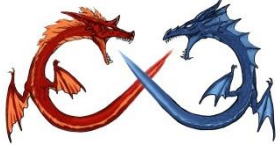

Grooved Surface (dimple)

The original concept of Using dimples & Grooved surfaces..

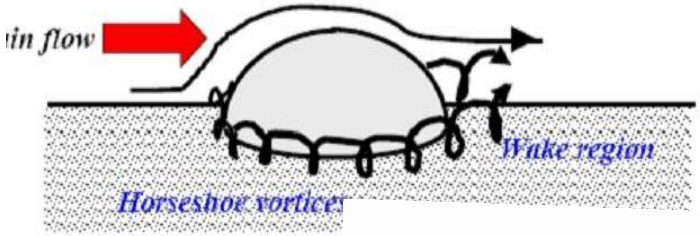

(b) P

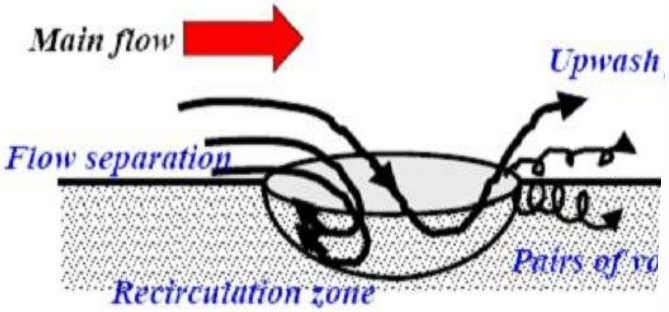

(a) Dimple

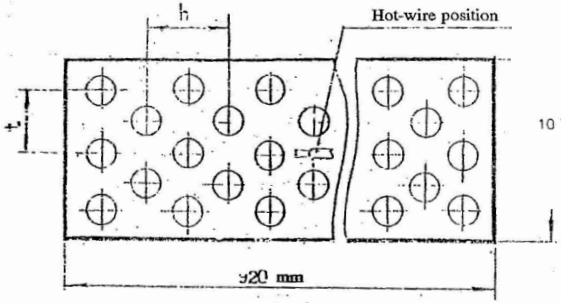

No.	D, mm	H, mm	R, mm	t, mm	h, mm	f, %
1	7.5	0.5	13.32	13.3	11.5	25
2	6.0	0.4	10.20	10.6	9.1	25
3	4.5	0.3	7.65	8.0	7.5	25
4	7.5	0.5	13.32	9.4	8.1	50
5	6.0	0.4	10.20	7.5	6.5	50
6	4.5	0.3	7.65	5.6	4.9	50
7	7.5	0.5	13.32	8.4	7.3	70
8	6.0	0.4	10.20	6.4	5.5	70
9	4.5	0.3	7.65	4.8	4.2	70

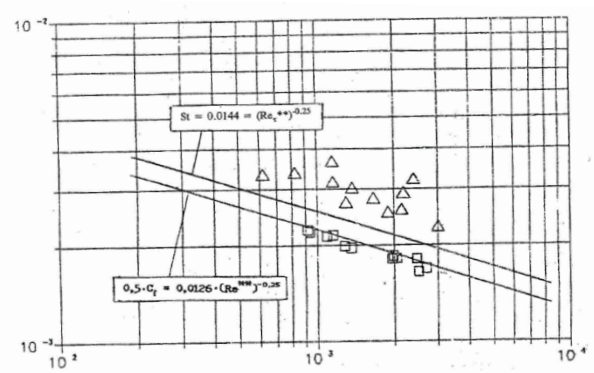

Fig. 13. Friction and heat transfer on indented walls.
□ - the dynamic (velocity) boundary layer; Δ - the thermal boundary layer.

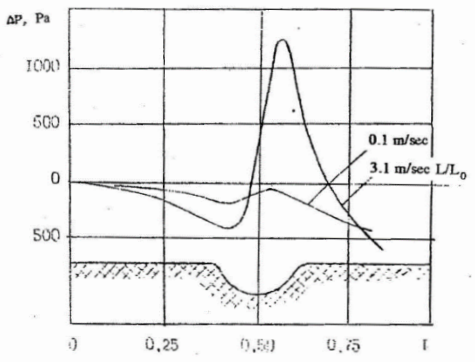

Fig. 10. Distribution of the pressure drop along the axis of a duct with an isolated hemispherical pit in the wall [15].

- Drag reduction
- Longitudinal Vortices

Grooved surface vs. interrupted surface

- Oblique Dimples with cannelure cannelure structure

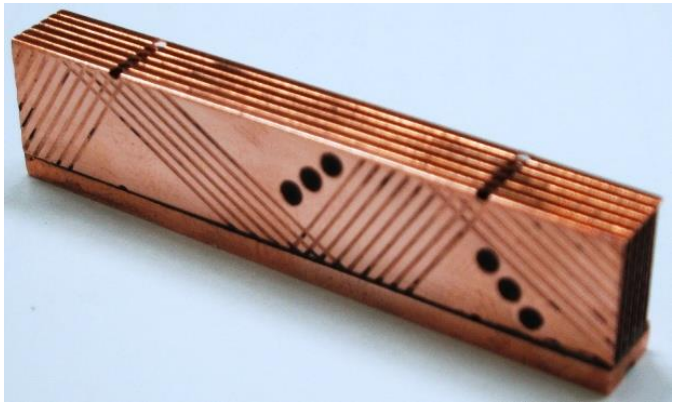

（plate fin）	(oblique dimple gap 4-12fin)
	
(oblique dimple gap 6-12 fin)	（cannelure fin I）
	
（cannelure fin II）	(oblique dimple gap 4-12 cannelure fin)
	
(oblique dimple gap 6-12 cannelure fin I)	(oblique dimple gap 6-12 cannelure fin II)
	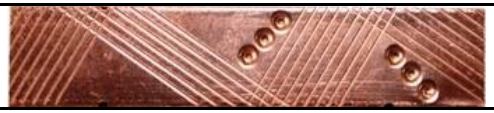

The original idea for oblique dimple..

- Concavity + Dimple
- Lengthen the flow path
- No need for significant amount dimples
  - Reduce the number of dimples to decrease the

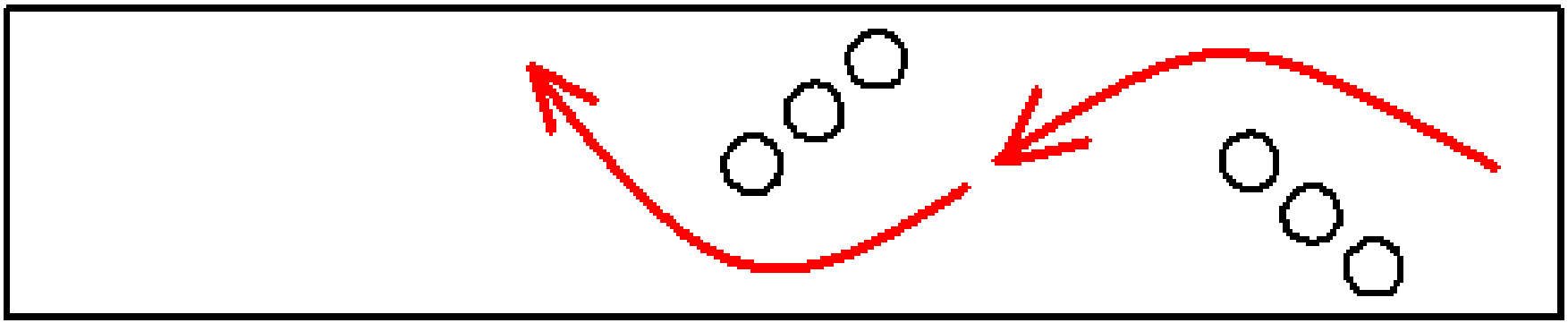

Results:

Approximate 20% increase HTC & 20% reduction in pressure drop

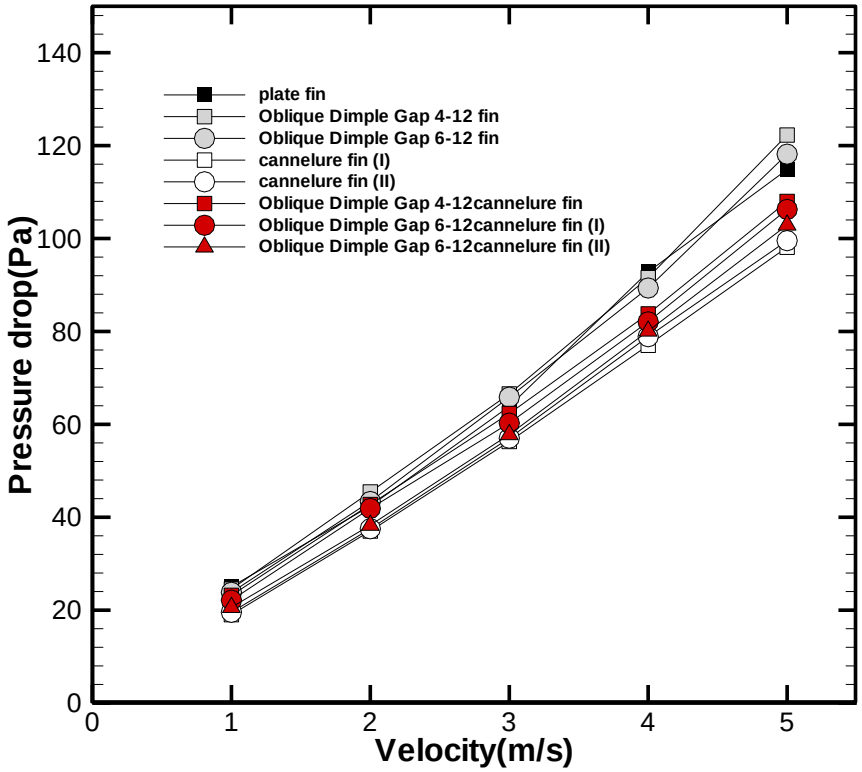

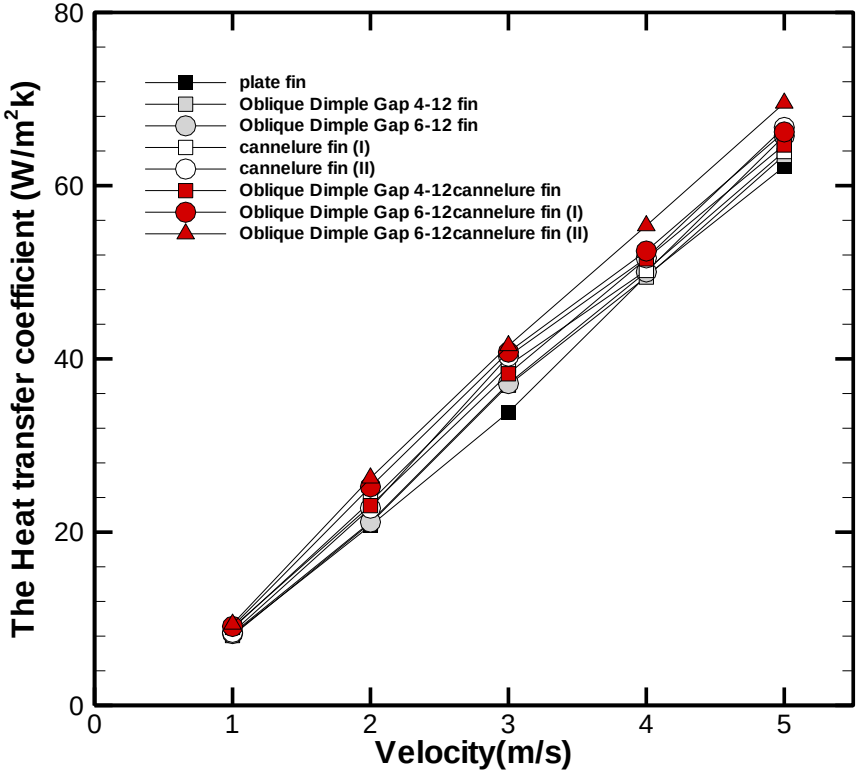

Performance & IR image

Plate fin(5 m/s)

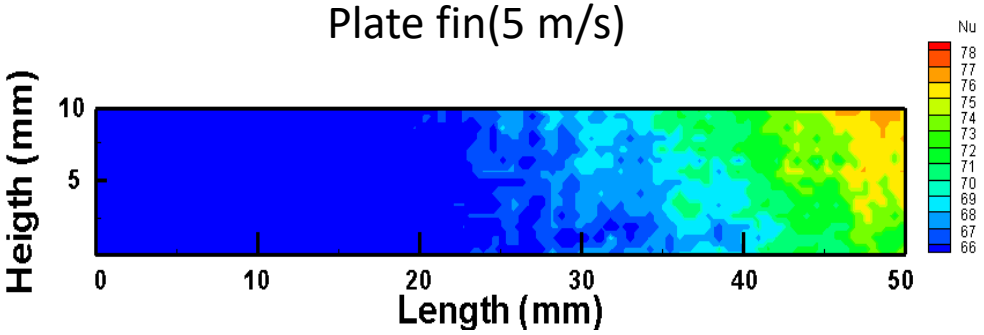

Gap 6-12 fin(5 m/s)

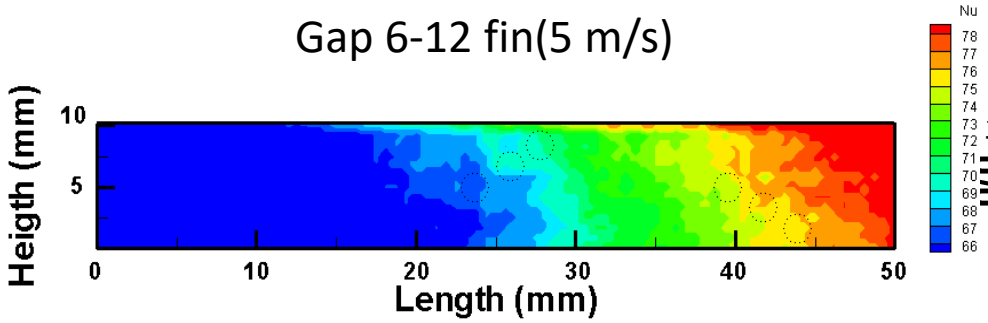

Cannelure fin II (5 m/s)

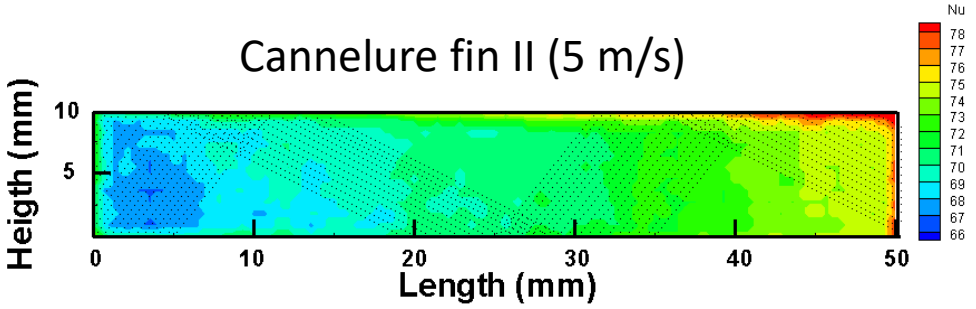

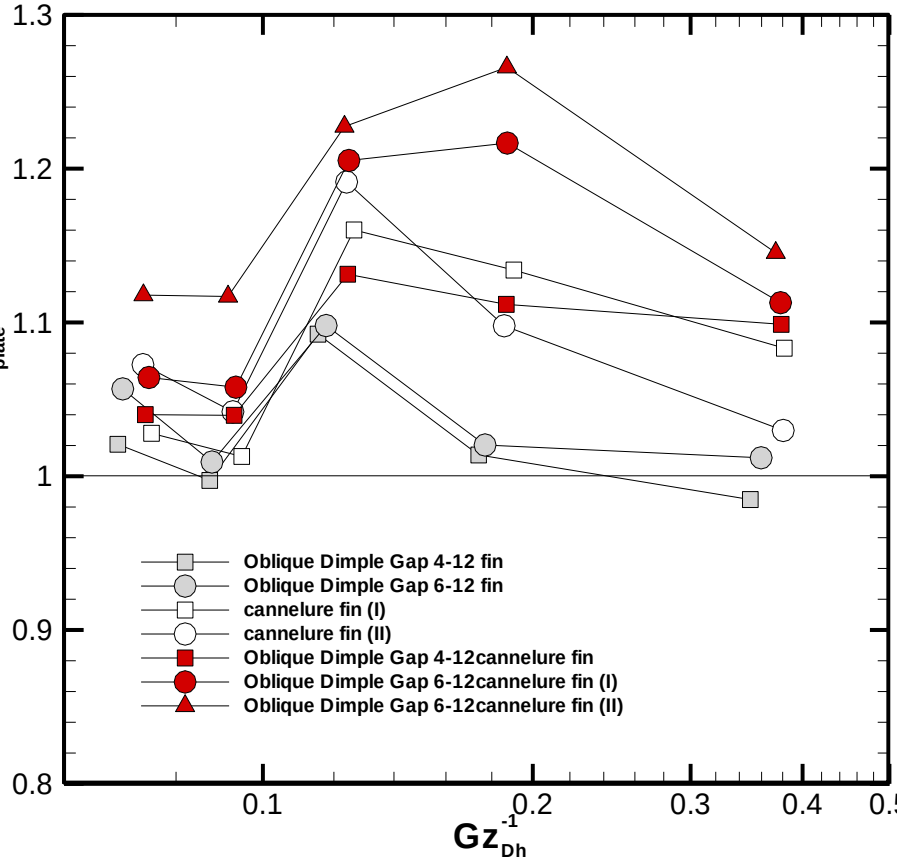

- Partial bypass design
  - Manipulating ΔT

A novel "partial bypass" concept to augment the performance of air-cooled heat exchangers, Int. J. Heat Mass transfer, 55 (2012) 5367–5372

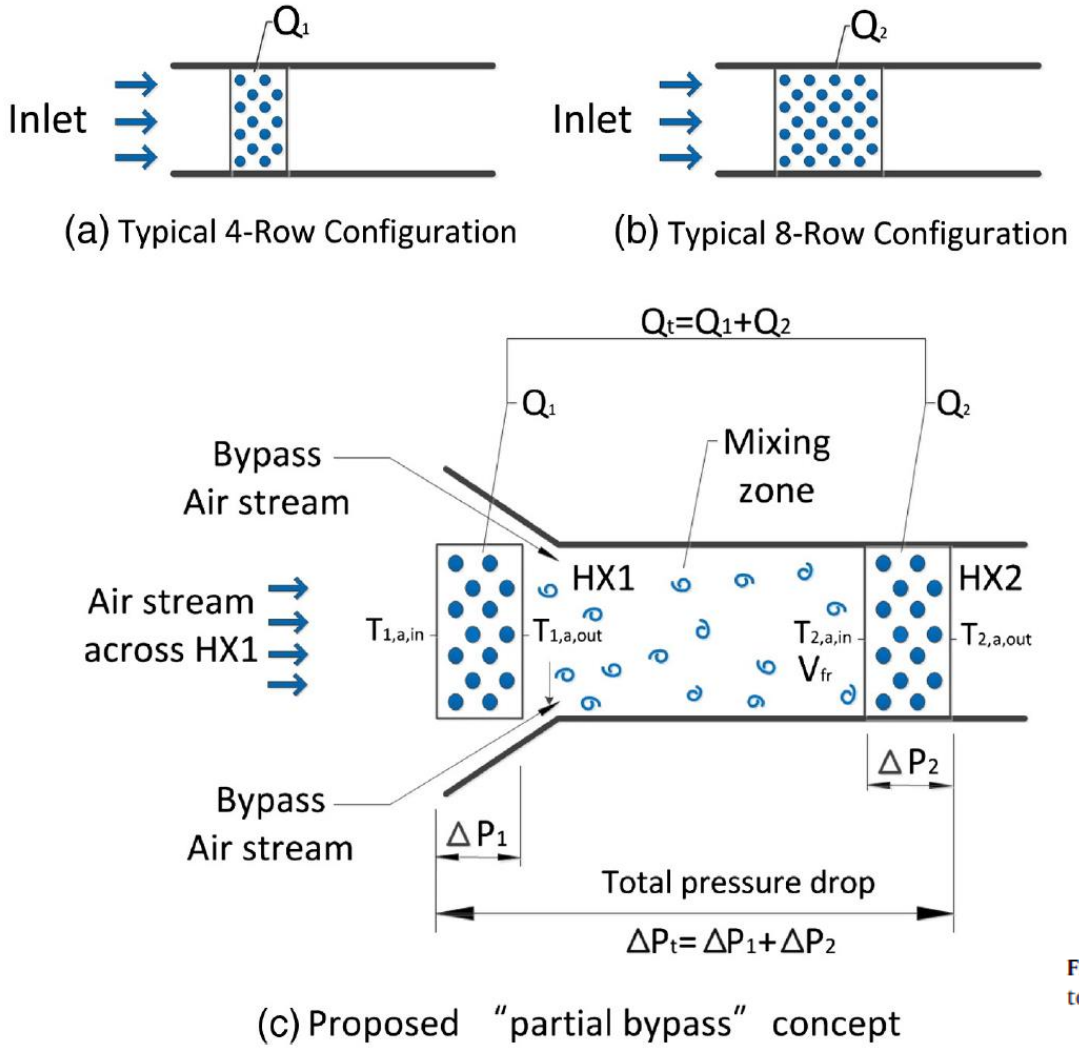

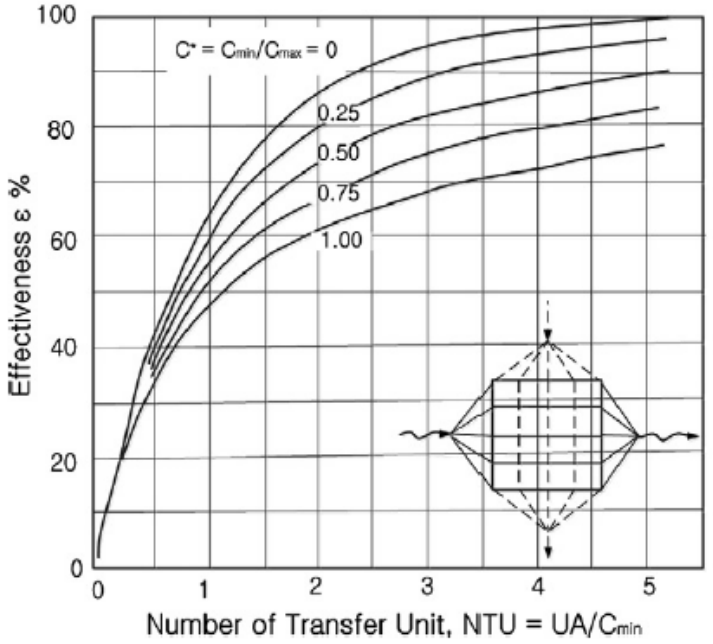

Fig. 2. Relation of the ε -*NTU* for unmixed/unmixed cross flow arrangement subject to variation of C^*.

matic of operation of the (1) 4-row heat exchanger; (2) 8-row heat exchanger; and (3) the proposed "partial bypass" heat exchanger.

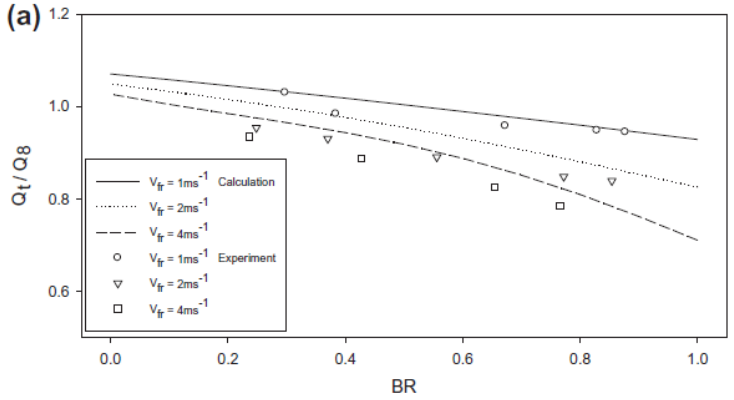

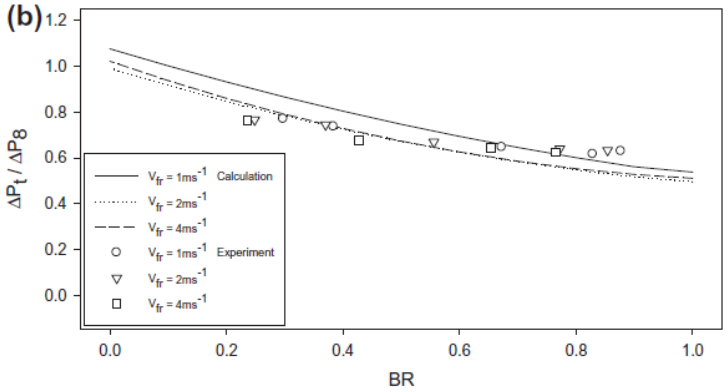

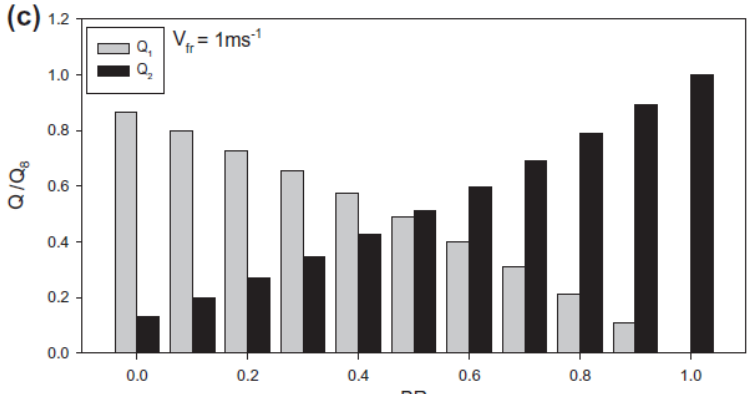

(a) Calculated results for QR vs. bypass ratio and its comparison with experimental measurements; (b) calculated results for PR vs. bypass ratio and its comparison with
experimental measurements; (c) fraction of heat transfer vs. bypass ratio for the first and second heat exchanger for Vfr = 1 m s1.

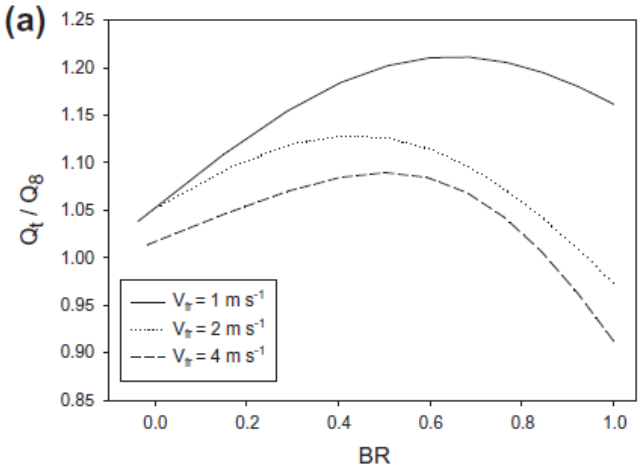

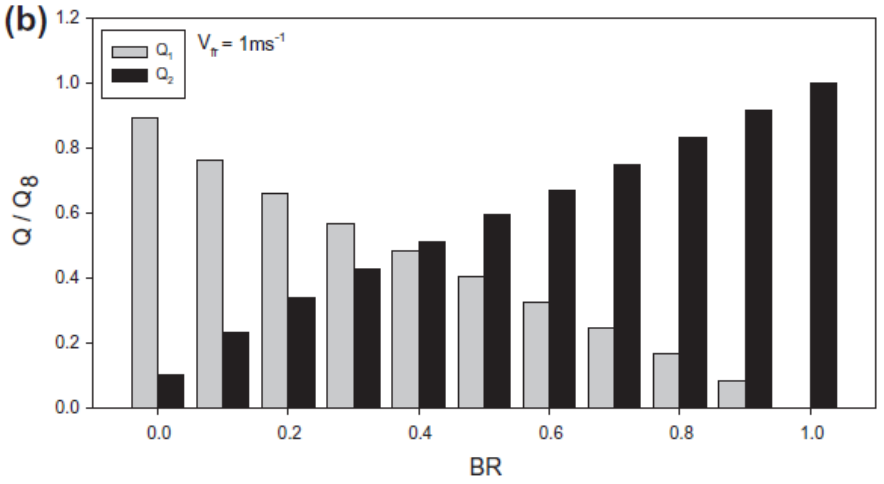

(a) Calculated results for Q/Q8 vs. bypass ratio subject to identical pumping power constraint with Vfr = 1, 2, and 4 m s1 at the second heat exchanger; (b) Fraction of heat transfer vs. bypass ratio for the first and second heat exchanger for Vfr = 1 m s1.

Effect of partial bypass on the heat transfer performance of dehumidifying coils, Int. Comm. in Heat and Mass Transfer 58 (2014) 132–137

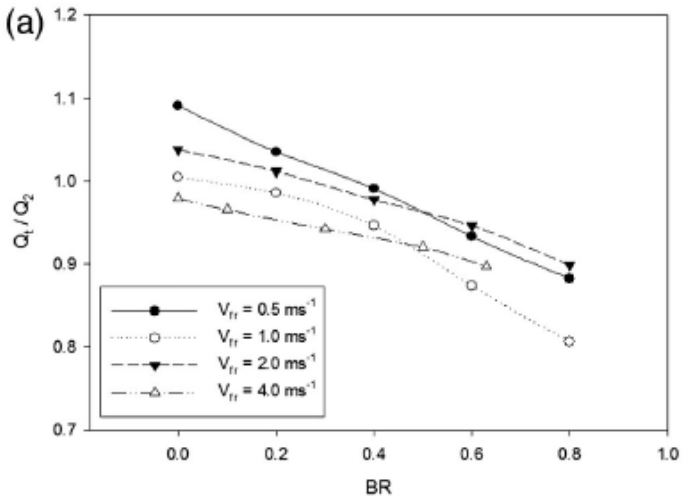

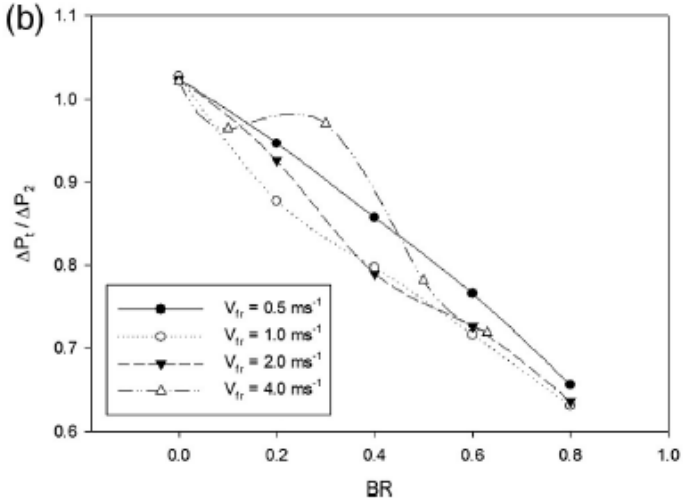

Fig. 5. (a) Experimental results for Q_R vs. bypass ratio for a 2-row coil under RH = 80%; (b) experimental results for P_R vs. bypass ratio for a 2-row coil under RH = 80%.

(b) Photo of the mixing device placed amid the first and the second heat exchanger.

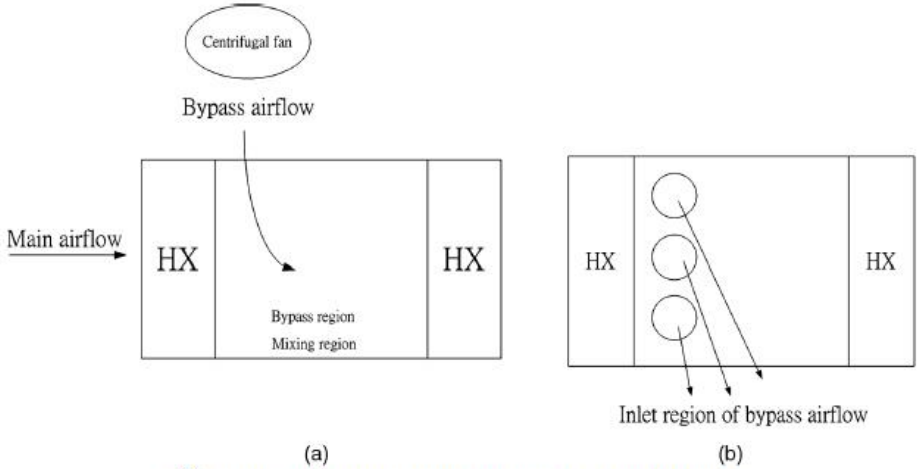

(c) Schematic of the bypass flow into the bypass device.

Fig. 2. Schematic of the test facility and the partial bypass device.

Plate	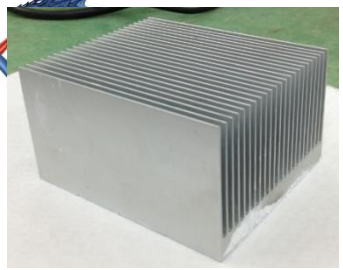	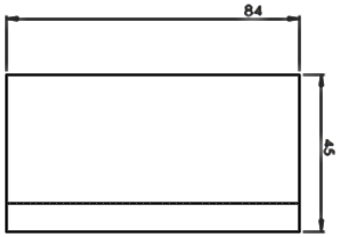
Step 1/3	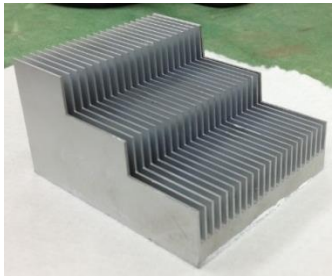	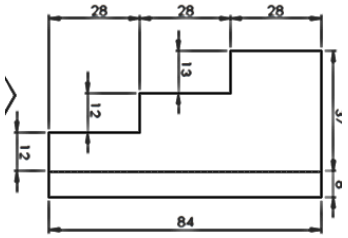
Step 1/2	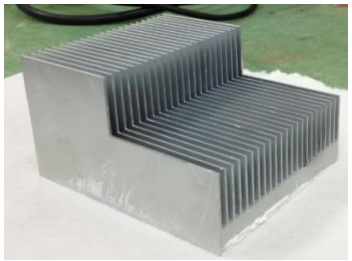	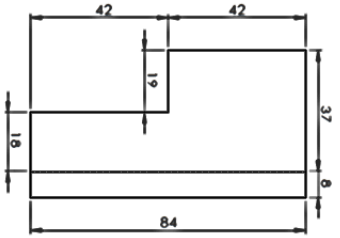
Trap 1/3	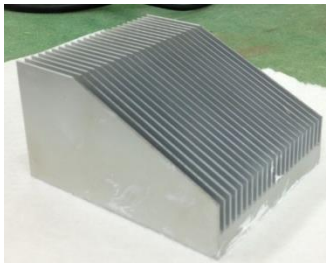	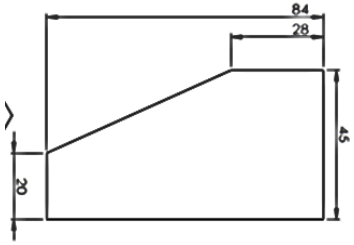
Trap 1/2	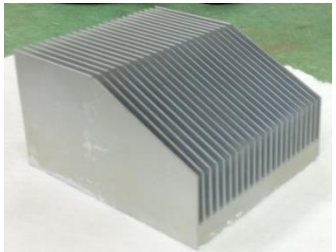	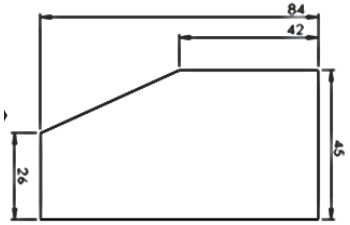

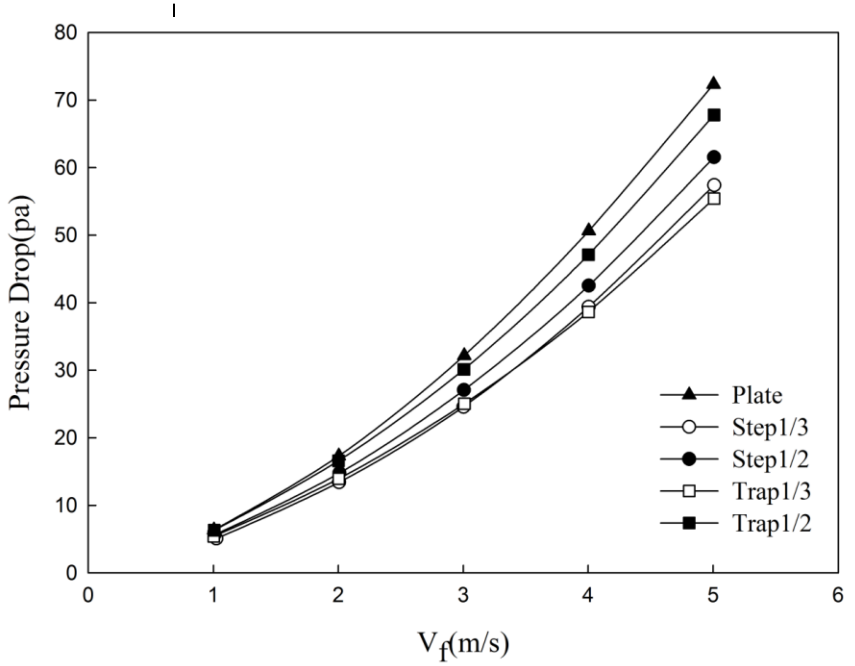

(a) Pressure drops vs. frontal velocity

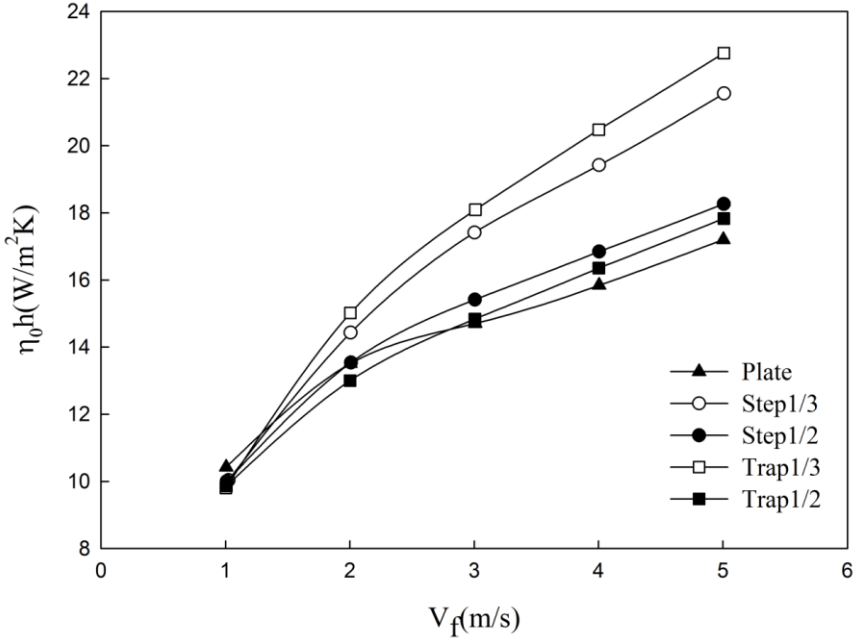

Thermal resistance vs. pumping power for all test samples

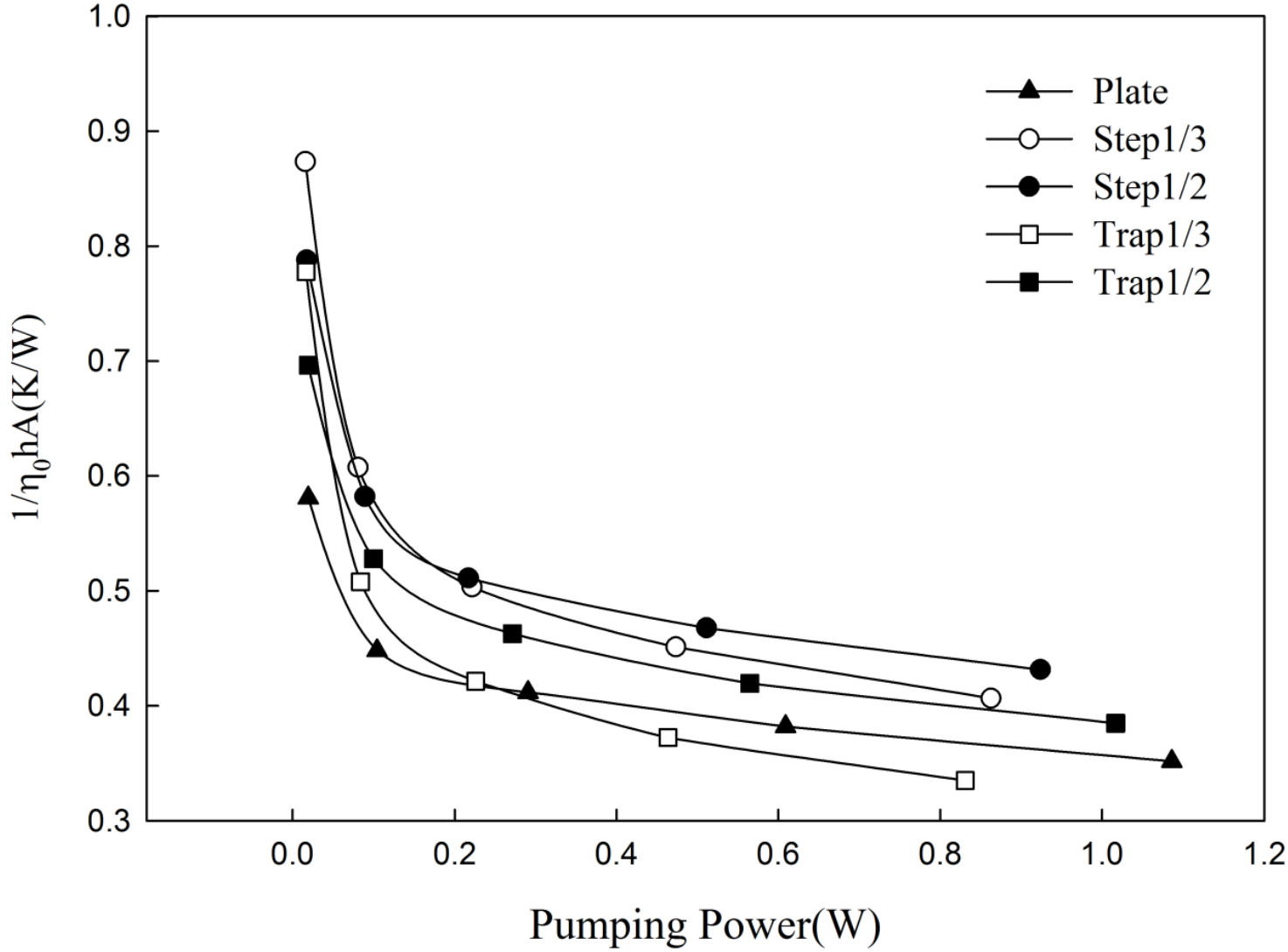

Partial bypass design

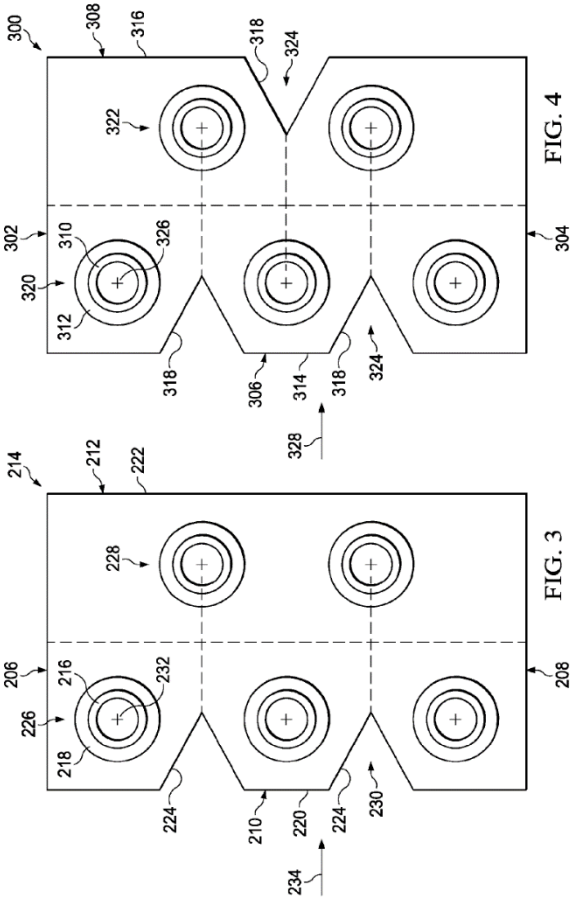

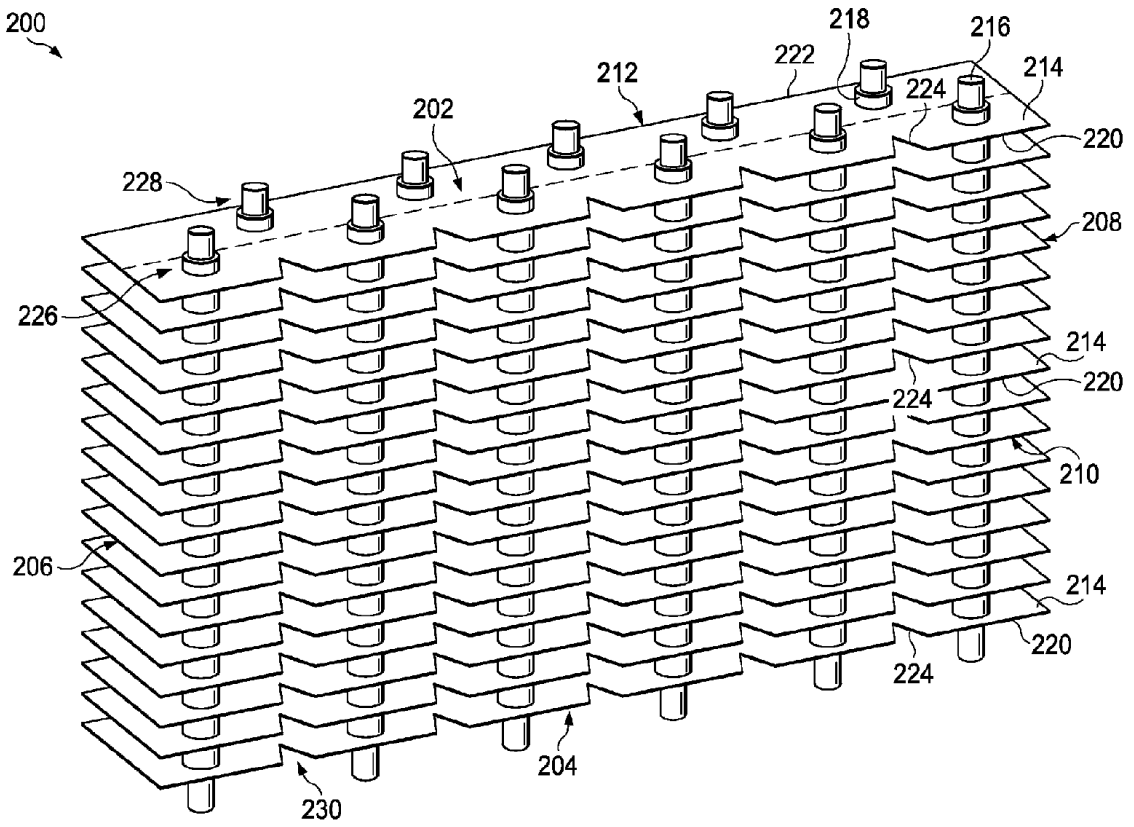

(19) **United States**
(12) **Patent Application Publication**
Groskreutz
(10) **Pub. No.: US 2015/0211807 A1**
(43) **Pub. Date: Jul. 30, 2015**

(19) **United States**

(12) **Patent Application Publication**

Hancock

(10) **Pub. No.: US 2017/0059188 A1**

(43) **Pub. Date: Mar. 2, 2017**

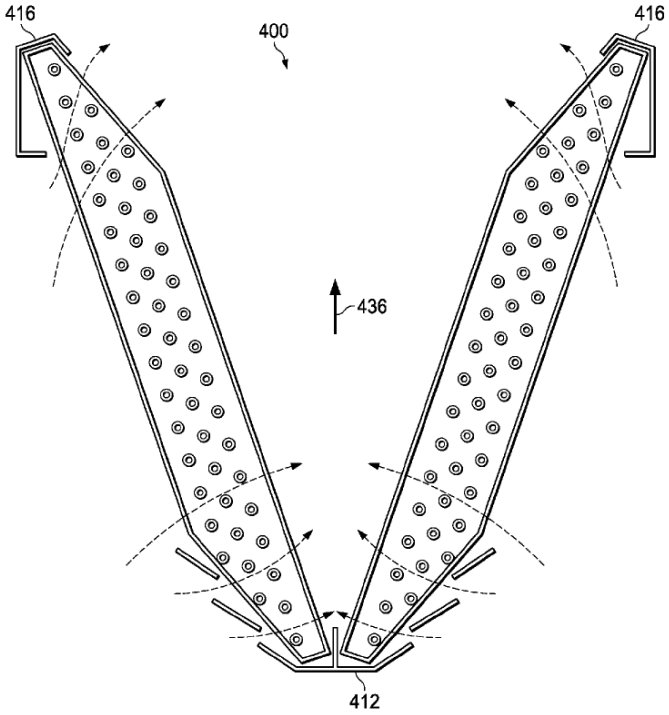

FIG. 4

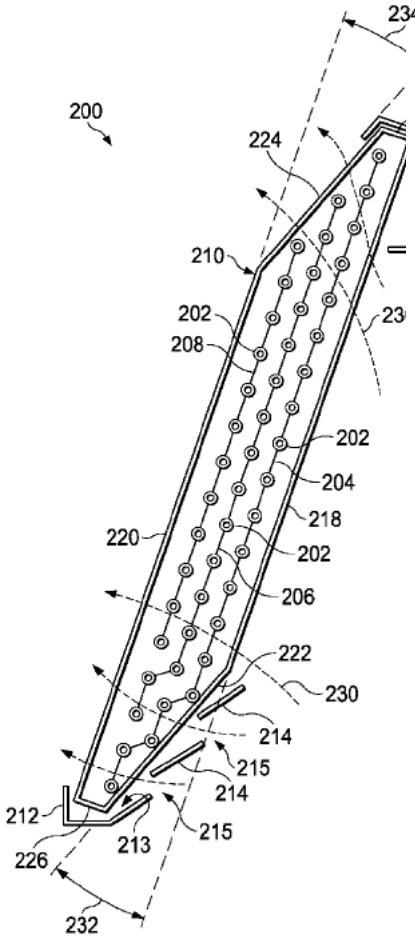

FIG. 2

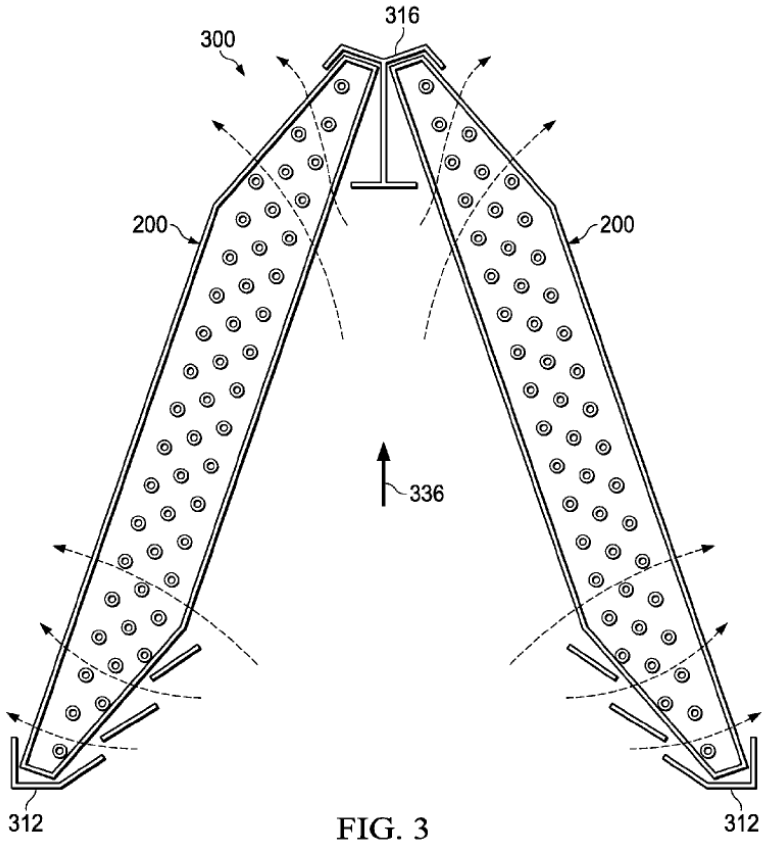

FIG. 3

Air-side heat transfer and pressure drop characteristics of accelerated flow evaporators, Int. J. Refig., Int. J. refrig. 34, (2011) 484-497
Reversed the “partial bypass” → Fails eventually

- Use as no-frost coil
- The designs are much inferior to the base line design (uniform one)

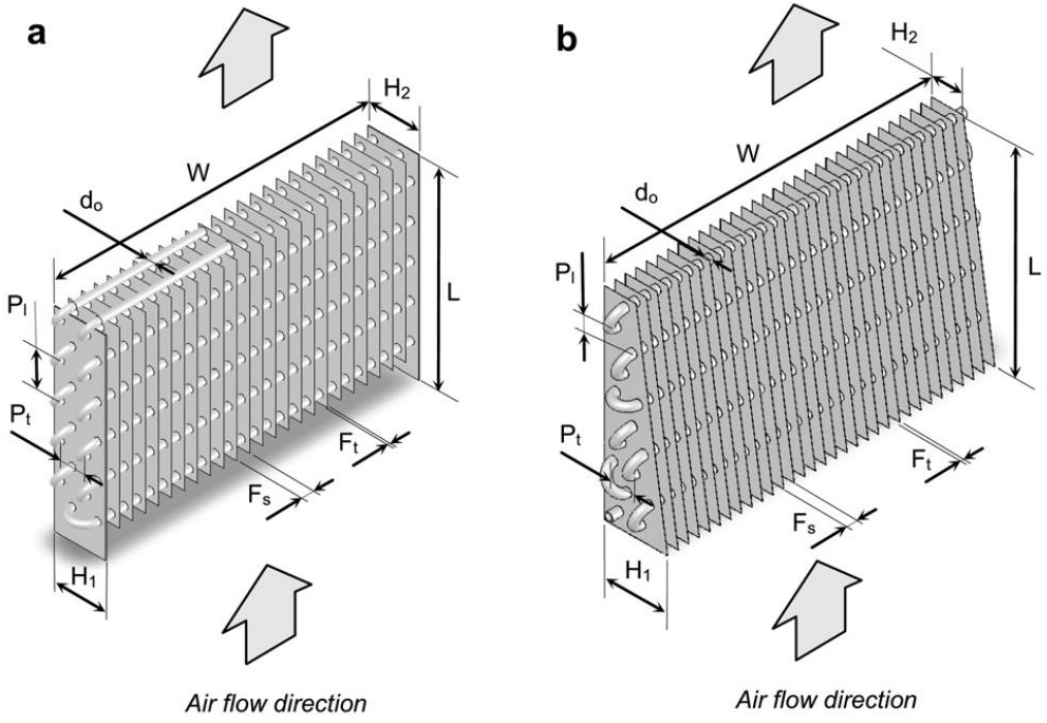

Fig. 1 – (a) Conventional no-frost evaporator; (b) accelerated flow evaporator.

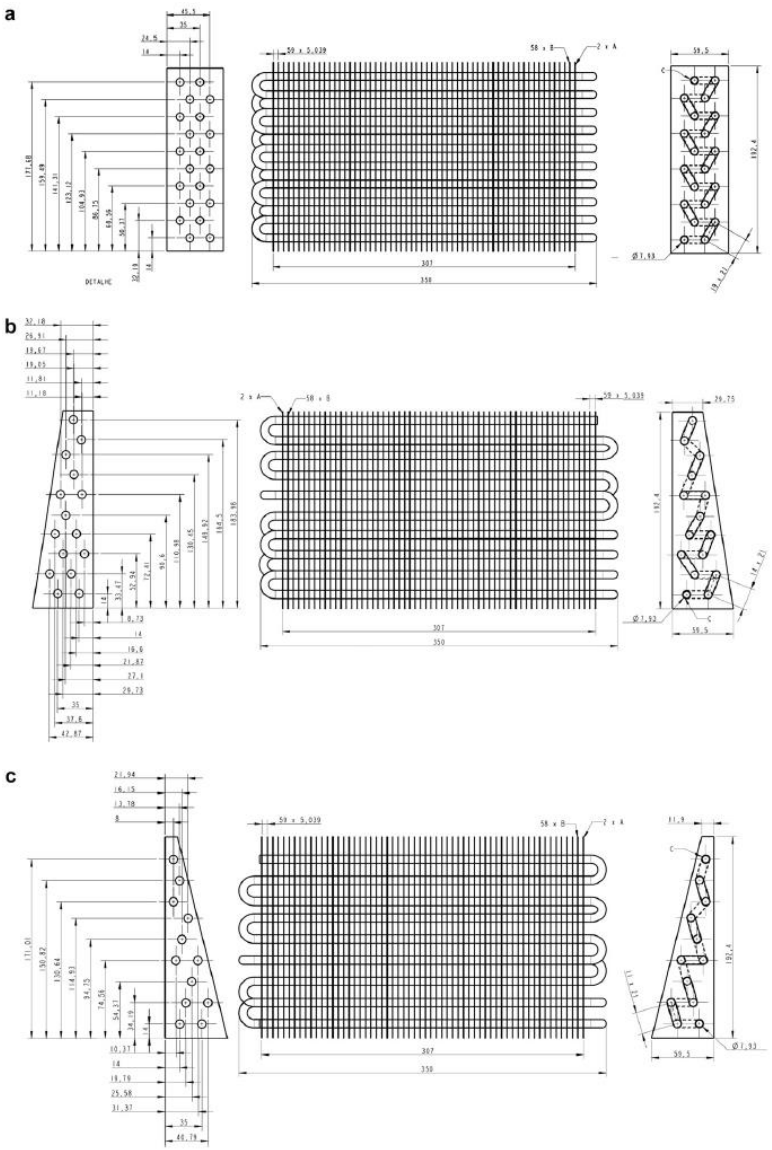

Fig. 2 – Real dimensions (in mm) of the AFE prototypes. (a) Evaporator #1, (b) Evaporator #4, (c) Evaporator #7.

Special Fin Design

Air Flow deflecting design

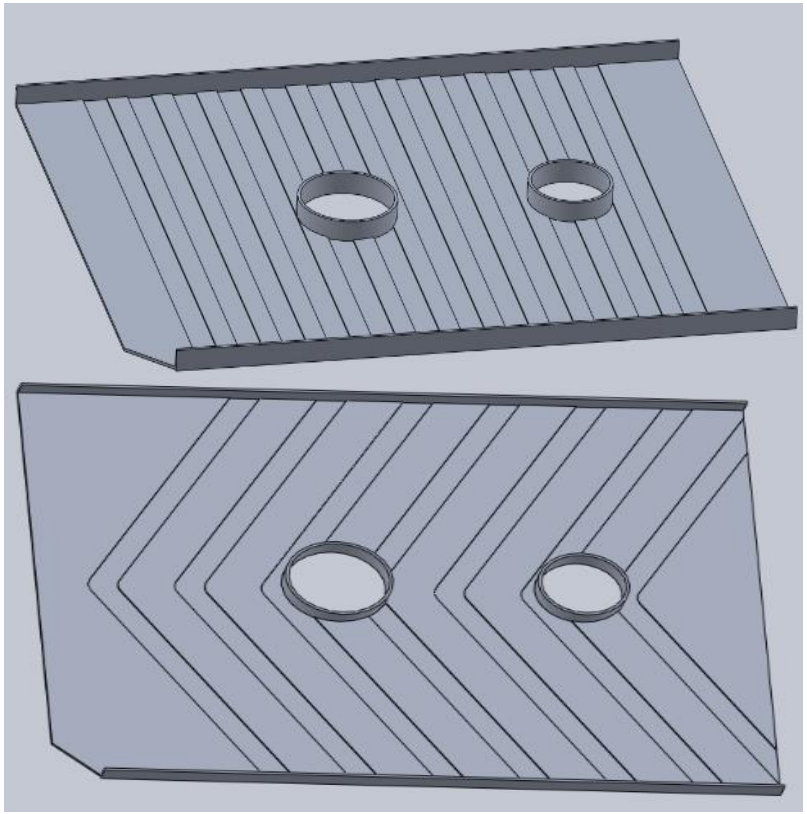

A study on heat sink performance using V-shaped cannelure structure fin. In Proceedings of the ASME 2015 International Technical Conference and Exhibition on Packaging and Integration of Electronic and Photonic Microsystems, San Francisco, 2015; Paper No. InterPACKICNMM2015-48043

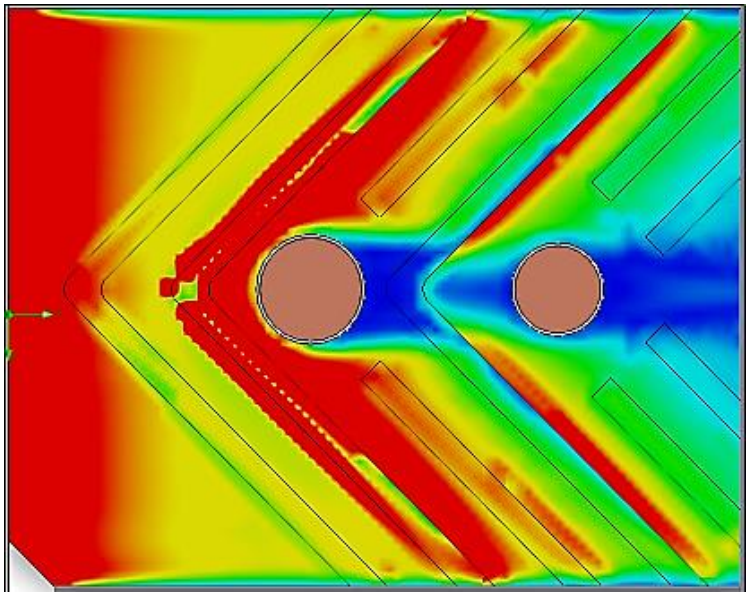

	h (W/m^2-K)	Δh (%)	ΔA (%)	Δh*A (%)	Pressure drop (Pa)	ΔP (%)
Plain fin	42.1	-	-	-	15	-
45 Degree V-shape	58.9	39.9	3.7	45.1	16	6.67
60 Degree V-shape	60.2	43.2	4.4	49.4	18	20.0
75 Degree V-shape	54.1	28.5	3.7	33.3	18	20.0

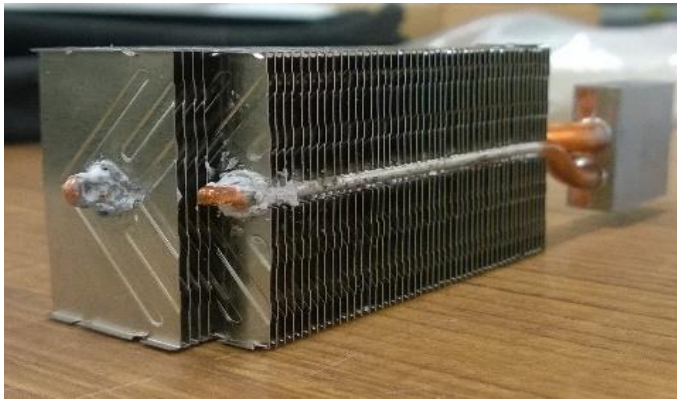

An experimental investigation on heat transfer enhancement of sprayed wire-mesh heat exchangers, Int. J. Heat mass transfer, 112 (2017) 699–708

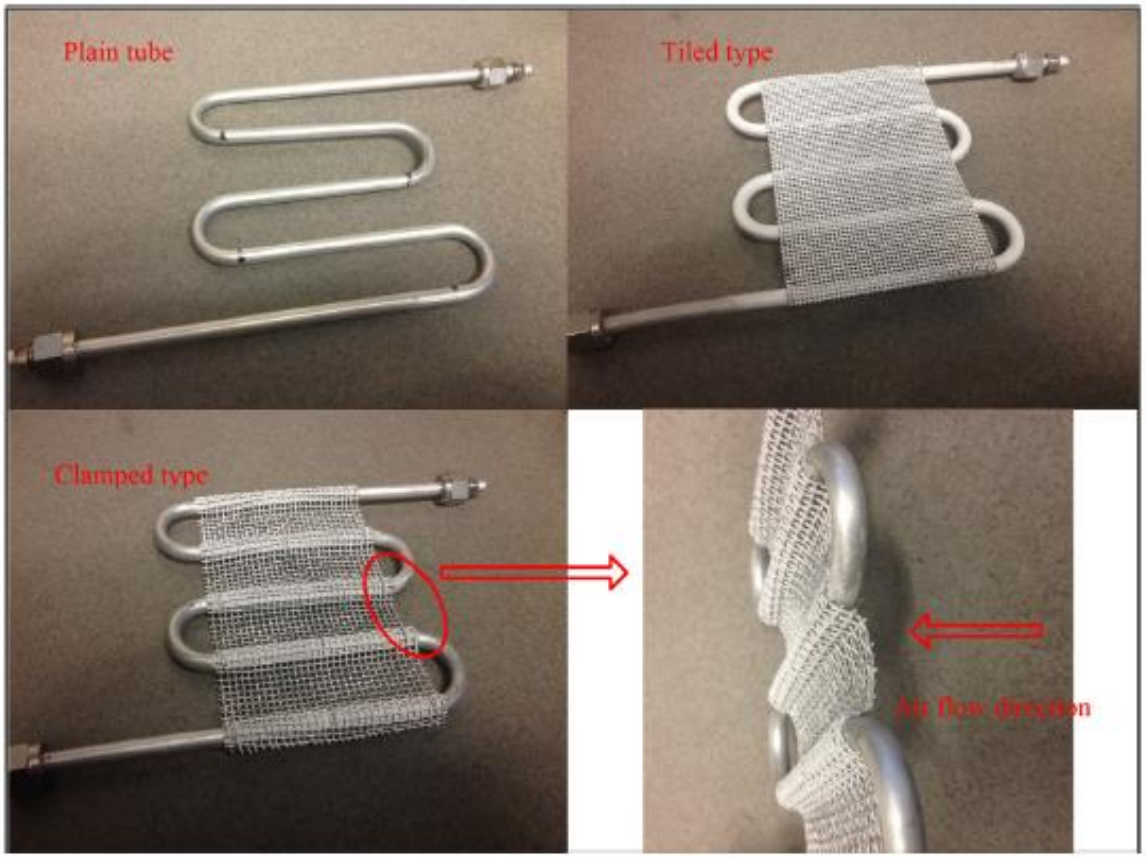

Fig. 3. Sample pictures of three types of heat exchangers.

Table 1
Experimental test conditions.

Wind tunnel side		Tube side	
Air velocity (m/s)	2, 5, 8, 10, 15, 20	Volumetric flow rate (L/min)	20.00
Pressure (MPa)	0.10	Pressure (MPa)	0.45
Temperature (°C)	Room temperature	Inlet temperature (°C)	100, 130, 150, 180, 200

- Wire mesh could be connected well with tube by spraying Al coating in both clamped and tiled types.
- All SPW heat exchangers can enhance the heat transfer coefficient compared with plain tubes. The maximum value of heat transfer enhancement is about 25.9% for the clamped 20PPI SPW heat exchanger.
- Classic pin-fin model was verified using data of wire temperature distribution for tube-wire heat exchanger and the efficiency compared with ideal fin has the maximum value of 76.7% for all

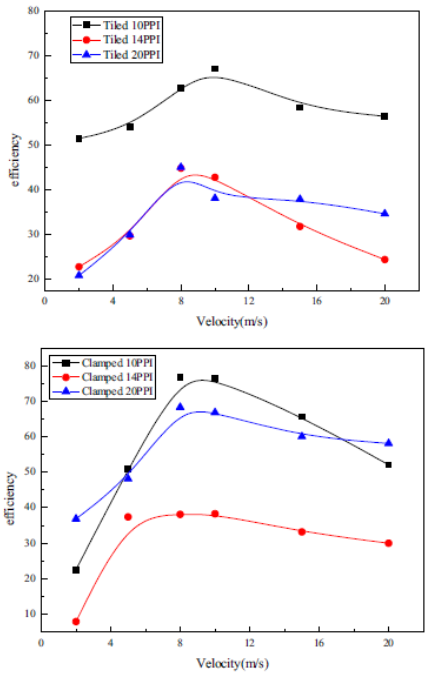

Fig. 14. SPW heat exchangers' efficiency under various wind tunnel velocities.

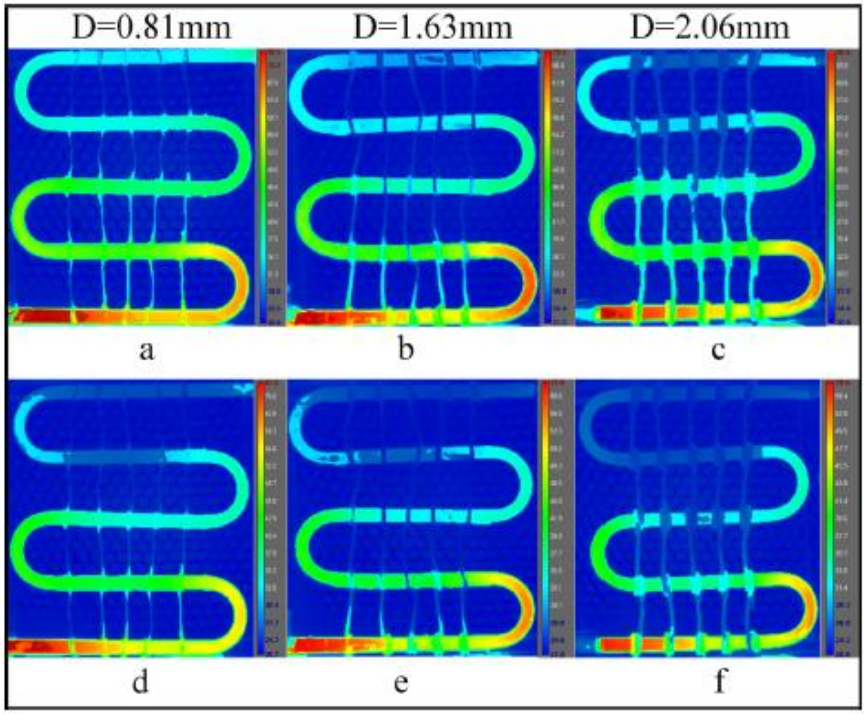

Fig. 10. Surface temperature distribution for tube-wire heat exchangers. (Tube inlet temperature: 150 °C, wind tunnel velocity: a–c: 8 m/s; d–f: 15 m/

Wire Structure Heat Exchangers—New Designs for Efficient Heat Transfer, Energies, Energies 2017, 10, 1341; doi:10.3390/en10091341

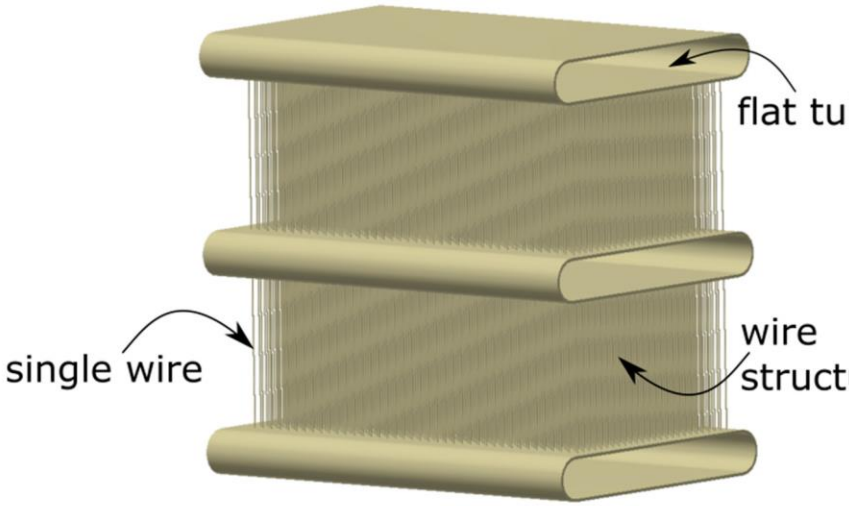

Figure 1. Concept of the flat tube wire heat exchanger design (FT WHX)

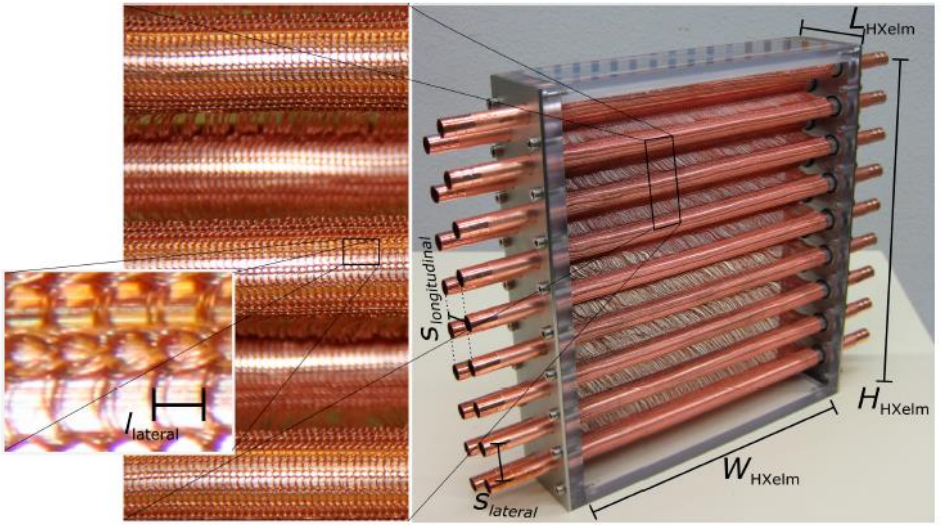

Figure 3. Round tube wire heat exchanger (RT WHX).

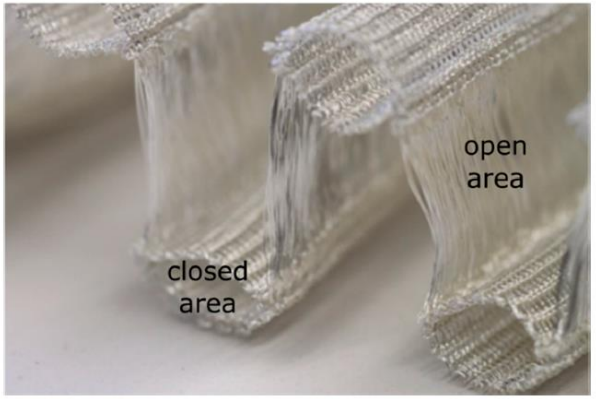

Figure 2. Knitted textile structure for a round tube heat exchanger. Air flows through the open area; tube insertion is in the closed area.

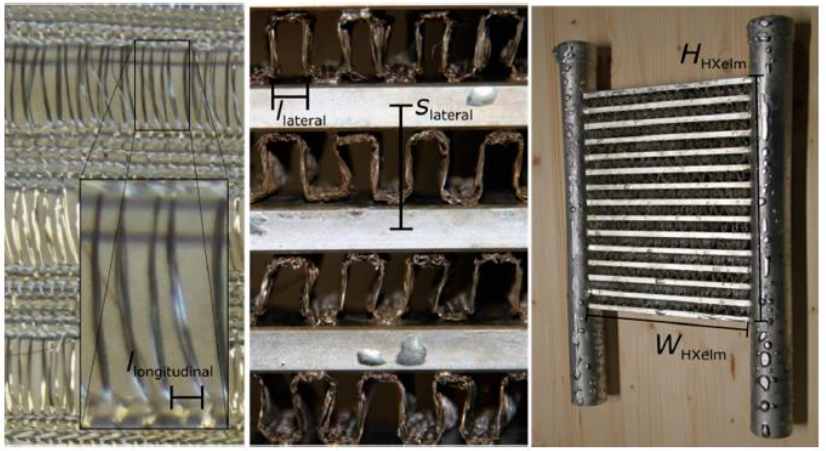

Figure 4. Flat tube wire heat exchanger (FT WHX).

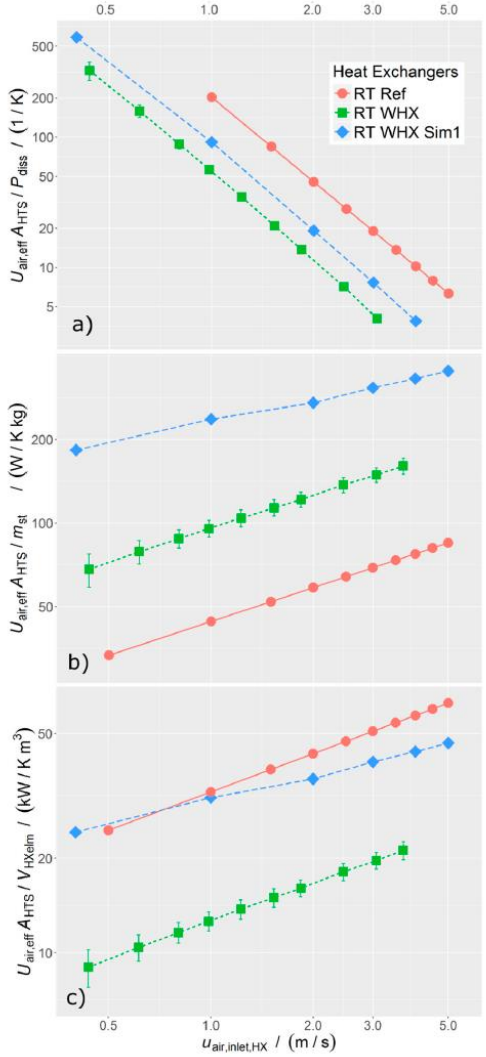

Figure 9. Results of the measured and simulated round tube wire heat exchangers (RT WHX and RT WHX Sim1) compared to a conventional fin-and-tube heat exchanger (RT Ref) in terms of (**a**) energetic efficiency; (**b**) mass efficiency; and (**c**) volume efficiency as a function of the air inlet velocity of the heat exchanger.

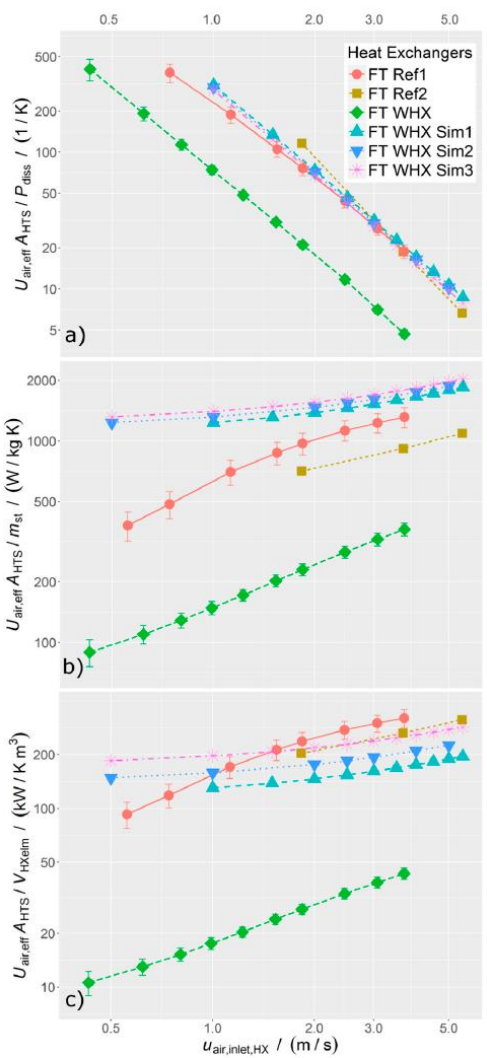

Figure 10. Results of the measured and simulated flat tube wire heat exchangers (FT WHX and FT WHX Sim) compared to a conventional louvered-fin flat tube heat exchanger (FT Ref) in terms of (**a**) energetic efficiency; (**b**) mass efficiency; and (**c**) volume efficiency as a function of the air inlet velocity of the heat exchanger.

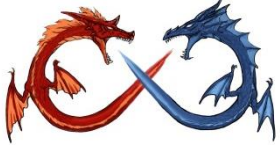

- The volume efficiency is in the same range for the simulated heat exchangers as it is for the reference.
- The energetic efficiency is lower in the case of the round tube wire heat exchanger simulation, but similar for the flat tube design.
- However, the key advantage is that the material efficiency of the wire heat exchangers is twice that of the reference heat exchanger with the same material. Thus, a reasonable application for wire structure heat exchangers would be lightweight design.

A numerical study on the air-side heat transfer of perforated finned-tube heat exchangers with large fin pitches, Int. J. Heat Mass Transfer, 100 (2016) 199–207

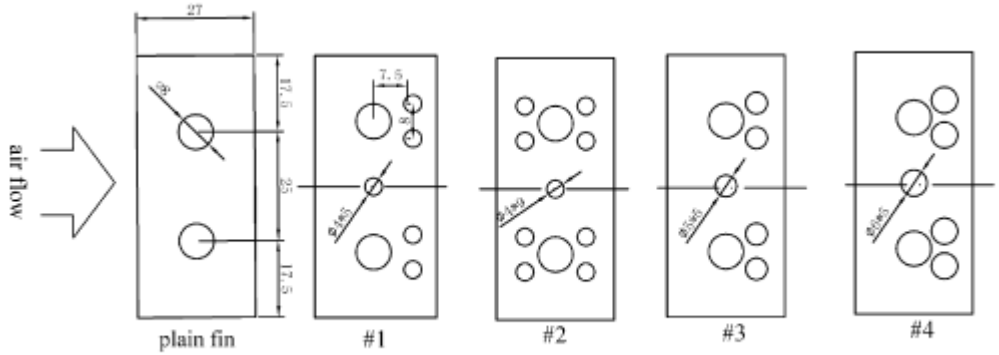

Fig. 3. The dimension of plain fin and four different perforated fins.

- An optimal perforation design is when the fin pitch is 10.0 mm.
- For the perforated FHEX with fin pitch of 10.0 mm, the j factor increases by 0.3% at Re = 750 and 8.1% at Re = 2350, respectively, with the optimal perforation design.
- The j factor increase for the perforated FHEXs compared with the plain FHEX is more obvious when the fin pitch is smaller. When the fin pitch varies from 20.0 mm to 7.5 mm, the increase in the j factor varies from 2.7% to 9.2% at Re = 2350.
- However, the simulated results show that the total heat transfer rate is reduced by 6.5% at Re = 750 when the fin pitch is 7.5 mm due to the heat transfer surfaces loss caused by perforations.

Heat transfer and pressure drop characteristics of peripheral-finned tube heat exchangers, Int. J. heat mass transfer, 55 (2012) 2835–2843

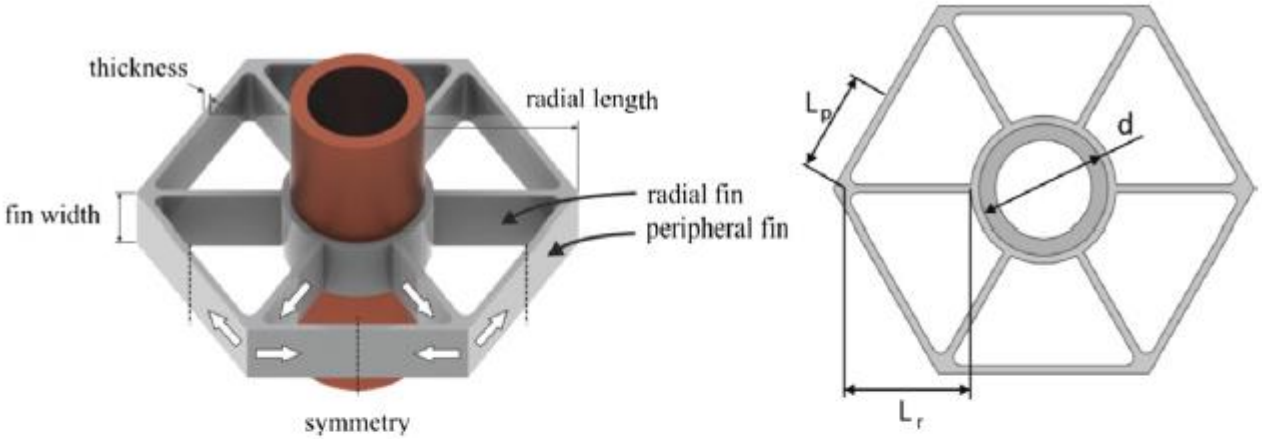

Fig. 3. Fin geometric parameters.

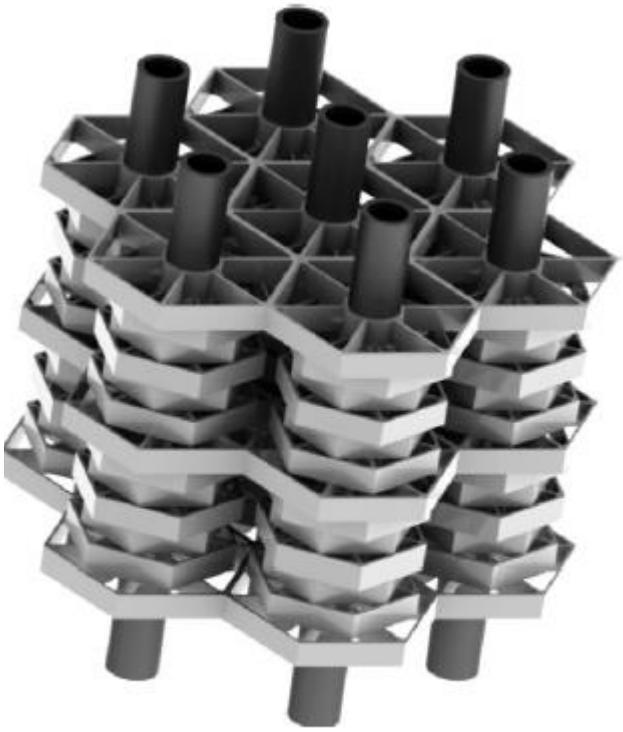

Fig. 1. The peripheral finned-tube geometry [12].

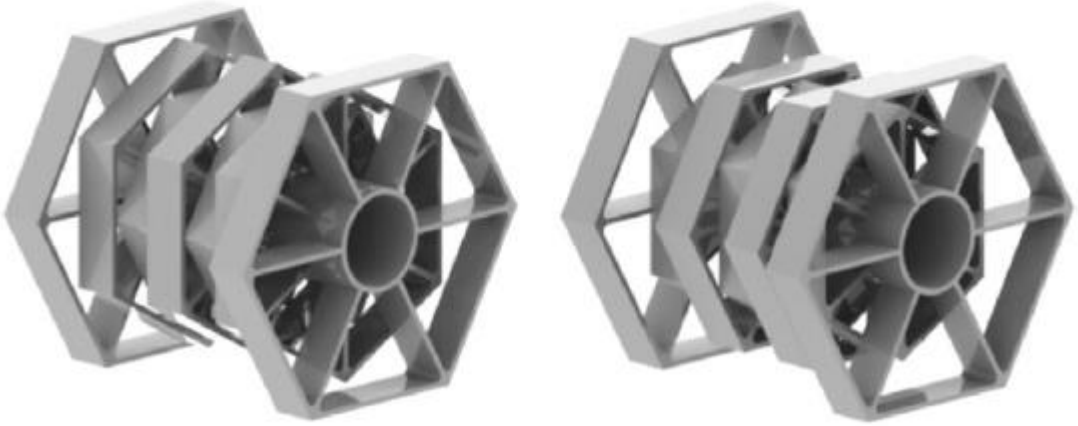

Fig. 4. Representation of a unit and its distribution. From left to right: (a) R_3, R_2, R_1, R_2, R_1, R_2, R_3 and (b) R_3, R_1, R_2, R_1, R_2, R_1, R_3.

Table 1
Geometric characteristics of the heat exchangers.

Sample	HX length (mm)/ no. tube rows	HX width (mm)/ no. units per tube	HX height (mm)	R_3 Radial length (mm)/no. of fins	R_2 Radial length (mm)/no. of fins	R_1 Radial length (mm)/no. of fins	Fin thickness (mm)	Surface area (m^2)/β (m^2/m^3)	Porosity	Distribution
A	128.6/5	148/6	56	12.1/70	9.0/180	7.0/120	0.5	0.4043/381	0.877	R_3, R_2, R_1, R_2, R_1, R_2
B	128.6/5	148/6	56	12.1/70	9.0/180	7.0/120	0.8	0.4083/385	0.810	R_3, R_2, R_1, R_2, R_1, R_2
C	128.6/5	148/6	56	12.1/70	9.0/120	7.0/180	0.8	0.3945/372	0.815	R_3, R_1, R_2, R_1, R_2, R_1
D	80.3/3	244/10	56	12.1/66	9.0/180	7.0/120	0.8	0.4083/372	0.810	R_3, R_2, R_1, R_2, R_1, R_2
E	67.3/3	292/12	47	9.5/78	7.0/216	5.5/144	0.8	0.3939/426	0.766	R_3, R_2, R_1, R_2, R_1, R_2

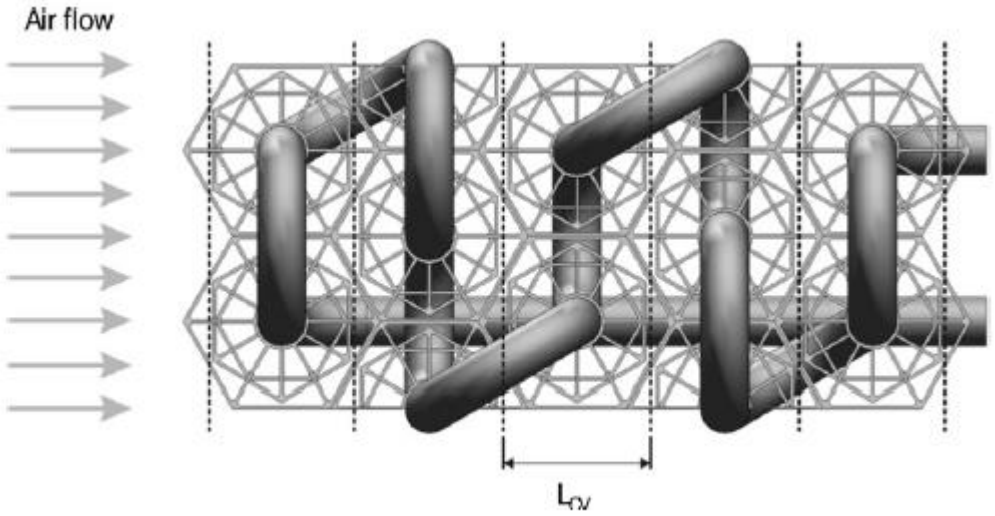

Fig. 6. Peripheral fin heat exchanger divided into control volumes.

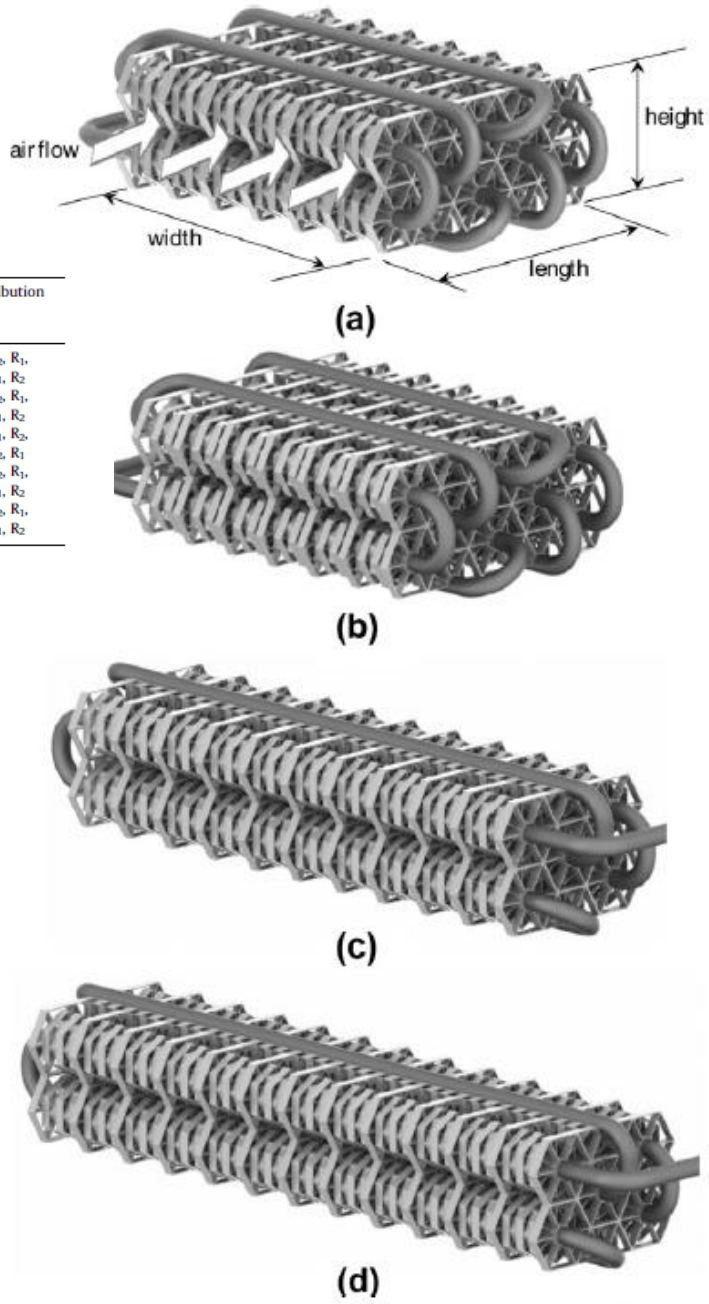

Fig. 2. Schematic view of the heat exchanger samples. (a) Sample A. (b) Sample C. (c) Sample D. (d) Sample E.

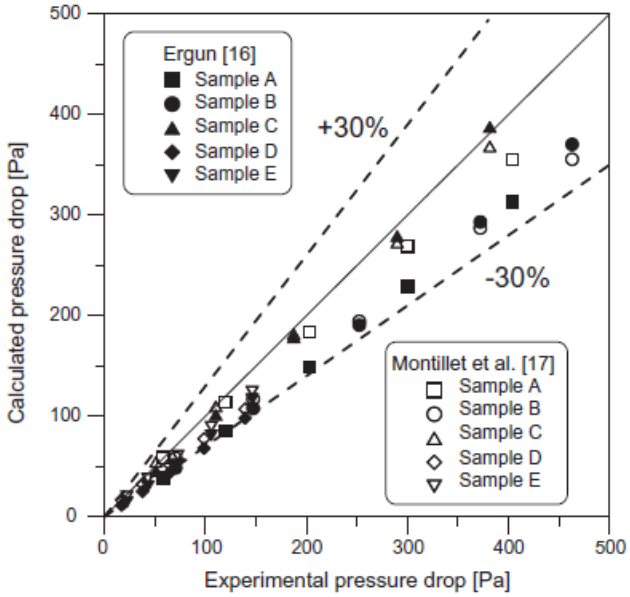

Fig. 9. Comparison of modeling and experimental results for the air-side pressure drop.

Table 2
Minimum, average and maximum values of the mean overall surface efficiency calculated according to the heat exchanger model.

Sample	Minimum	Average	Maximum
A	0.876	0.912	0.955
B	0.935	0.958	0.987
C	0.945	0.964	0.987
D	0.960	0.978	0.993
E	0.984	0.991	0.999

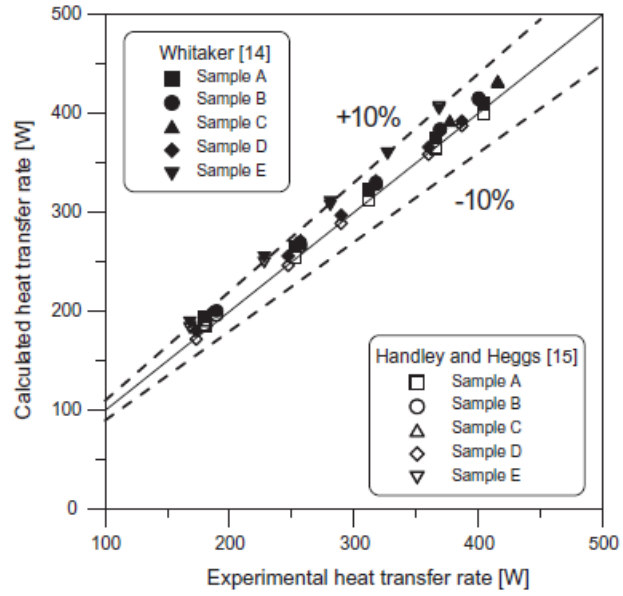

Fig. 10. Comparison of modeling and experimental results for the heat transfer rate.

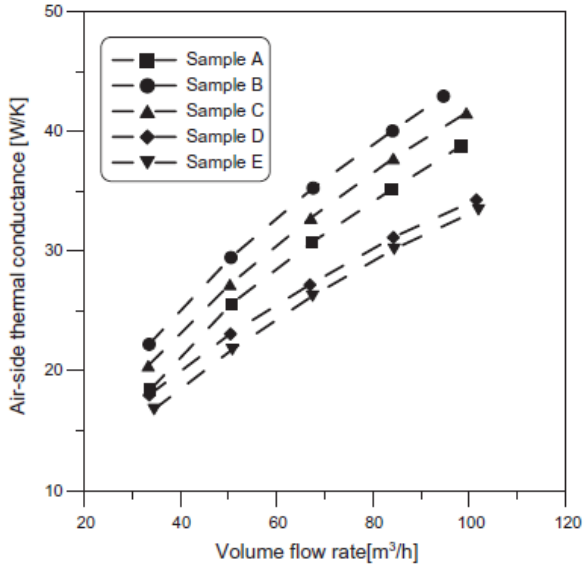

Fig. 7. Air-side thermal conductance as a function of the air flow rate.

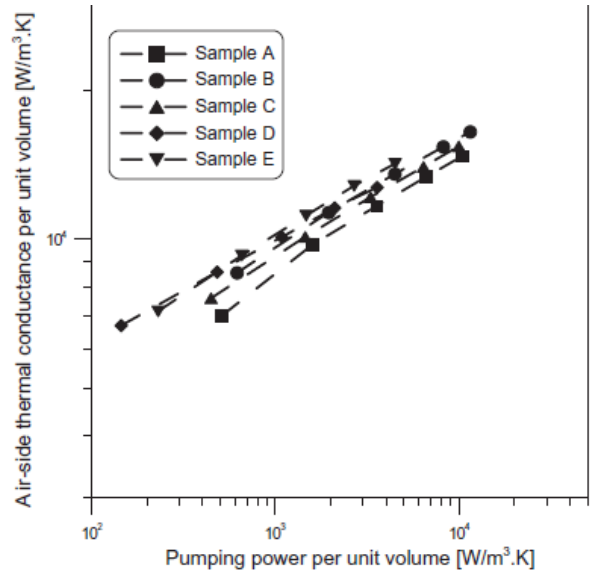

Fig. 8. Air-side thermal conductance per unit volume as a function of the pumping power per unit volume.

Other Concept for Fin Design : Design by Non-uniformity

1. Place the enhancement at low heat transfer region.
2. Check the effective local temperature difference. Placing enhancements at those having lower temperature difference are generally more effective.

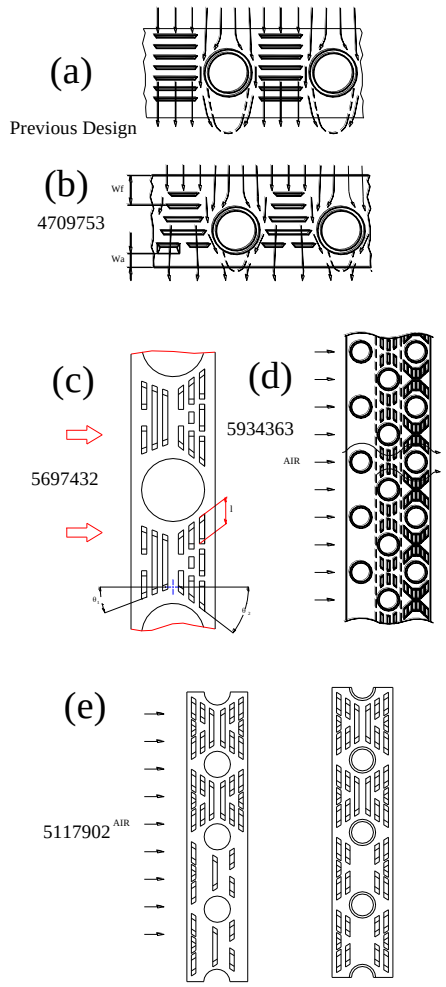

Variable (Asymmetry design)

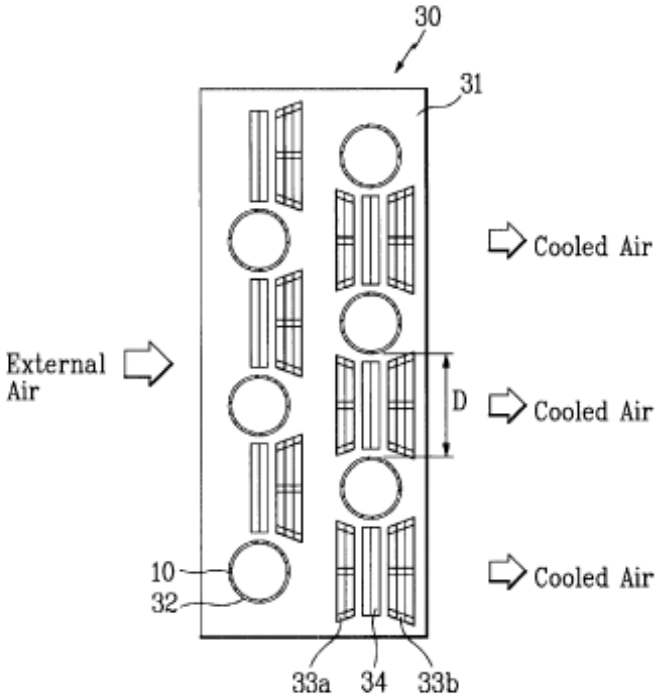

(a) US patent 6334326.

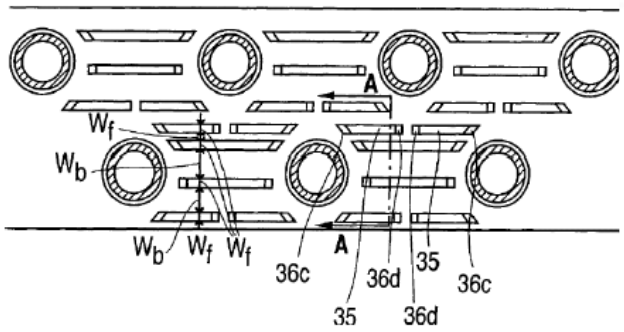

(b) US patent 6227289.

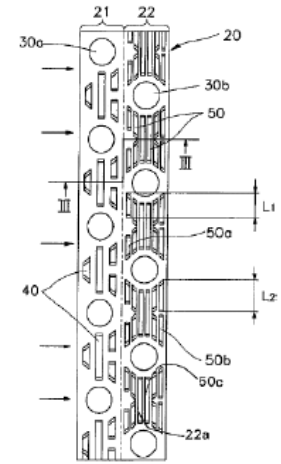

(c) US patent 6026893.

Fig. 13. Schematic of the US patents of 6334326, 6227289, and 6026893.

Fig. 13. (*Continued*)

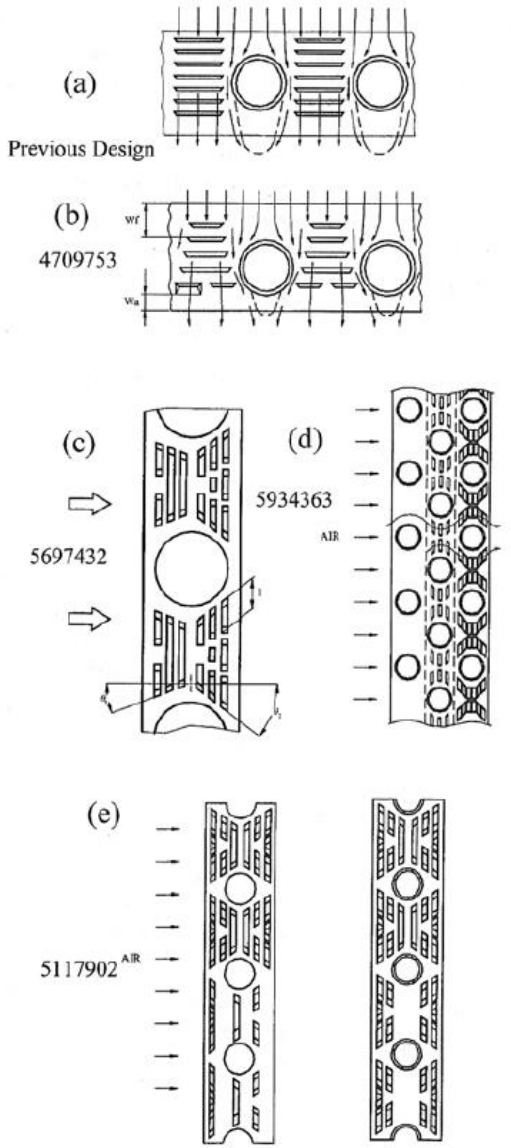

FIGURE 12 Schematic of the US patents of 4709753 5697432, 5934363 and 5117902.

The Influence of Strip Location on the Pressure Drop and Heat Transfer Performance of a Slotted Fin, Numerical Heat Transfer, Part A, 52: 463–480, 2007

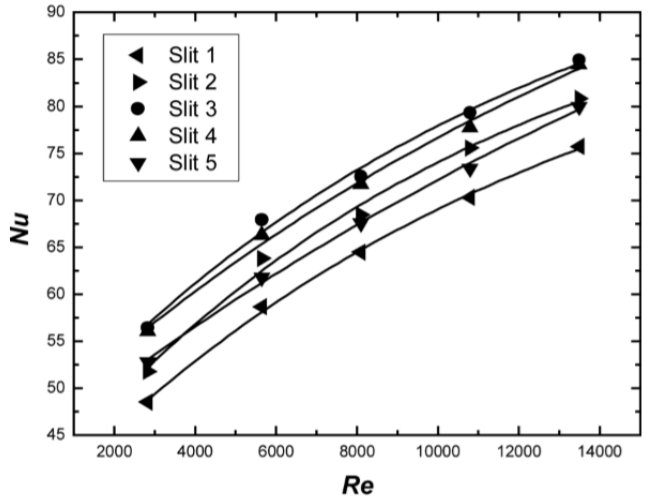

Figure 4. Comparison of Nu among five slit arrangements.

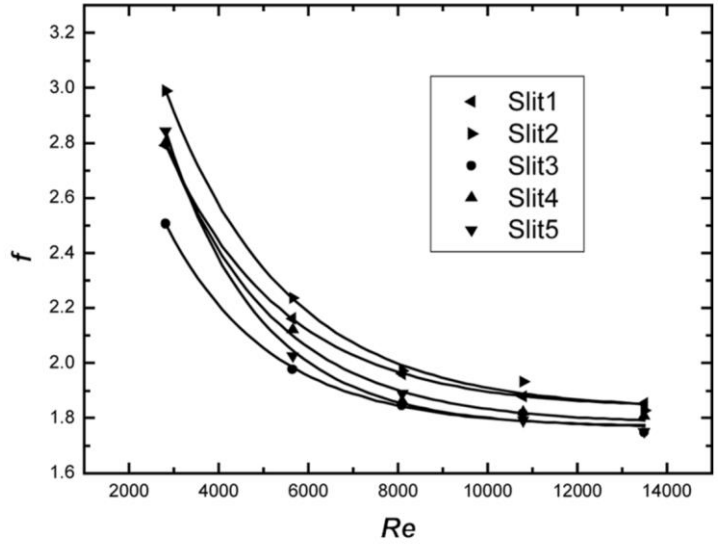

Figure 6. Comparison of friction factors among five slit arrangements.

Table 1. Simulation conditions

Tube outside diameter	19.1 mm
Longitudinal tube pitch	25.0 mm
Transverse tube pitch	25.0 mm
Fin thickness	0.3 mm
Fin pitch	2.5 mm
Strip width	2.0 mm
Strip height	1.25 mm
Tube temperature	308 K
Inlet air temperature	403 K
Inlet frontal velocity	2–10.0 m/s

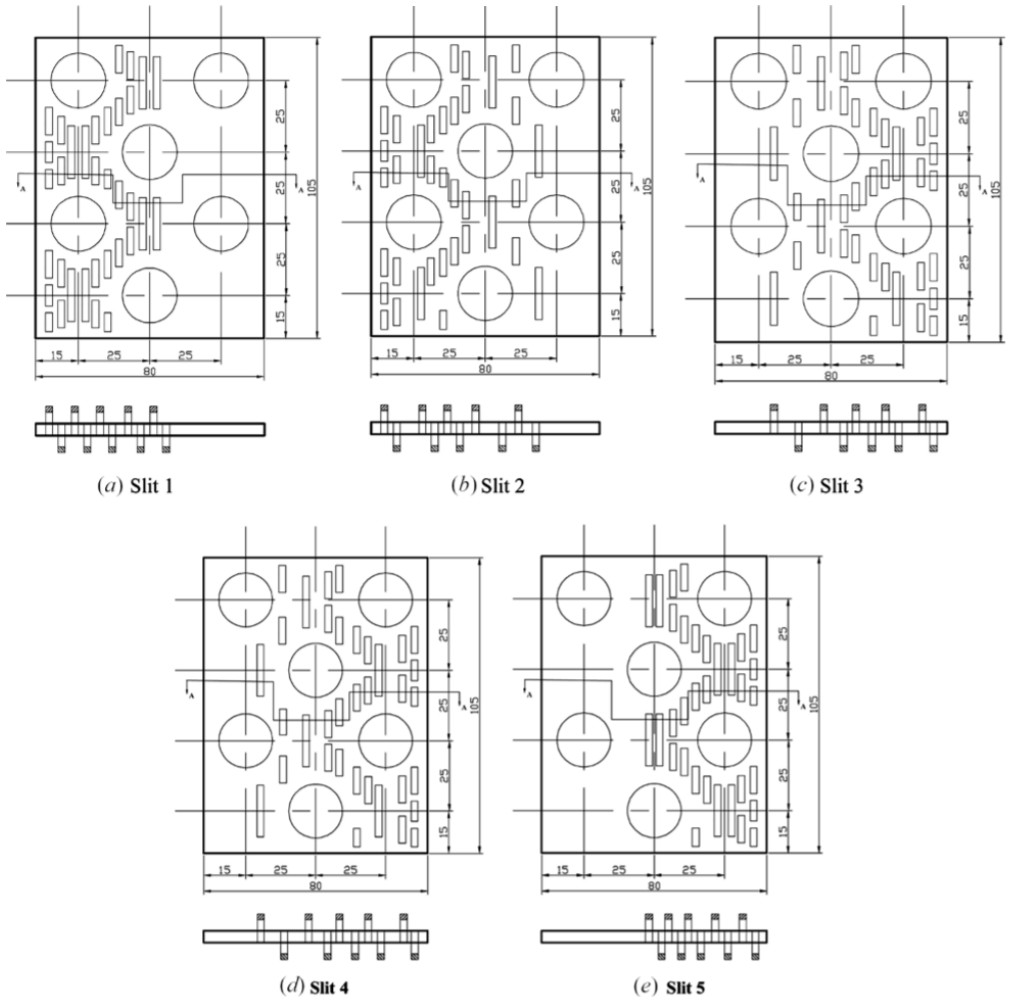

Defrosting Coil

US 9,528,779 B2
Dec. 27, 2016

Fig. 13

12

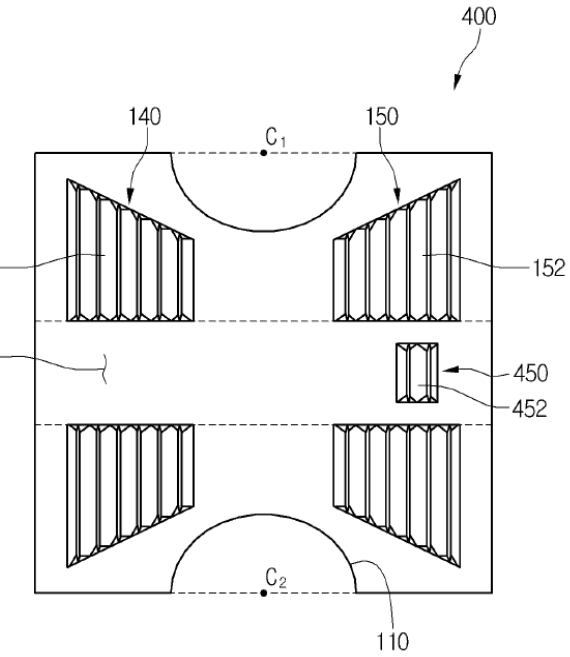

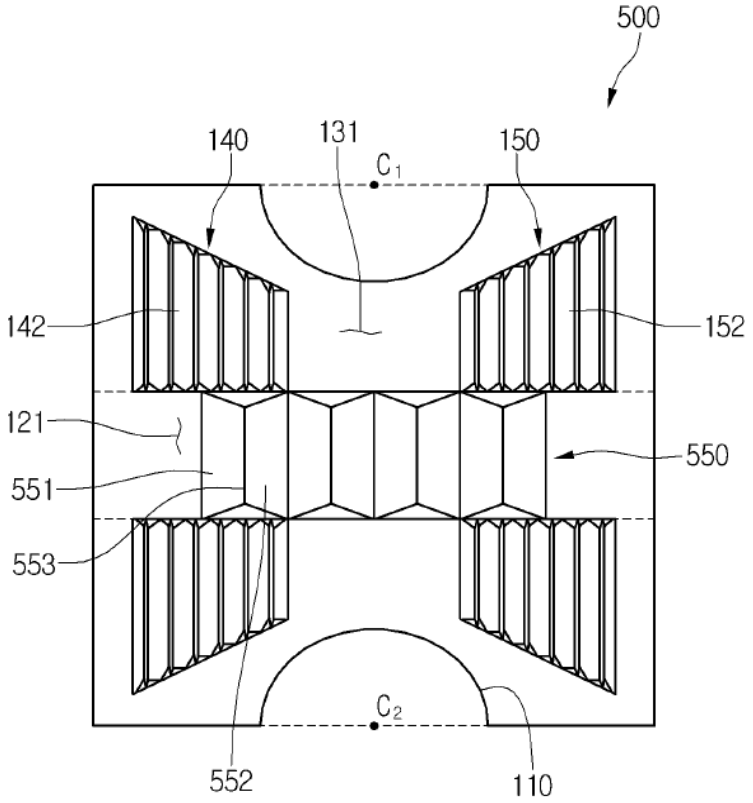

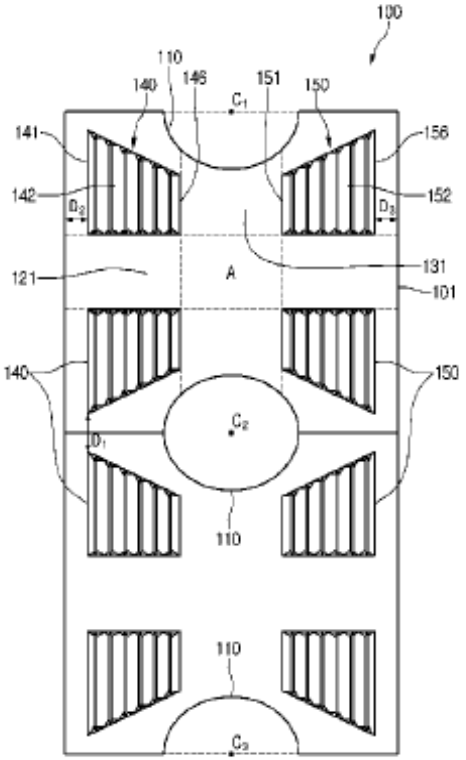

Effect of a micro-grooved fin surface design on the air-side thermal-hydraulic performance of a plain fin-and-tube heat exchanger, Int. J. Refrig., 36 (2013) 1078-1089

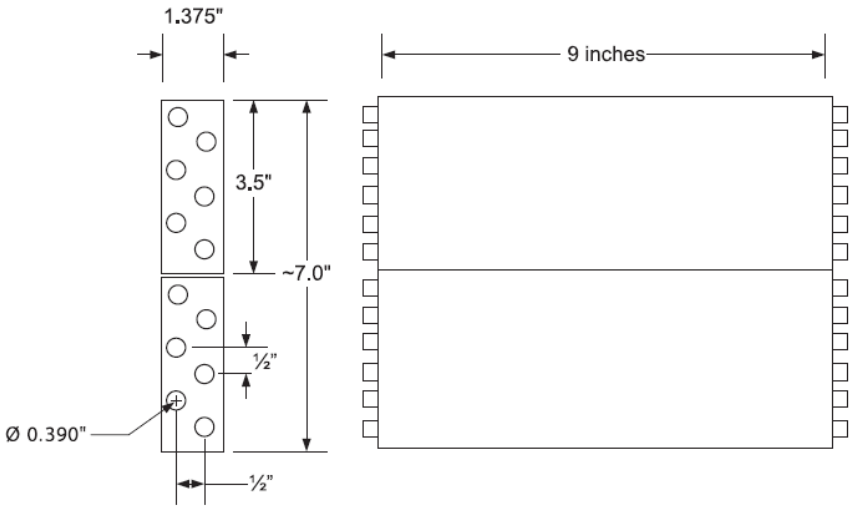

Fig. 3 – Schematic of the relevant coil geometry.

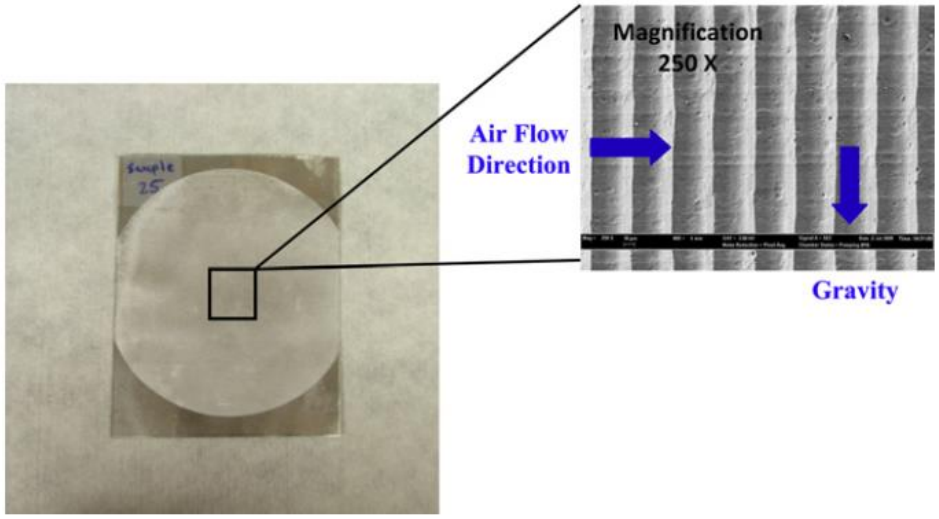

Fig. 2 – Photo of a representative fin sample prepared for Coil #2 with SEM image showing underlying microstructure after wet etching.

Table 2 – Description of the fin surfaces used for heat exchanger prototype construction.

	Coil #1	Coil #2	Coil #3	Coil #4
Fin surface conditions	Baseline surface	Channels: 15 μm width, 9–10 μm depth + silane coating	Channels: 50 μm width, 15–16 μm depth + silane coating	Fin surface exposed to a 300 W O_2 plasma for 10 min

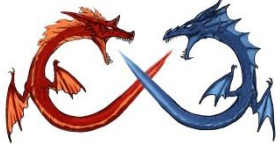

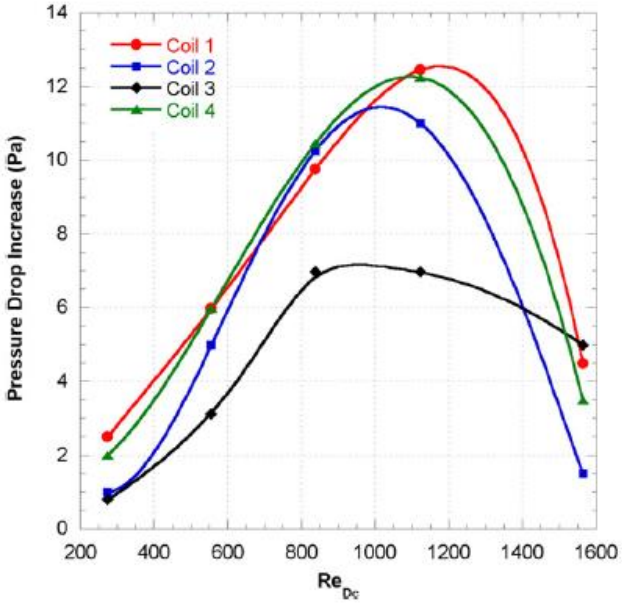

Fig. 10 – Change in pressure drop between dry and wet conditions.

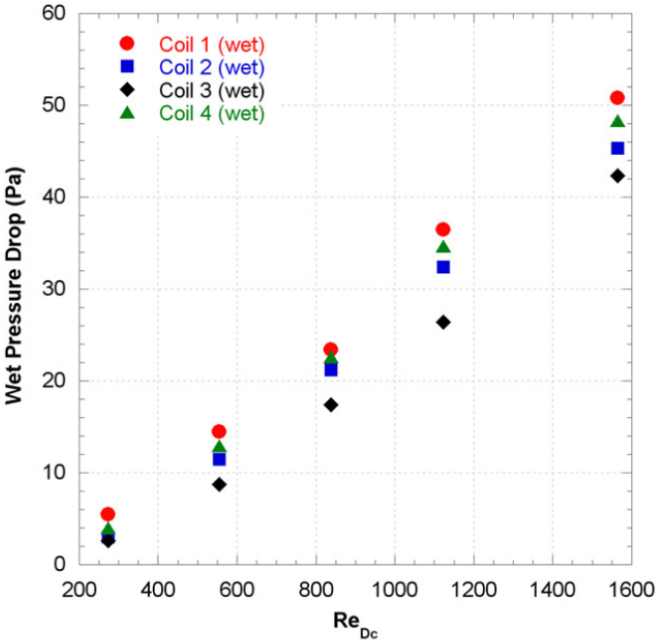

Fig. 9 – Air-side pressure drop during wet tests.

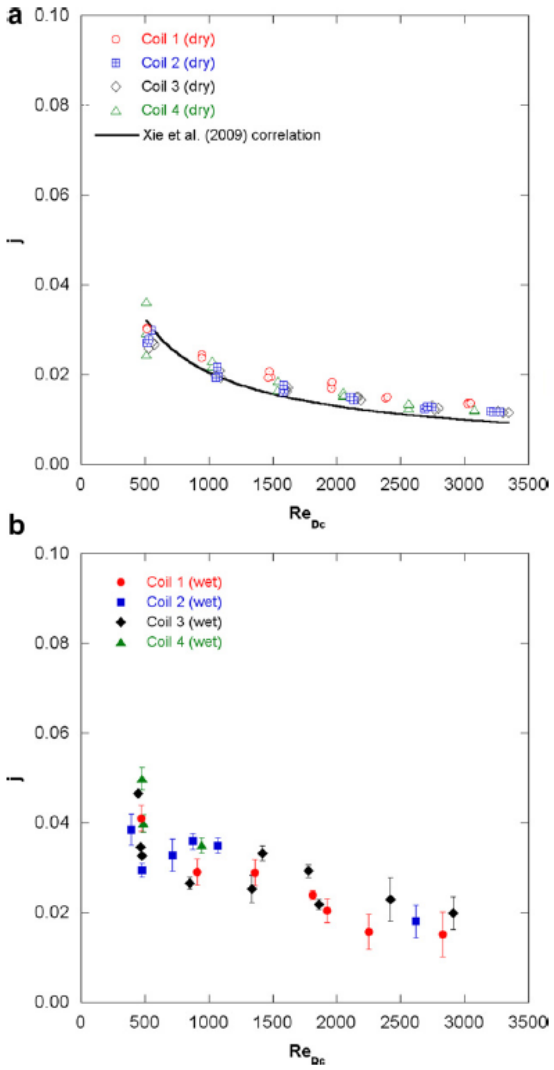

Fig. 11 – Air-side sensible j factor under both dry and wet conditions.

Table 4 – Durability of the dynamic contact angle data.

		Feb. 2010[a]	Mar. 2010[b]	Sept. 2010[b]	Mar. 2011[b]
Coil #1	Advancing angle	87.81°	105.82°	104.28°	105.41°
	Receding angle	25.23°	66.96°	72.45°	82.07°
Coil #2	Advancing angle	62.60°	100.64°	116.11°	110.78°
	Receding angle	18.66°	60.94°	78.43°	79.10°
Coil #3	Advancing angle	73.74°	104.50°	105.64°	104.78°
	Receding angle	22.24°	72.56°	74.68°	76.05°
Coil #4	Advancing angle	87.81°	91.93°	100.10°	101.22°
	Receding angle	25.23°	31.45°	51.38°	60.52°

Note:
a Feb. 2010: fin surfaces without silane coating.
b Mar. 2010, Sept. 2010, and Mar. 2011: fin surfaces with coating.

(19) United States
(12) Patent Application Publication
Jin et al.
(10) Pub. No.: US 2017/0198984 A1
(43) Pub. Date: Jul. 13, 2017

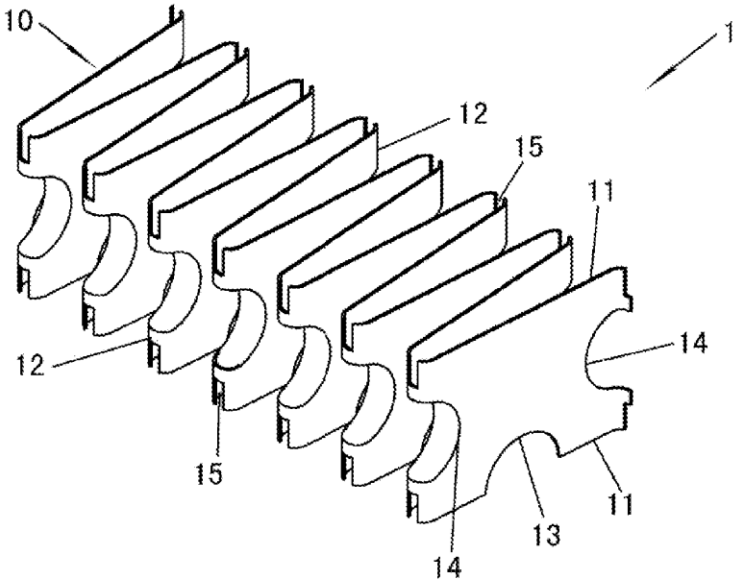

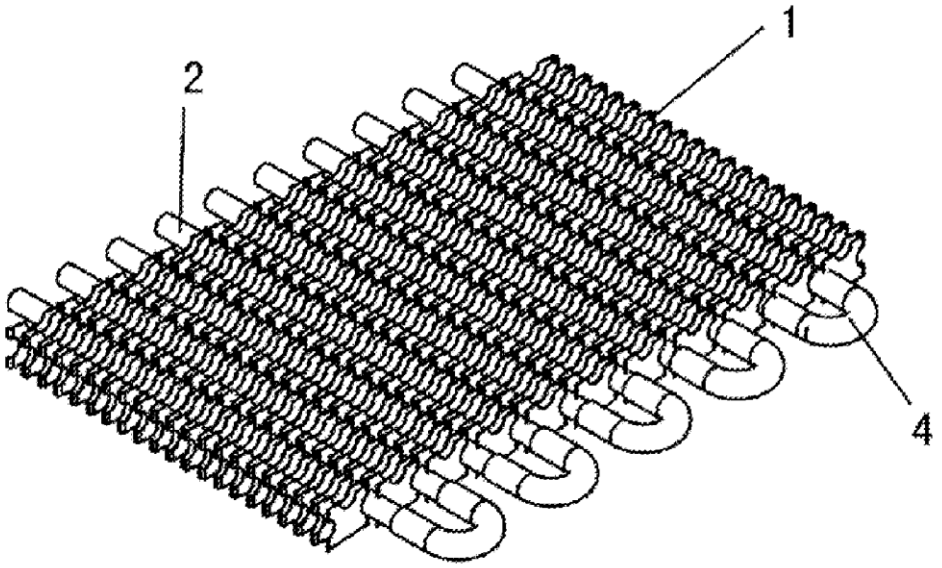

Fig.1

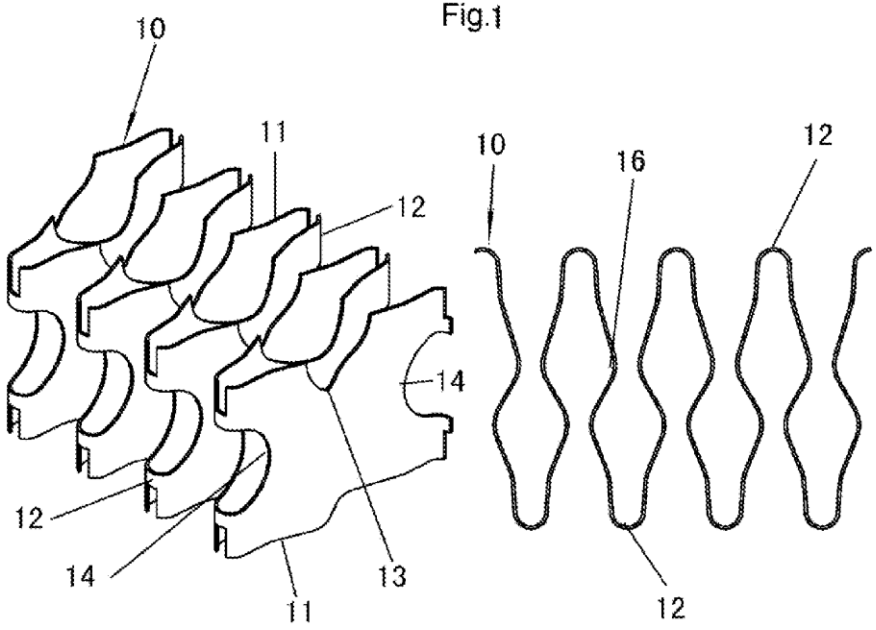

Analytical analysis and experimental verification of interleaved parallelogram heat sink, Applied Thermal Engineering 112 (2017) 739–749

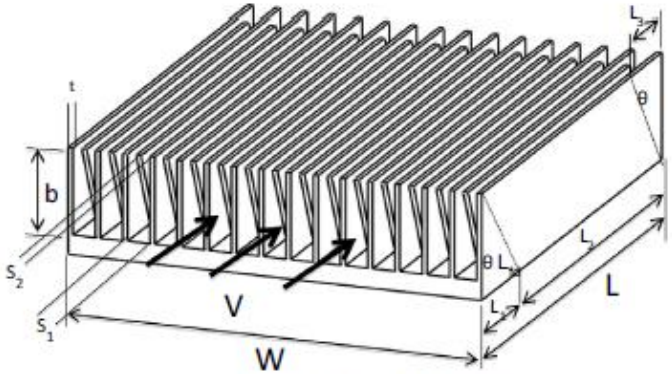

(a) Proposed IPFM configuration.

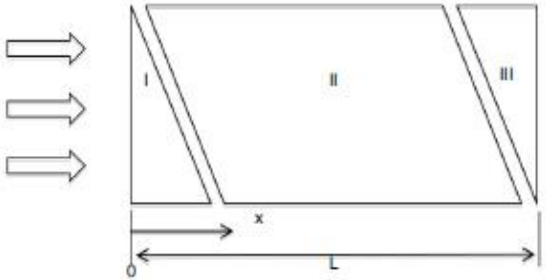

(b) The IPFM model fin module can be divided into 3 parts.

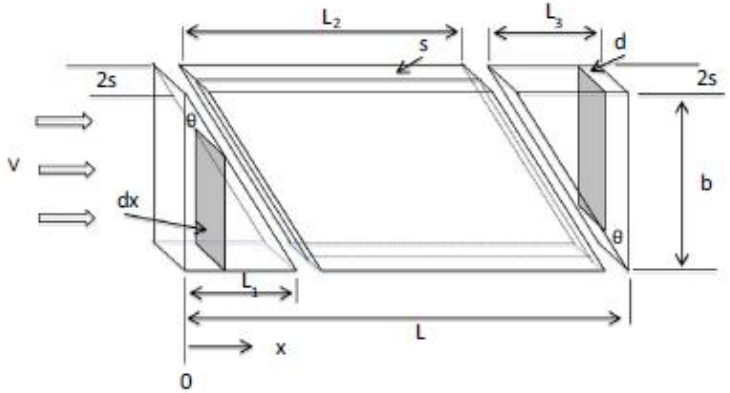

(c) Notations of the IPFM design.

Fig. 3. Schematic of the proposed IPFM design and related notations.

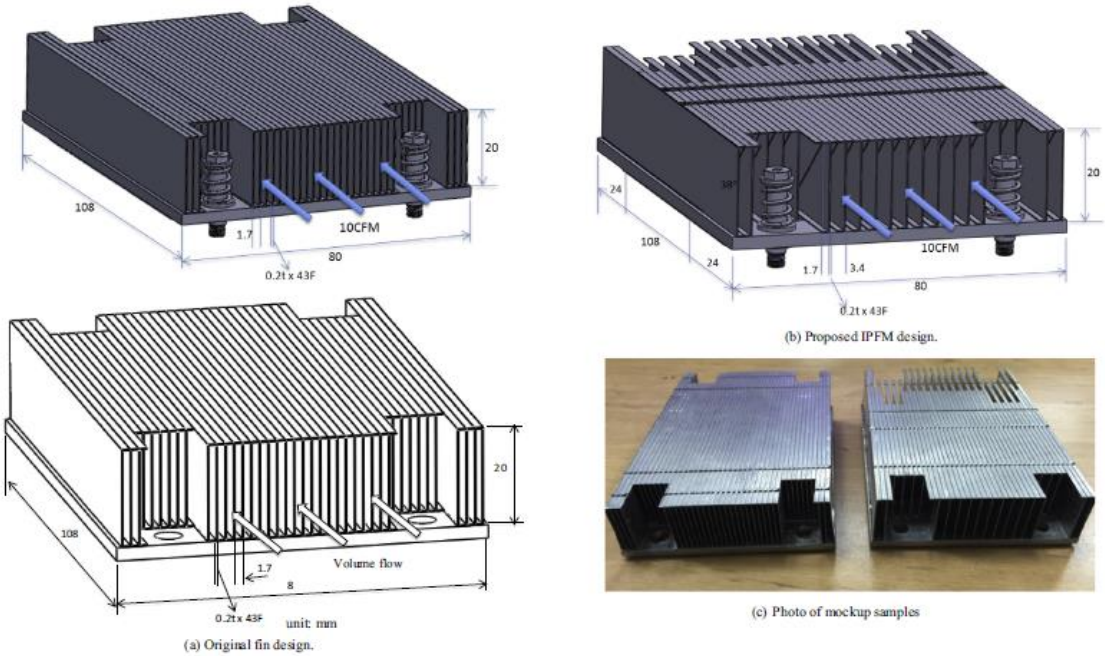

(a) Original fin design.

(b) Proposed IPFM design.

(c) Photo of mockup samples

Fig. 5. Actual implementation of the heat sinks for the original and the proposed IPFM design.

- Alternating Fin Design

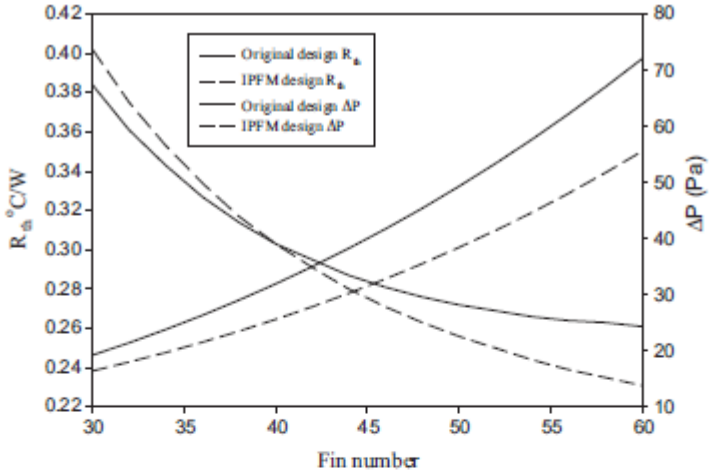

(a) Results for 10 CFM

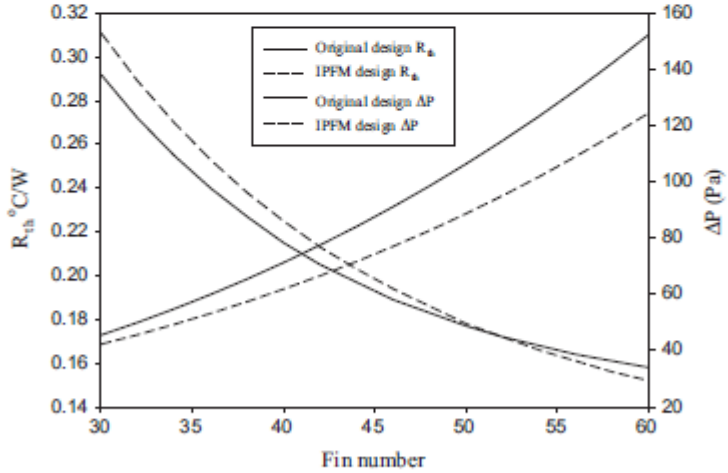

(b) Results for 20 CFM

Fig. 8. Analytical calculations and comparisons of the influence of fin number on the heat transfer and frictional performance for the conventional and IPFM design.

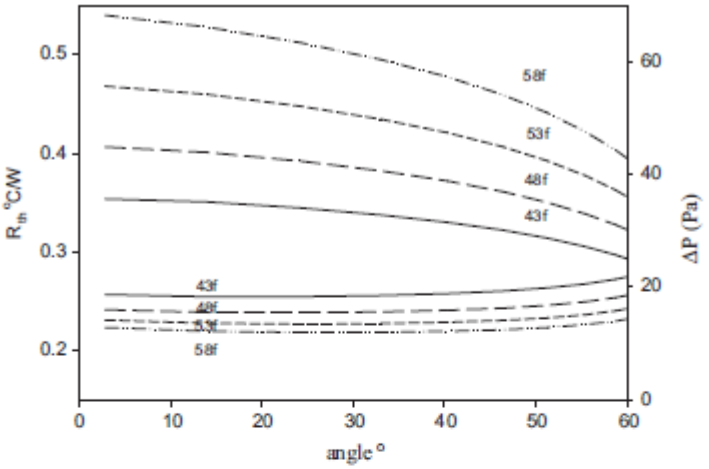

(a) Results for 10 CFM

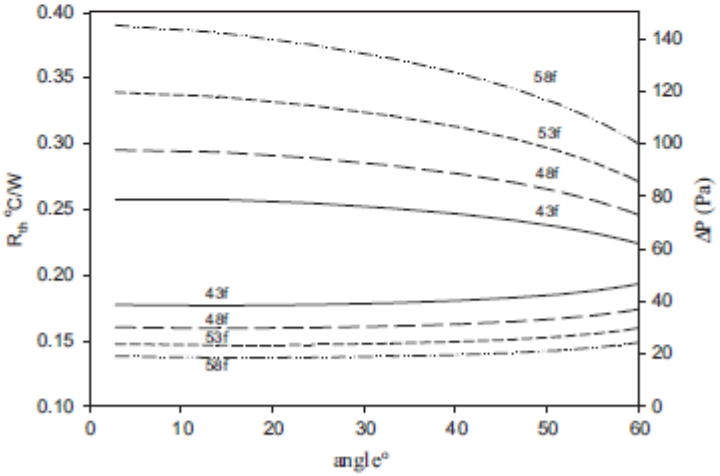

(b) Results for 20 CFM

Fig. 9. Analytical calculations and comparisons of the influence of cut angle on the heat transfer and frictional performance of the present IPFM design.

Porous design.. Usually not so effective, requires further modifications..

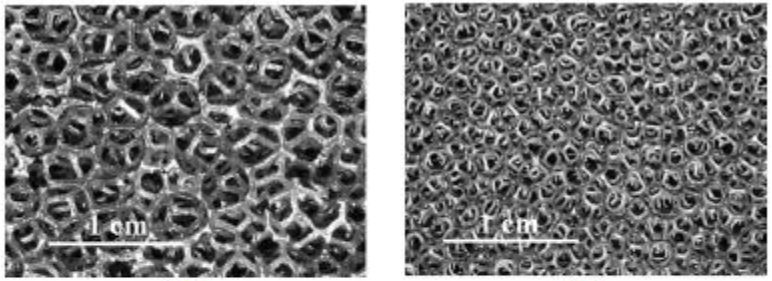

Figure 4. Typical metal foam. Reprinted with permission from [19]. Copyright 2014 Elsevier. (**a**) Sample is with 5 PPI (pore per inch) having a porosity of 95%; (**b**) Sample is with 10 PPI (pore per inch) having a porosity of 95%.

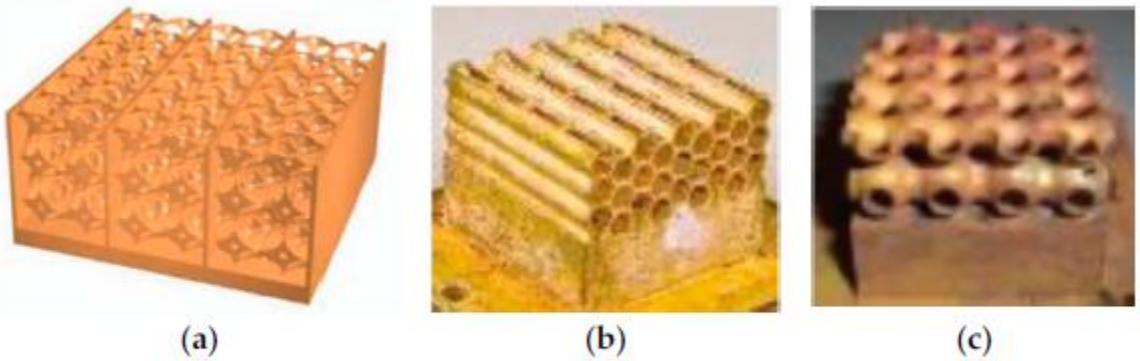

Figure 5. Fin structure tested by Krishnan et al. Reprinted with permission from [24]. Copyright 2012 IEEE. (**a**) Fin metal foam heat sink; (**b**) slotted hexagon heat sink; (**c**) Schwartz type heat sink.

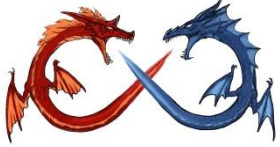

Conclusions

- Interrupted surfaces are applicable for comparatively large spacing and higher operational velocity (say 1.7 mm & $V_{fr} > 2$ m/s).
- LVGs are effective with less number and comparatively large fin spacing.
- Con-cavity and dimple is quite effective in heat transfer and pressure drop reduction, provided the numbers are low.
- Cannelure structure may reduce the boundary layer thickness to further reduce pressure drop.
- Combined designs are implemented and are proved to be effective.
- Porous design seems to be less effective for fin-and-tube applications.
- The partial bypass design is applicable in some limited ranges.
- Manipulating ΔT can be effective at low velocity regime.
- Asymmetry design can be quite useful for locating the enhancement at poor heat transfer regime.

感謝聆聽

敬請賜教

王啟川
Tel: +886-3-5712121 ext. 55105
E-mail:ccwang@mail.nctu.edu.tw